Chemical-Scale Studies of the Nicotinic Acetylcholine Receptor: Insights from Amide-to-Ester Backbone Mutagenesis

Thesis by

Kristin Rule Gleitsman

In Partial Fulfillment of the Requirements

for the Degree of

Doctor of Philosophy

Division of Chemistry and Chemical Engineering
California Institute of Technology
Pasadena, California
2010

(Defended April 12, 2010)

Acknowledgements

First and foremost I would like to thank my advisor, Professor Dennis Dougherty, who has supported me throughout my graduate career both personally and professionally. Although it took me longer than most to find my way in the lab, I have come to appreciate the level of intellectual freedom he affords his graduate students. While this meant plenty of room to make (and learn from) mistakes in the first few years of my graduate career, it has ultimately fostered a degree of independence that I believe will serve me well throughout my scientific career. There is nothing like graduate school to instill a strong sense of humility, occasionally trending toward insecurity, so these acknowledgements would not be complete without thanking Dennis for being there with words of encouragement at critical moments during the last five and a half years.

The expertise of Professor Henry Lester and his laboratory were critical to the completion of the research contained in this thesis. Henry's depth of knowledge and experience in the field of electrophysiology provided essential perspective for interpreting unusual results. In addition, Henry served as a wellspring of experimental suggestions, whose value lay not only in the ideas themselves, but also in honing my critical thinking skills in deciding which experiments to pursue. Of the Lester lab, I am particularly indebted to Dr. Rigo Pantoja for helping me design and execute my single-molecule TIRF experiments.

I would also like to thank my committee, Professors Peter Dervan, Harry Gray, and Shu-ou Shan. Their guidance and advice have been invaluable, especially when planning the next steps in my career. In addition, it has truly been a pleasure to interact with people who are not only brilliant, but also kind, encouraging, and interesting. I only wish there had been more opportunities for interaction.

Past and present members of the Dougherty lab have certainly shaped my graduate school experience. In particular, the candid humor of Dr. Michael Torrice was incredibly important in getting me through some rough patches. Likewise, Jai Shanata has been an incredible colleague and friend. Several chapters of this thesis (4 and 5, in particular) would not have been possible without his intellectual contribution, as well as moral support. Sean Kedrowski has also been a pleasure to work with since he joined the lab. More recently, he and Ethan Van Arnam have been extremely tolerant of the not infrequent baby-induced disruptions to our otherwise quiet bay. I owe my deepest gratitude to the entire lab for their support of me and their enthusiastic acceptance of my daughter, Malina, over the past year, as I attempted to juggle new motherhood with research and thesis writing. In particular, Ariele Hanek not only helped in proofreading parts of this document, but also brought us numerous delicious meals in the early weeks of Malina's life. Nyssa Puskar has been an exceptional colleague over the last year, acting as a sounding board for proposal ideas and other professional quandaries, as well as being an excellent copy editor. Although I wouldn't accuse Nyssa of being quiet, her unassuming manner has come to define the meaning of "still waters run deep" for me. Finally, I must thank Angela Blum for indulging my desire to do one last project as I was finishing up in the lab by agreeing to tackle the experimental component of the research described in Chapter 7 (and for proofreading that chapter).

Since moving to Pasadena more than five years ago, I have been blessed in the friendships that I have made here. I specifically want to mention Heidi Privett, Michael Adams, and Valerie Scott. Their friendship over the years has had a tremendous impact on my life, more than I can even begin to describe here.

Several people from my pre-Caltech existence also deserve acknowledgement. My mother has provided support and encouragement my entire life. Her sacrifices through difficult

times in our family's history ensured that I had the opportunity to pursue my passions. My awe of what she was able to accomplish as a single parent has only increased over the years, especially since becoming a parent myself. My biology teacher from high school, Spike Black, initially sparked my interest in science. My freshman chemistry professor, Dr. Bob Olsen, is the reason that I decided to major in chemistry in the first place. Karen Wovkulich, herself currently a graduate student in the physical sciences, has been with me every step of the way- choosing the seat next to her in first semester freshman year is one of those happy twists of fate that likely changed the course of my life. Not only did she help inspire my early passion for chemistry, by providing help with problem sets and friendly competition, she also introduced me to my husband.

I also owe an enormous debt of gratitude to my husband, Wolfe Gleitsman. Beginning with his willingness to follow me to California in the fall of 2004, Wolfe has supported me in innumerable ways throughout my graduate career. Most recently, he has been sharing in the adventure of new parenthood, whether that meant staying up with Malina so that I could get some much needed sleep or filling in for gaps in childcare so that I could complete some final experiments. And to Malina, who will not remember this somewhat hectic chapter in our life, thank you for the excited smiles when I come home in the evening, for the occasional night of good sleep, and for just being the charming little person you are.

Abstract

This thesis describes the use of peptide backbone amide-to-ester mutations to study the structure and function of ligand-gated ion channels. The research described herein has been done on the muscle nicotinic acetylcholine receptor, a prototypical ligand-gated ion channel in the cys-loop superfamily. Backbone mutagenesis in these proteins provides insight into specific intermolecular interactions that are critical to function, as well as answering more fundamental questions about the role of the peptide backbone in long-range conformational changes in these allosteric receptors.

Chapter 2 describes the identification of a key hydrogen bond near the binding site that is involved in the gating pathway. We found that the backbone N-H of a loop C residue makes a hydrogen bond to an anionic side chain of the complementary subunit upon agonist binding. The hydrogen bonding partner is not the residue predicted by structural data, but instead an aspartate that was originally believed to participate directly in agonist binding.

In chapter 3 we consider the involvement of the peptide backbone in the binding-induced conformational changes that lead to channel gating. Single backbone mutations in the β-sheet-rich extracellular domain were well tolerated, whereas two proximal backbone mutations led to nonfunctional receptors. These results support a model in which backbone movements in the outer β-sheet are important for receptor function.

Chapter 4 describes a new method - **e**lucidating **l**ong-range **f**unctional **c**oupling in **a**llosteric **r**eceptors (ELFCAR) - that should be broadly applicable to determining functional roles of residues in allosteric receptors.

Chapters 5 and 6 describe electrophysiological and computational investigations into the role of amide-to-ester mutations in the aromatic binding box of the nicotinic receptor.

Echoing the results of chapter 3, these mutations largely reveal an overall tolerance of backbone mutations in the binding site.

Finally, in chapter 7, we explore the use of ester and N-methyl backbone modifications to uncover the role of conformational changes at an unusual vicinal disulfide bond near the tip of the C-loop. Using ab initio calculations, we demonstrate that N-methylation and esterification of this ring structure in model peptides dramatically impacts its *cis-trans* conformational preferences.

Table of Contents

List of Figures

List of Tables

Chapter 1: An Introduction to Chemical-Scale Neuroscience

1.1 Toward a Chemical-Scale Understanding of the Brain

For centuries, the human brain has inspired generations of scientists and non-scientists alike. With a hundred billion nerve cells wired together to form an estimated million billion synapses that endow our species with thought, emotion, and consciousness, it is the most complex structure, natural or artificial, on earth.[1] As such, unraveling its mysteries remains a formidable challenge for the 21st century and beyond. Until relatively recently, most systematic studies of brain function took a "black box" approach. Theories were formulated and tested using behavioral endpoints with the goal of predicting or treating behavior, ignoring how the brain creates that behavior. To accomplish a more complete understanding of the human brain and move beyond behavior-based therapies, scientists had to break open the veritable black box within our skulls and interrogate brain function on the cellular and molecular levels.

This odyssey began just over a century ago, with the development of a rudimentary appreciation of how cells in the brain are connected.[2] It is now well established that nerve cells in the brain, or neurons, have branchlike extensions called axons and dendrites that they use to communicate with one another. Information is passed from one neuron to another through a combination of electrical and chemical signals. A nerve impulse travels down the axon of one neuron until it reaches the synapse, or gap between neurons. The electrical signal then triggers the release of small-molecule neurotransmitters that diffuse across the synapse and bind to receptors on the neighboring neuron. In binding to and activating receptors on the neighboring neuron, these neurotransmitters initiate a new electrical signal that then further propagates the message. This process is called synaptic transmission, and its regulation is believed to underlie

much of higher brain function. As a result, much work in modern neuroscience is devoted to understanding the synapse.

1.2 The Nicotinic Acetylcholine Receptor: The Prototypical Cys-Loop Receptor

Arguably some of the most interesting synaptic proteins are those involved in mediating neuronal communication by binding neurotransmitters. The neurotransmitters that mediate synaptic transmission activate two classes of receptors: G protein-coupled receptors (GPCRs) and ligand-gated ion channels. While GPCRs are critical in modulating synaptic transmission, the majority of fast synaptic transmission in the brain is mediated by ligand-gated ion channels. These receptors respond directly to the binding of small-molecule neuroreceptors by opening an integral pore within 1-100 ms.

The Cys-loop superfamily of ligand-gated ion channels constitutes an important class of these fast-acting neuroreceptors.[3-5] Among this superfamily of ion channels are the receptors that bind serotonin, acetylcholine, and nicotine, and their functions are implicated in a variety of neurological disorders. The Cys-loop receptors are comprised of a pentamer of subunits arranged around a central ion-conducting pore. Subunits further share a homologous superstructure, including a large extracellular domain, which is involved in agonist binding; four transmembrane domains (M1-M4), which form the central ion-conducting pore; and a short extracellular carboxy terminus. Early studies on the Cys-loop family were made possible in large part because the abundance of one member of this family, the muscle subtype of the nicotinic acetylcholine receptor (nAChR) found in the cells of electric organs of the *Torpedo* electric ray.[6] For this reason, the muscle nAChR has historically been the best-characterized member of the Cys-loop family and is generally considered the prototypical Cys-loop receptor.

The muscle nAChR consists of four distinct subunits with the stochiometry $\alpha_2\beta\gamma\delta$.[7] This affords the receptor with two nonequivalent binding sites formed at the interface between the α-subunit (principal component) and the γ- or δ-subunit (complementary component). Several noncontiguous regions of both the principal and complementary subunits contribute amino acids to the compact pocket that is the agonist binding site. The structure of the nAChR is illustrated in figure 1.1A-E. These regions are referred to as loops A, B, and C (principal) and D, E, and F (complementary) (Figure 1.1B,C). Five highly conserved residues form what is known as the aromatic binding box (Figure 1.1E) and include αY93 (loop A), αW149 (loop B), αY190 and αY198 (loop C), and γW55 or δW57 (loop D). The face of αW149 makes a cation-π interaction with the endogenous agonist, acetylcholine, constituting a major non-covalent binding interaction.[8] Other residues in the aromatic binding box have been proposed to play a role in shaping the agonist binding site and transmitting binding events to channel opening events;[9-12] a process referred to as gating. Furthermore, the motions of the C-loop are strongly implicated in the gating process.[10, 13-16]

Gating culminates in the opening of the central ion-conducting pore within the transmembrane domain. The second transmembrane α-helix lines the channel pore, with each subunit contributing several highly conserved hydrophobic residues to the gate of the channel. Of these, the L9' residue (simplified transmembrane numbering system for the M2 domain[17]) resides at approximately the halfway point and comprises the narrowest constriction point in the Cryo-EM structure of the *Torpedo* nAChR (Figure 1.1D).[16] It has been demonstrated to play a critical role in gating, and mutating this residue to a more polar amino acid stabilizes the pore in an open, ion-conducting conformation.[18, 19]

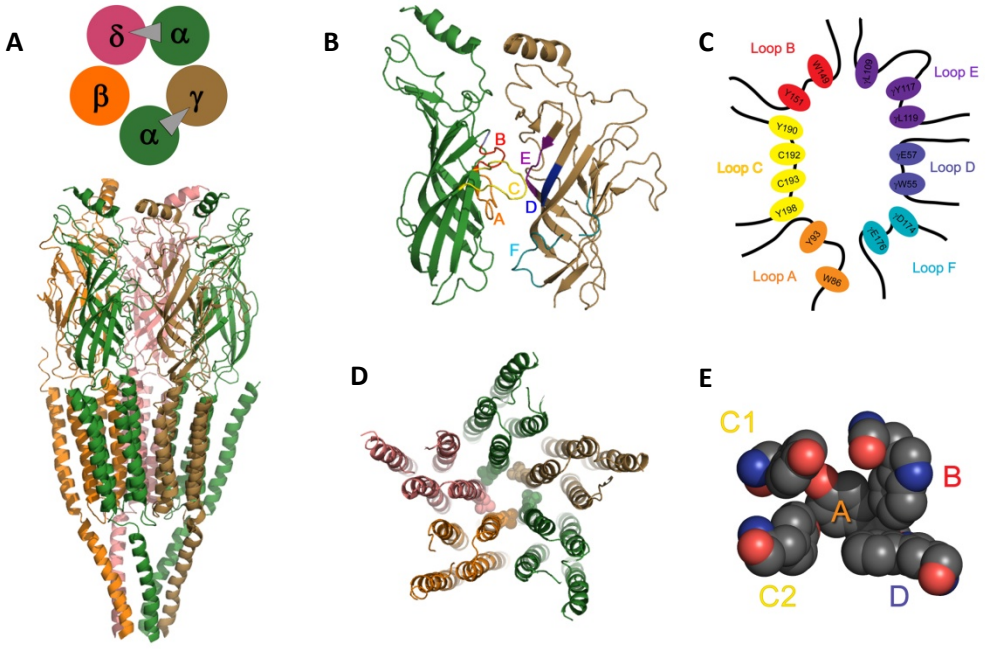

Figure 1.1. The general topology of the muscle nAChR. (A) The muscle nAChR has two α1 (green), one β1 (orange), one γ (brown), and one δ (pink) subunit arranged around a central ion-conducting pore. The binding sites (grey triangles) are at the αγ and αδ interfaces. (B) The binding sites are located within the largely β-sheet extracellular domain with contributions from six loops: A (orange, primary subunit), B (red, primary subunit), C (yellow, primary subunit), D (blue, complementary subunit), E (purple, complementary subunit), and F (cyan, complementary subunit). (C) Amino acid contributions to the agonist binding site from the loops. (D) The transmembrane region is comprised of four transmembrane-spanning helices from each subunit. The second transmembrane helix (M2) lines the ion-conducting pore. The L9' residue is highlighted as space-filling. (E) The structure of the aromatic binding box, with contributions from loops A, B, C (primary subunit), and D (complementary subunit).

1.3 Heterologous Expression of Synaptic Proteins and Electrophysiological Characterization

The synapse itself is a dizzyingly complex structure. It not only contains the receptors and ion channels that bind various neurotransmitters, but also numerous scaffolding proteins that control spatial arrangements and signaling proteins involved in downstream cascades beyond the simple further propagation of the electrical signal. Many of these proteins interact with each other and these interactions are constantly in flux, both spatially and temporally. Untangling this web of interactions is the focus of cellular neuroscience and is an immensely important goal for eventually understanding brain function. To fully do this, however, we must understand something about the synaptic proteins on a molecular level. The most efficient way

of interrogating the structure and function of these synaptic proteins is to isolate them from the seeming chaos of the synapse. Thus, studying the molecules of the synapse requires us to leave the synapse.

Heterologous expression of proteins provides an elegant way of expressing these synaptic proteins in a controlled native like environment without the overwhelming complexity of the synapse. In particular, the large size of a *Xenopus oocyte* (1 mm) makes it particularly advantageous as a vessel for the expression of synaptic proteins such as ligand-gated ion channels. The size affords relative ease both in terms of (1) the delivery of the genetic material that encodes the synaptic protein and (2) characterizing the behavior of the expressed protein. When the expressed protein is an ion channel, electrophysiology provides a sensitive assay that is a direct measure of function. In the synapse, the creation of an electrical current by the flow of ions through the ion channel (Figure 1.2A) allows for the further propagation of the signal in synaptic transmission. In the case of a heterologously expressed ion channel, however, generated current provides a convenient and extremely sensitive readout of function.

Receptor function can be assayed at the whole-cell level, using the response of all the ion channels being expressed in the cell membrane, or on the single-channel level, looking at a single channel opening and closing. For whole-cell characterization, the aggregate passage of ions through the expressed ion channels produces a cell current measurable by two-electrode voltage clamp.[20, 21] When the concentration of agonist increases, the net current also increases as more receptors are in an active ion-conducting state (Figure 1.2B). Thus, a range of agonist concentrations is used to construct a dose-response relationship for the ion channel (Figure 1.2C). This is, in turn, fitted to the Hill equation to give the EC_{50}, or effective concentration at half maximum response, which is a convenient metric for assessing ion channel function. A loss

of ion channel function is marked by an increase in the whole-cell EC_{50}, where higher concentrations of agonist are necessary to evoke the same response (Figure 1.2C, green curve). Conversely, if the ion channel opens in response to lower concentrations of agonist (gain-of-function), this would be reflected by a lower EC_{50} value (Figure 1.2C, blue curve).

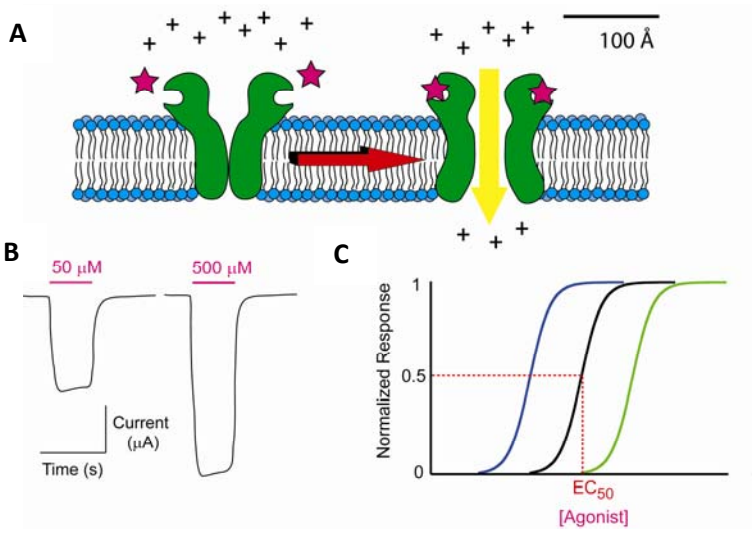

Figure 1.2: Basics of an electrophysiology assay. A) Agonist (pink stars) binding to the ion channel promotes channel opening. Once open, the channel allows the passage of ions across an otherwise impermeable membrane, producing a measurable current. B) Examples of current response to varying agonist concentrations. C) Example dose-response curves. The black curve represents the dose-response relation of an unmodified (wild-type) receptor. The blue and green curves show shifts in this relationship in response to gain-of-function and loss -of-function mutations, respectively.

The goal of taking the ion channels out of the synapse is to characterize their structure and function, which can be accomplished using conventional site-directed mutagenesis. Replacing a single amino acid residue with one of the other 20 canonical amino acids can A) provide a sense of the importance of a particular residue and B) provide clues as to the role of that amino acid in overall protein function. However, the structural variation available in the 20 natural amino acids is neither broad nor systematic enough to enable an in depth, chemical-scale understanding of protein structure and function. For instance, if we wish to understand the role of a glutamate residue in a protein- its participation in hydrogen bonding, for example- we could conventionally mutate to an alanine residue to completely remove the side chain

functionality. A less dramatic mutation would involve replacing the carboxylate of glutamate with an amide (e.g., glutamine). However, this alters both the hydrogen bonding ability and the steric properties of the side chain (Figure 1.3). Interpreting changes in function is thus complicated by effects that are secondary to the question at hand. If we want to understand the role of charge, a nitro functionality (nitrohomoalanine, in this case) would provide a sterically similar, but charge-neutral alternative to the carboxylate of glutamate. Of course, the nitro functionality is absent among the natural amino acids.

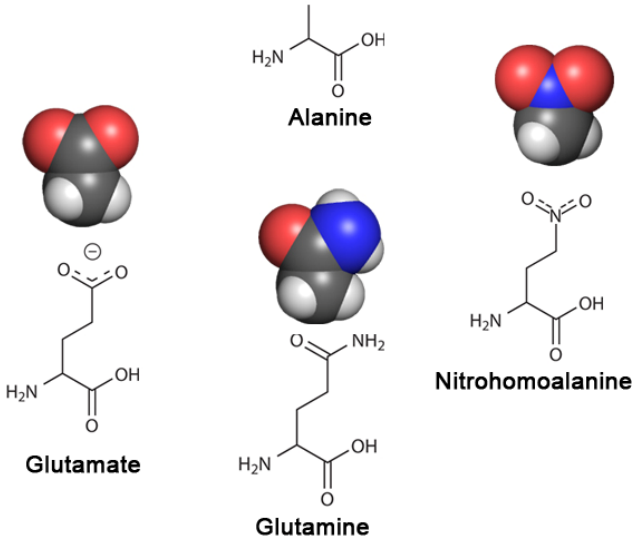

Figure 1.3: Natural and unnatural amino acids for testing the function of the glutamate side chain.

In addition to the limited chemical functionality of the twenty natural amino acids, some structural modifications, such as altering the peptide backbone, are impossible using conventional mutagenesis. Unnatural amino acid mutagenesis allows us to move past these limitations and achieve the precise control over structural variation that we desire.

1.4 Unnatural Amino Acid Incorporation

The nonsense suppression methodology was developed in the late 1980s to allow researchers to site specifically incorporate unnatural amino acids.[22-24] In normal protein synthesis, the ribosome decodes messenger RNA by matching set three-nucleotide codes, or codons, with the anticodon region of a tRNA molecule bearing the specified amino acid. The nonsense suppression method borrows one of the cell's stop codons (typically UAG or UGA) to

serve as the codon for the unnatural amino acid. An orthogonal suppressor tRNA with a complementary anticodon that recognizes the stop codon bears the desired unnatural amino acid. The result is that instead of terminating at the appropriated stop codon, the ribosome incorporates the unnatural amino acid into the growing polypeptide chain (Figure 1.4).

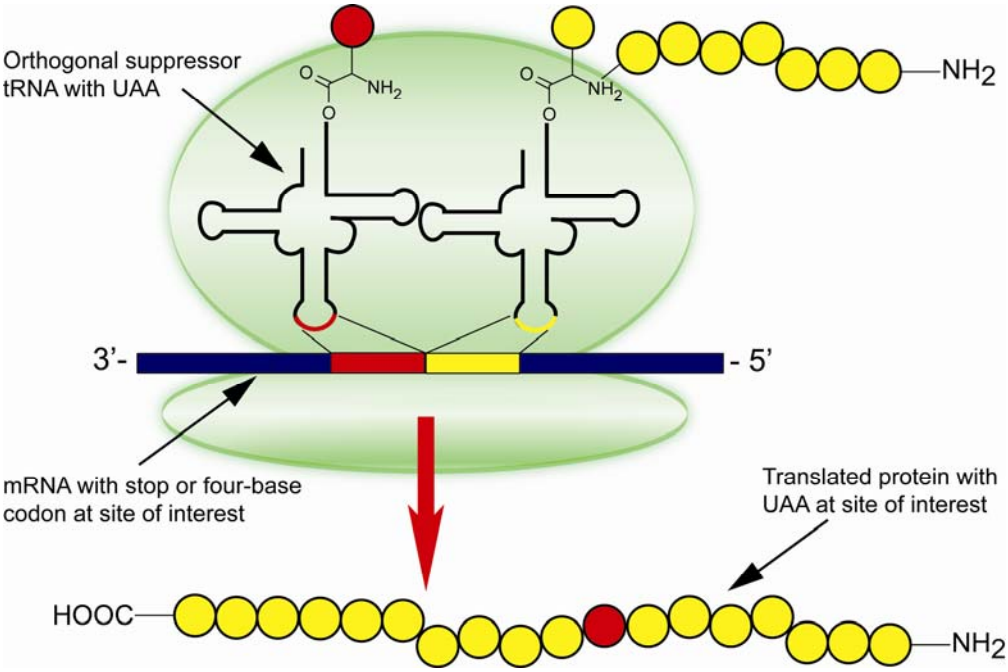

Figure 1.4: Overview of unnatural amino acid incorporation using the nonsense and frameshift suppression methodologies.

A related, alternative method for unnatural amino acid incorporation uses a four-base codon instead of a stop codon.[25, 26] This method uses a suppressor tRNA with a matching four-base anticodon to incorporate the unnatural amino acid and suppress the shift in reading frame that would normally occur when the ribosome encounters a four-base codon. Appropriately, this method is known as frameshift suppression.

Both methods require the same basic combinations of simple molecular biology and chemical synthesis (Figure 1.5).[27-29] Using standard mutagenesis protocols, the gene for the target protein is mutated to contain a stop or four-base codon at the site of interest and

subsequently used to transcribe the mRNA transcript. The suppressor tRNA lacking the final two nucleotides of the acceptor stem (C and A) is likewise transcribed in vitro. These final nucleotides of the acceptor stem are used as a handle for the unnatural amino acid, both of which are chemically synthesized separately before being chemically joined. Once prepared, the dCA-amino acid is ligated onto the truncated tRNA body using the T4 RNA ligase. Injecting the prepared mRNA and tRNA into the *Xenopus oocyte* provides the necessary genetic material for the cellular machinery to translate, process, and transport the target protein to the cell membrane. An incubation period of 18- 48 hours is required for this process, after which the impact of the unnatural amino acid at the site of interest can be assayed.

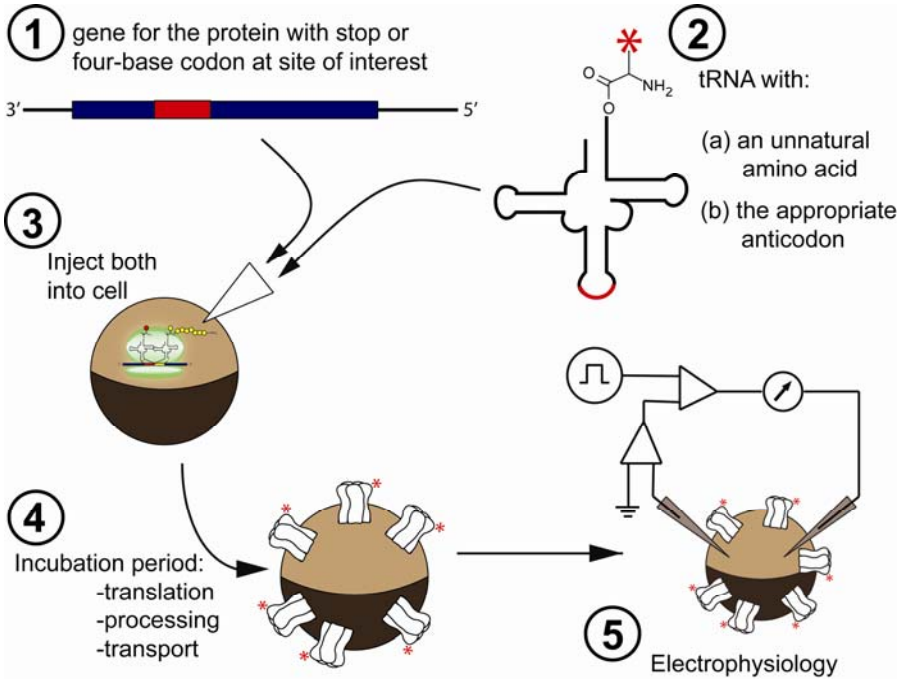

Figure 1.5: Implementation of the nonsense or frameshift methodologies for incorporating unnatural amino acids into ion channels in *Xenopus laevis* oocytes.

Control experiments are simultaneously performed to ensure the fidelity of unnatural amino acid incorporation. Injecting mRNA alone tests for readthrough of the stop or four-base codon by the ribosome. The impact of misacylation, a process in which the cell's synthetases

append a natural amino acid onto the exogenous tRNA body, can be controlled for by injecting the mRNA along with suppressor tRNA with no amino acid appended to the acceptor stem. Both readthrough and misacylation can lead to a heterogeneous population of proteins, obscuring the impact of the unnatural amino acid at the site of interest. Finally, wild-type recovery experiments, in which the natural amino acid is appended to the suppressor tRNA, ensure that normal protein function can be recovered using the nonsense or frameshift suppression methodology.

1.5 α-Hydroxy Acid Incorporation for Probing the Peptide Backbone

The power of unnatural amino acid mutagenesis is that it allows us to ask, and answer, otherwise inaccessible questions about protein structure and function. One prime example of this is the ability to modify the peptide backbone by incorporating unnatural α-hydroxy acids. Upon incorporation, α-hydroxy acids confer backbone flexibility by removing the amide bond rigidity and disrupting the hydrogen binding ability of a residue. Hydrogen bonding ability is critical for secondary protein structure, as it is a key component of both α-helices and β-sheets (Figure 1.6). In addition, individual backbone-to-side chain and backbone-to-backbone hydrogen bonds can play a significant role in modulating protein function.

By replacing an amino acid with an α-hydroxy acid, the critical NH is replaced by an oxygen, thus eliminating the ability of the residue to act as a hydrogen bond donor. This mutation also diminishes the ability of the neighboring carbonyl to act as a hydrogen bond acceptor, as the carbonyl of an ester is a weaker hydrogen bond acceptor than that of an amide. This mutation also potentially introduces unfavorable electrostatic interactions between the ester oxygen and the amide carbonyl (Figure 1.6). Overall, however, the amino-to-hydroxy acid

mutation is subtle, maintaining the original side chain properties and the amide backbone conformational properties (i.e., bond lengths, angles, cis/trans preferences).

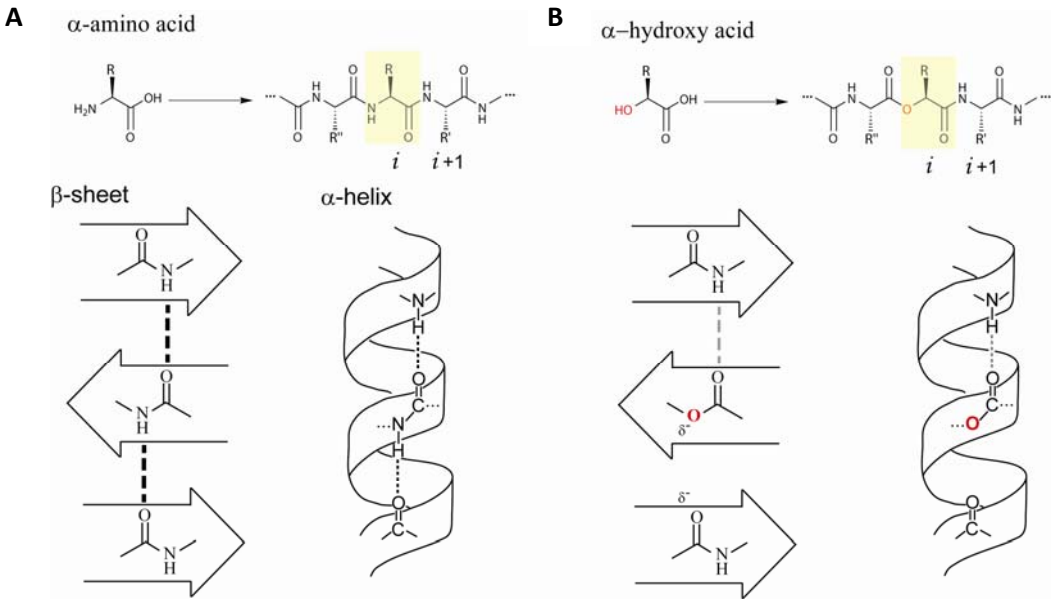

Figure 1.6: Amide-to-ester mutations. A) Normal α-amino acid incorporation in a polypeptide and its hydrogen bonding patterns in β-sheets and α-helices. B) The impact of α-hydroxy incorporation on hydrogen bonding in α-helices and β-sheets.

1.6 Dissertation Research

This dissertation describes one *in silico* and three experimental studies that consider the impact of ester backbone mutations in the extracellular domain of the muscle nAChR. One additional chapter describes a method for using whole-cell data to more fully characterize the functional impact of a mutation.

Chapter 2 describes the discovery of a specific intersubunit hydrogen bond between the backbone of a residue in the C-loop and the side chain in the complementary binding subunit. This resolved the role of a conserved asparagine residue originally thought to directly participate in agonist binding. In chapter 3, the role of the peptide backbone is considered more broadly in

the context of the outer β-sheet that connects the agonist binding site to the transmembrane domain. We determined that single α-hydroxy mutations were well tolerated in this region, causing only minor functional perturbations. However, the presence of two nearby backbone esters was extremely detrimental to receptor function. Chapter 4 discusses the ELFCAR methodology for using readily obtainable whole-cell data to determine whether a particular mutation impacts channel gating. This method is particularly useful for elucidating gating function in residues that are physically removed from the channel gate, such as those in and around the binding site. Chapter 5 discusses the impact of amide-to-ester mutations in the agonist binding box. Finally, chapter 6 discusses the complementary use of molecular dynamics to understand the effect of α-hydroxy acid incorporation.

1.7 References:

1. Green, T., Heinemann, S.F. & Gusella, J.F. Molecular neurobiology and genetics: investigation of neural function and dysfunction. *Neuron* **20**, 427-44 (1998).
2. Ramón y Cajal, S., Pasik, P. & Pasik, T. v. <1, 3 > (Springer, Wien ; New York, 1999).
3. Miller, P.S. & Smart, T.G. Binding, activation and modulation of Cys-loop receptors. *Trends Pharmacol Sci*.
4. Dougherty, D.A. Cys-loop neuroreceptors: structure to the rescue? *Chem Rev* **108**, 1642-53 (2008).
5. Sine, S.M. & Engel, A.G. Recent advances in Cys-loop receptor structure and function. *Nature* **440**, 448-55 (2006).
6. Eldefrawi, M.E. & Eldefrawi, A.T. Characterization and partial purification of the acetylcholine receptor from Torpedo electroplax. *Proc Natl Acad Sci U S A* **69**, 1776-80 (1972).
7. Taly, A., Corringer, P.J., Guedin, D., Lestage, P. & Changeux, J.P. Nicotinic receptors: allosteric transitions and therapeutic targets in the nervous system. *Nat Rev Drug Discov* **8**, 733-50 (2009).
8. Zhong, W. et al. From ab initio quantum mechanics to molecular neurobiology: a cation-pi binding site in the nicotinic receptor. *Proc Natl Acad Sci U S A* **95**, 12088-93 (1998).
9. Celie, P.H. et al. Crystal structure of acetylcholine-binding protein from Bulinus truncatus reveals the conserved structural scaffold and sites of variation in nicotinic acetylcholine receptors. *J Biol Chem* **280**, 26457-66 (2005).
10. Hansen, S.B. et al. Structures of Aplysia AChBP complexes with nicotinic agonists and antagonists reveal distinctive binding interfaces and conformations. *EMBO J* **24**, 3635-46 (2005).
11. Rucktooa, P., Smit, A.B. & Sixma, T.K. Insight in nAChR subtype selectivity from AChBP crystal structures. *Biochem Pharmacol* **78**, 777-87 (2009).
12. Williams, D.K., Stokes, C., Horenstein, N.A. & Papke, R.L. Differential regulation of receptor activation and agonist selectivity by highly conserved tryptophans in the nicotinic acetylcholine receptor binding site. *J Pharmacol Exp Ther* **330**, 40-53 (2009).
13. Gao, F. et al. Solution NMR of acetylcholine binding protein reveals agonist-mediated conformational change of the C-loop. *Mol Pharmacol* **70**, 1230-5 (2006).
14. Mukhtasimova, N., Lee, W.Y., Wang, H.L. & Sine, S.M. Detection and trapping of intermediate states priming nicotinic receptor channel opening. *Nature* **459**, 451-4 (2009).
15. Shi, J., Koeppe, J.R., Komives, E.A. & Taylor, P. Ligand-induced conformational changes in the acetylcholine-binding protein analyzed by hydrogen-deuterium exchange mass spectrometry. *J Biol Chem* **281**, 12170-7 (2006).
16. Unwin, N. Refined structure of the nicotinic acetylcholine receptor at 4A resolution. *J Mol Biol* **346**, 967-89 (2005).
17. Miller, C. Genetic manipulation of ion channels: a new approach to structure and mechanism. *Neuron* **2**, 1195-205 (1989).
18. Filatov, G.N. & White, M.M. The role of conserved leucines in the M2 domain of the acetylcholine receptor in channel gating. *Mol Pharmacol* **48**, 379-84 (1995).
19. Labarca, C. et al. Channel gating governed symmetrically by conserved leucine residues in the M2 domain of nicotinic receptors. *Nature* **376**, 514-6 (1995).

20. Hodgkin, A.L. & Huxley, A.F. A quantitative description of membrane current and its application to conduction and excitation in nerve. *J Physiol* **117**, 500-44 (1952).
21. Hodgkin, A.L. & Huxley, A.F. Movement of sodium and potassium ions during nervous activity. *Cold Spring Harb Symp Quant Biol* **17**, 43-52 (1952).
22. Bain, J.D. et al. Site-specific incorporation of nonnatural residues during in vitro protein biosynthesis with semisynthetic aminoacyl-tRNAs. *Biochemistry* **30**, 5411-21 (1991).
23. Ellman, J., Mendel, D., Anthony-Cahill, S., Noren, C.J. & Schultz, P.G. Biosynthetic method for introducing unnatural amino acids site-specifically into proteins. *Methods Enzymol* **202**, 301-36 (1991).
24. Noren, C.J., Anthony-Cahill, S.J., Griffith, M.C. & Schultz, P.G. A general method for site-specific incorporation of unnatural amino acids into proteins. *Science* **244**, 182-8 (1989).
25. Hohsaka, T., Ashizuka, Y., Taira, H., Murakami, H. & Sisido, M. Incorporation of nonnatural amino acids into proteins by using various four-base codons in an Escherichia coli in vitro translation system. *Biochemistry* **40**, 11060-4 (2001).
26. Rodriguez, E.A., Lester, H.A. & Dougherty, D.A. In vivo incorporation of multiple unnatural amino acids through nonsense and frameshift suppression. *Proc Natl Acad Sci U S A* **103**, 8650-5 (2006).
27. Dougherty, D.A. Physical organic chemistry on the brain. *J Org Chem* **73**, 3667-73 (2008).
28. Nowak, M.W. et al. In vivo incorporation of unnatural amino acids into ion channels in Xenopus oocyte expression system. *Methods Enzymol* **293**, 504-29 (1998).
29. Nowak, M.W. et al. Nicotinic receptor binding site probed with unnatural amino acid incorporation in intact cells. *Science* **268**, 439-42 (1995).

Chapter 2: An Intersubunit Hydrogen Bond in the Nicotinic Acetylcholine Receptor that Contributes to Channel Gating

This research was originally published in Journal of Biological Chemistry. Kristin Rule Gleitsman, Sean M. A. Kedrowski, Henry A. Lester, Dennis A. Dougherty J. Biol. Chem. **2008**, *283*, 35638-35643.

2.1 Abstract

The muscle nicotinic acetylcholine receptor (nAChR) is a large, allosteric, ligand-gated ion channel with the subunit composition $\alpha_2\beta\gamma\delta$. Though much is now known about the structure of the binding site, relatively little is understood about how the binding event is communicated to the channel gate, causing the pore to open. Here we identify a key hydrogen bond near the binding site that is involved in the gating pathway. Using mutant cycle analysis with the novel unnatural residue α-hydroxyserine (Sah), we find that the backbone N-H of αS191 in loop C makes a hydrogen bond to an anionic side chain of the complementary subunit upon agonist binding. However, the anionic partner is not the glutamate predicted by the crystal structures of the homologous acetylcholine binding protein (AChBP). Instead, the hydrogen bonding partner is the extensively researched aspartate γD174/δD180—which had originally been identified as a key binding residue for cationic agonists.

2.2 Introduction

The Cys-loop family of ligand-gated ion channels is involved in mediating fast synaptic transmission throughout the central and peripheral nervous systems{Corringer, 2000 #8; Grutter, 2001 #10; Karlin, 2002 #11}. These neuroreceptors are among the molecules of learning, memory, and sensory perception, and they are implicated in numerous neurological disorders, including Alzheimer's disease, Parkinson's disease, and schizophrenia. The muscle nicotinic acetylcholine receptor (nAChR) is arguably the best-studied member of the Cys-loop family. This heteropentameric receptor is composed of homologous, but functionally distinct, subunits

arranged symmetrically around a central ion-conducting pore with the stoichiometry $\alpha_2\beta\gamma\delta$. The agonist binding sites are located at the interfaces between the αγ and αδ subunits. The binding of two agonist molecules induces a conformational change that leads to the opening of the ion channel.

It is now widely appreciated that a tryptophan residue (αW149) plays a key role in neurotransmitter binding by forming a cation-π interaction with the quaternary ammonium group of acetylcholine{Zhong, 1998 #15}, a result supported by structural data. However, many other important residues in the immediate vicinity of the binding site have been identified. In a classic experiment on the *Torpedo* nAChR (a close homologue of the muscle subtype), Czajkowski and Karlin concluded that a key aspartate (γD174/δD180) from the complementary binding subunit could come within 9 Å of the agonist binding site{Czajkowski, 1991 #1}. Mutation of this residue severely impacted receptor function, leading to a proposal that the negative charge of this aspartate interacted with the positive charge of the agonist{Czajkowski, 1995 #2; Czajkowski, 1993 #3}. Subsequently, however, both the crystal structure of acetylcholine-binding protein (AChBP, a soluble protein homologous to the extracellular domain of the nAChR){Brejc, 2001 #16} and the 4 Å cryo-EM structure of *Torpedo* nAChR{Miyazawa, 1999 #12; Unwin, 2005 #36} showed that this residue is positioned quite far from the agonist binding site (Figure 2.1). Single-channel studies suggest that this residue is primarily important for ligand-induced channel gating rather than agonist binding{Akk, 1999 #14; Sine, 2002 #13}.

γD174/δD180 is part of loop F, the most remote of the six loops originally proposed by Changeux to contribute to the agonist binding site{Corringer, 2000 #8}. In the carbamylcholine-bound AChBP structure{Sixma, 2003 #32}, a different F loop anionic residue, γE176/δE182 (AChBP E163), is positioned near loop C of the agonist binding site (Figure 2.1). Specifically,

γE176/δE182 is within hydrogen bonding distance of the backbone N-H at αS191, which is located on the C loop between the aromatic binding box residue αY190 and the vicinal disulfide formed by αC192 and αC193. Loop F is generally disordered in the AChBP and nAChR structures, and hydrogen-deuterium exchange mass spectrometry on AChBP reveals that loop F and loop C are the most conformationally dynamic segments of the protein{Shi, 2006 #6}. It is generally accepted that agonist binding draws loop C inward, capping the aromatic binding pocket{Hansen, 2005 #7; Sixma, 2003 #32}. In contrast, crystal structures of AChBP with antagonists bound reveal loop C pulled away from the agonist binding site{Hansen, 2005 #7}. Distinctions between antagonist- and agonist-induced motion have also been observed in loop F{Hibbs, 2006 #33}. As such, many investigators favor a gating model involving a contraction of the agonist binding site around an agonist molecule that is largely mediated by movements in loops C and F, though little is known about the nature of the specific interactions involved in this systolic motion.

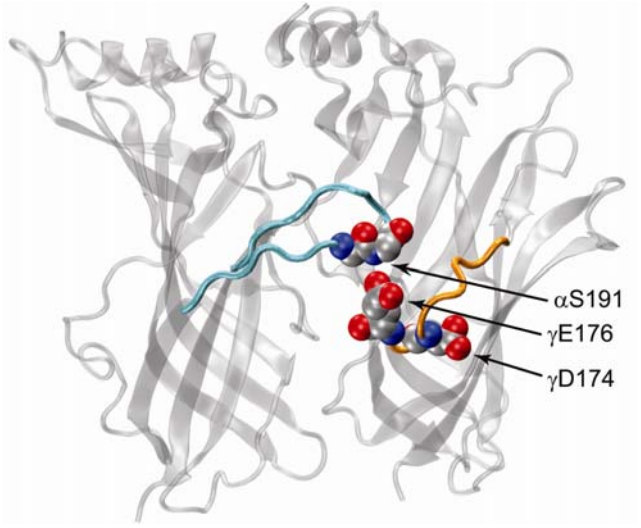

Figure 2.1. Structure of AChBP with carbamylcholine bound (pdb: 1UV6); numbering as in nAChR. Residues considered here are shown in space-filling. The C loop (cyan) and F loop (orange) are highlighted. In this structure, the C and F loops have closed around the bound agonist (agonist not shown). A carboxylate oxygen (red) of γE176 is within hydrogen bonding distance of the backbone NH (blue) of αS191.

In the present work we evaluate several anionic residues in loop F and potential interactions with loop C. Using a combination of natural and unnatural mutagenesis, we find that, indeed, the backbone N-H of αS191 does make a hydrogen bond to a loop F residue.

However, the partner is not the glutamate seen in the AChBP crystal structure. Instead, the aspartate (γD174/δD180) originally identified by Czajkowski and Karlin is the hydrogen bonding partner.

2.3 Results

A Backbone Mutation at αS191 Has a Large Impact on Receptor Function

In the process of probing the backbone flexibility surrounding the nAChR binding box, we mutated αS191 to α-hydroxyserine (Sah). This produces an ester backbone linkage at this position, while preserving the side chain. Along with increasing backbone flexibility, this mutation removes the hydrogen bond-donating N-H group and replaces it with a non-hydrogen bond-donating O (Figure 2.2, 2.3). We have performed similar backbone mutations at several positions throughout the nAChR, and typically the consequences are not dramatic{England, 1999 #31; Cashin, 2007 #17}. However, at αS191, this subtle mutation leads to a 40-fold increase in EC_{50} (Table 2.1 & Figure 2.2b). We also made alanine and α-hydroxyalanine (Aah) mutations at this site. The side chain mutation alone had minimal impact on receptor function, producing no shift in EC_{50}. However, receptor function of the αS191Aah mutant was dramatically impaired relative to αS191Ala, confirming that the backbone—and not the side chain—at αS191 is important for receptor function.

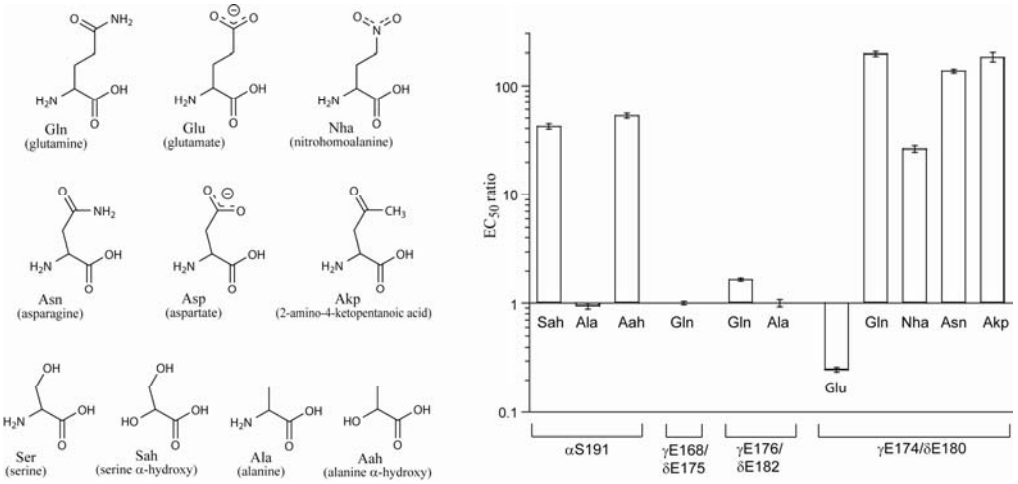

Figure 2.2 (A) Natural and unnatural residues used in this study. (B) EC_{50} ratios (mutant/wild type) for natural and unnatural substitutions at four sites in the extracellular domain. For glutamine and Nha, EC_{50} ratios were calculated with reference to glutamate instead of wild type (aspartate).

Mutant	EC_{50} (μM)	Double Mutant	EC_{50} (μM)	ΔΔG (kcal/mol)
αβγδ	1.2 ± 0.04			
αS191βγδ Sah	50 ± 2.3			
αβγE176AδE182A	1.2 ± 0.08	αS191SahβγE176AδE182A	32 ± 1.7	0.27 ± 0.06
αβγE176QδE182Q	2.0 ± 0.10	αS191SahβγE176QδE182Q	51 ± 2.4	0.29 ± 0.03
αβγE168QδE175Q	1.2 ± 0.02	αS191SahβγE168QδE175Q	37 ± 1.2	0.18 ± 0.05
αβγD174EδD180E	0.3 ± 0.01	αS191SahβγD174EδD180E	15 ± 0.90	0.12 ± 0.05
αβγD174QδD180Q	59 ± 2.0	αS191SahβγD174QδD180Q	96 ± 5.2	1.9 ± 0.05
αβγD174NhaδD180Nha	7.9 ± 0.40	αS191SahβγD174NhaδD180Nha	31 ± 1.9	1.4 ± 0.05
αβγD174NδD180N	160 ± 2.7	αS191SahβγD174NδD180N	190 ± 12	2.1 ± 0.05
αβγD174AkpδD180Akp	220 ± 19	αS191SahβγD174AkpδD180Akp	190 ± 12	2.3 ± 0.15
αS191βγδ Ala	1.1 ± 0.06	αS191AlaβγD174NδD180N	230 ± 8.0	0.25 ± 0.04
αS191βγδ Aah	63 ± 2.4	αS191AahβγD174NδD180N	130 ± 7.6	2.5 ± 0.04

Table 2.1. EC_{50} values ± the standard error of the mean for mutations made in this study. In all cases the β-subunit contains a L9'S mutation.

Evaluating anionic residues on loop F

To evaluate the potential hydrogen bond from αS191 to γE176/δE182, we made several mutations at this glutamate. Surprisingly, all mutations have minimal impact, suggesting no critical role for this residue. Another nearby loop F glutamate residue, γE169/δE175, was also evaluated. Again, no significant impact is seen.

In sharp contrast, even the subtlest mutations at γD174/δD180 produce large effects on receptor function, a result that others have also seen{Czajkowski, 1991 #1; Czajkowski, 1995 #2; Martin, 1996 #5; Martin, 1997 #4}. We first studied asparagine, glutamate and glutamine mutations at this site. The γD174E/δD180E mutant exhibits a modest ~3-fold decrease in EC_{50}. However, the γD174N/δD180N and γD174Q/δD180Q mutants produce substantial (>100-fold) changes to the EC_{50} (Figure 2.2b and Table 2.1).

Fundamentally, the results of these conventional mutations strongly implicate the side chain of γD174/δD180 in an electrostatic interaction, such as an ion pair or hydrogen bond. However, changing the side chain functionality from a carboxylate to an amide not only neutralizes the charge on the side chain, it also desymmetrizes it and introduces a potential hydrogen bond donor. To better understand the role of γD174/δD180, we incorporated two unnatural amino acids.

Nitrohomoalanine (Nha) is an analogue of glutamate that contains a nitro (NO_2) group, which is isosteric and isoelectronic to a carboxylate, but it has no charge and is a much weaker hydrogen bond acceptor (Figure 2.2a).[*] Incorporation of Nha at γD174/δD180 yields a slightly less dramatic effect than the γD174N/δD180N and γD174Q/δD180Q mutants, producing a 24-

[*] Although nitroalanine, the analogue of aspartate, would be ideal, it is not chemically compatible with the nonsense suppression methodology. Given that the mutation γD174E/δD180E produces a very modest EC_{50} shift and that γD174N/δD180N and γD174Q/δD180Q show similar effects on receptor function, the comparison of Nha to Glu can be considered meaningful.

fold shift in EC_{50} relative to γD174E/δD180E (Figure 2.2b). Thus, charge neutralization at this site significantly affects receptor function but cannot fully account for the EC_{50} shift seen in the γD174N/δD180N and γD174Q/δD180Q mutants.

The second unnatural amino acid analogue incorporated at γD174/δD180 was 2-amino-4-ketopentanoic acid (Akp). Akp is isoelectronic to Asp, but possesses a methyl ketone functionality in place of the carboxylate (Figure 2.2a). As such, Akp is a desymmetrized analogue of Asp—similar to Asn—but it has different electrostatic properties (less polar, weaker hydrogen bond acceptor, and cannot donate a hydrogen bond). When Akp is incorporated at γD174/δD180, its effect upon receptor function is roughly as deleterious as the Asn mutation (Figure 2.2b).

Mutations at individual binding sites (αβγD174Nδ and αβγδD180N) showed substantial (~50-fold) and approximately equivalent increases in whole cell EC_{50}.

Mutant cycle analysis reveals a strong interaction between the αS191 backbone and the side chain of γD174/δD180

Mutant cycle analysis was performed between several of the side chain mutations at γD174/δD180 and the αS191Sah mutation (Figure 2.3, 2.4). Briefly, mutant cycle analysis is used to determine the pairwise interaction energy between two residues in a protein using the equation given in Figure 2.3. If the two residues do not interact, the change in free energy for the simultaneous mutation of both residues should simply be the sum of the free energy of each of the individual mutations. However, for residues that interact, the change in free energy for the double mutation will be non-additive. EC_{50}-based mutant cycle analysis has been used to

investigate interactions in Cys-loop receptors by other researchers{Kash, 2003 #18; Price, 2007 #19; Venkatachalan, 2008 #20}.

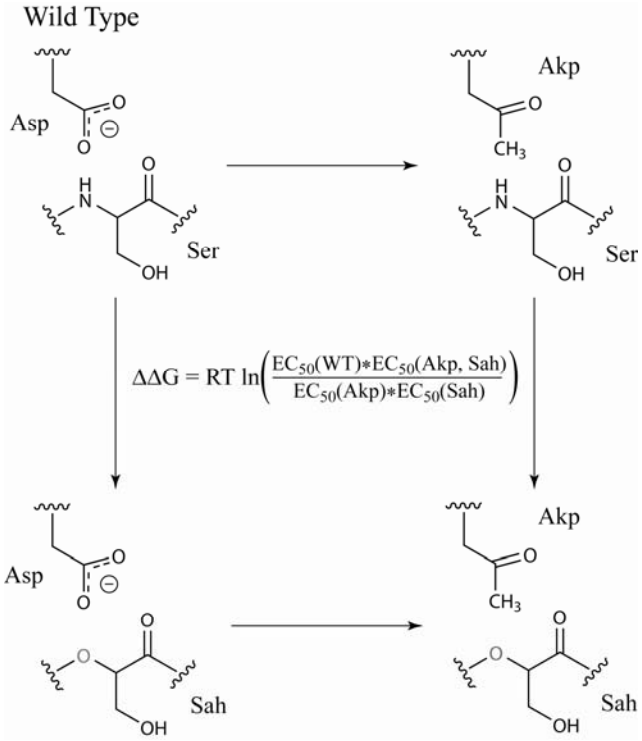

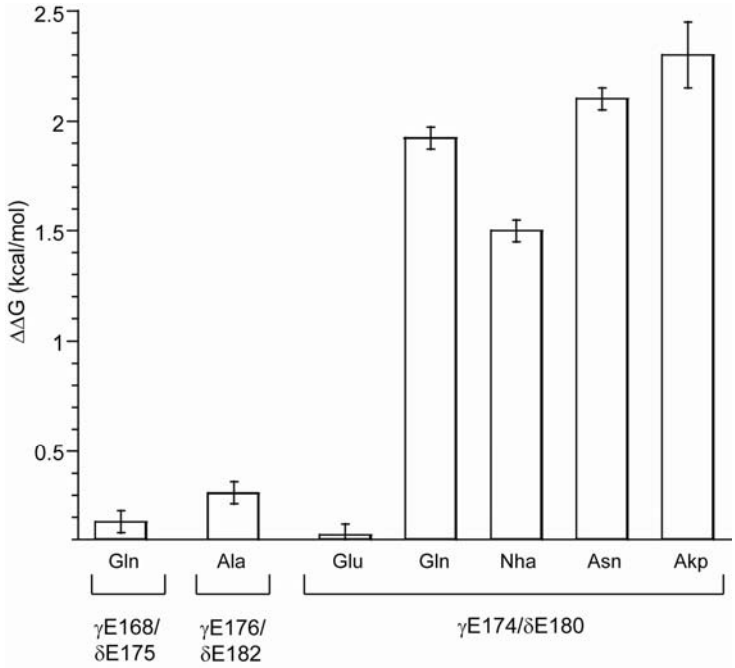

Figure 2.4: Coupling energies between various side chain mutants in the complementary binding subunit and the backbone mutation at αS191 (αS191Sah). For glutamine and Nha, free energy calculations were made with reference to glutamate instead of wild type (aspartate).

Lengthening the side chain (γD174E/δD180E) has no impact on the interaction between these two residues (ΔΔG = 0.12 kcal/mol). In contrast, mutant cycle analysis between γD174N/δD180N and αS191Sah indicates a large energetic coupling (ΔΔG = 2.1 kcal/mol). A smaller but still quite significant effect is seen for the mutant cycle analysis between γD174Nha/δD180Nha and αS191Sah (ΔΔG = 1.4 kcal/mol). Mutant cycle analyses of γD174N/δD180N with αS191A and αS191Aah further support the conclusion that the interaction between these residues involves the backbone of αS191 and not the side chain (αS191Ala: ΔΔG = 0.25; αS191Aah: ΔΔG = 2.3 kcal/mol). Not surprisingly, comparable mutant cycle analyses of the two glutamates of loop F, γE176/δE182 and γE169/δE175, with αS191Sah showed no significant coupling.

2.4 Discussion

The AChBP crystal structures transformed the study of nAChRs by providing high resolution structural data about the ligand binding domain of these proteins. In addition to refining our existing structural knowledge of the receptor—obtained from decades of careful biochemical research—it served as a valuable starting point for new structure-function studies on the receptor. However, AChBP is not a ligand-gated ion channel and, in fact, shares less than 25% homology with its nearest Cys-loop relative, the α7 nAChR{Brejc, 2001 #16}. As such, some fundamental structural differences must exist between AChBP and actual Cys-loop receptors, particularly pertaining to residues involved in mediating communication between the binding site and the ion channel pore.

Arguably the biggest discrepancy between the AChBP structures and prior biochemical studies of the nAChR concerns the loop F residue γD174/δD180. A remarkable cross-linking study in the *Torpedo* nAChR indicated that this residue can come within 9 Å of the vicinal

disulfide on the C loop, located at the heart of the agonist binding site{Czajkowski, 1991 #1}. Yet, in AChBP the residue that aligns with γD174/δD180 is not at all near the agonist binding site. In addition, the cryo-EM structure of the *Torpedo* nAChR, which is believed to be in the desensitized or closed state, places this residue tucked deeply inside a β-sheet-lined hydrophobic pocket, over 15 Å from loop C{Miyazawa, 1999 #12; Unwin, 2005 #36}.

While γD174/δD180 is remote to the agonist binding site in AChBP, another loop F anionic residue, γE176/δE182, appears to make a hydrogen bond to a backbone N-H that is integral to the aromatic box of the agonist binding site when the agonist carbamylcholine is bound. Using nonsense suppression methodology, we have been able to specifically remove the backbone N-H in question by replacing αS191 with its α-hydroxy analogue. Consistent with the AChBP images, this subtle structural change has a large effect on receptor function, suggesting that a hydrogen bond to this moiety is important. However, consistent with prior mutational analyses{Czajkowski, 1995 #2; Czajkowski, 1993 #3; Martin, 1996 #5}, we find that γE176/δE182 does not play a large role in receptor function. This suggests that AChBP does not provide an accurate model of the muscle nAChR in this region. Given that the sequence alignment in this region shows a number of insertions in nAChR relative to AChBP—combined with the fact that the F loop is believed to be involved in gating the nAChR (AChBP does not gate)—it is not surprising that AChBP would be an unreliable model here.

Our results indicate that the hydrogen-bonding partner for the backbone N-H of αS191 in the nAChR is instead the side chain of γD174/δD180. Based on the available structural and functional data, we suggest that this hydrogen bond exists in the open state only{Akk, 1999 #14; Martin, 1996 #5; Martin, 1997 #4}. As others have seen, a number of mutations of this side chain profoundly affect receptor function. Here we employ several relatively subtle mutations.

The fact that substantial functional consequences are seen suggests a precise structural role for this side chain in at least one state crucial for activating the channel. Furthermore, all mutations at γD174/δD180 that significantly impact function also show strong coupling to the αS191Sah backbone mutation via mutant cycle analysis. The nature of the coupling is as one would expect from the hydrogen bonding model: mutation at either site has a strong effect; however, once the αS191Sah mutation is introduced—removing any possible hydrogen bonding interaction—mutations at γD174/δD180 have a *much* smaller impact. Interestingly, no specific role for the side chain of αS191 is found, as the αS191A mutant gives essentially wild type behavior.[†] However, when the alanine side chain is combined with the α-hydroxy backbone mutation, the same coupling to γD174/δD180 is observed.

We propose that the movement of loop F of the complementary subunit from a position remote to the agonist binding site to one of close proximity to loop C of the principal subunit is a key early structural change associated with nAChR gating. Driving this structural reorganization is the formation of a hydrogen bond between the side chain of γD174/δD180 and the backbone N-H of αS191. In the closed state of the wild-type receptor, αS191 and the C loop project out into solution, away from the bulk of the receptor, while γD174/δD180 of the F loop projects deep within a hydrophobic cavity. Though the energetic desolvation penalty of burying a charged residue within a hydrophobic cavity is significant[‡], it alone is apparently not sufficient to overcome other structural elements that bias this conformation of the F loop. However, agonist binding induces a centripetal movement of the C loop, bringing the backbone N-H of αS191 in closer proximity to the F loop. This structural change makes possible a hydrogen bond between γD174/δD180 and the C loop backbone. We hypothesize that the formation of this hydrogen

[†] In AChBP structures, the αS191 side chain also makes hydrogen bonds toγE176/δE182.

[‡] Based on the hydrophobicity constant, π, the expected desolvation penalty for an aspartic acid residue would be on the order of 1 kcal/mol ({Eisenberg, 1986 #38}

bond, along with the energetic solvation benefit of moving γD174/δD180 into an aqueous environment, provides sufficient driving force to move γD174/δD180 out of its pocket, inducing a movement of the F loop toward the C loop.[§] This structural rearrangement of loop F contributes to the gating pathway. Using rate-equilibrium free energy relationships, Auerbach and coworkers have also concluded that γD174/δD180 moves early in the gating process{Grosman, 2000 #9}.

Our results provide an explanation for the cross-linking studies of Czajkowski and Karlin{Czajkowski, 1991 #1}, and they are not in conflict with available structural information. The cryo-EM images of the *Torpedo* receptor show greater than 20 Å separation between αS191 and γD174/δD180 in the closed state. Still, the distance of less than 9 Å that is suggested by the cross-linking studies is plausible, provided that the residues are free to move closer, as occurs in our model of channel gating. A comparison of AChBP structures with and without agonist bound likewise shows that motions of loops C and F are the dominant structural rearrangements that occur when agonist binds. The fact that the hydrogen bond acceptor in loop F differs between AChBP and nAChR is not surprising, given that loop F is strongly implicated in nAChR gating and AChBP did not evolve to have a gating function.

This model is also consistent with the γD174/δD180 mutants described here. Lengthening the sidechain of this key F loop residue (γD174E/δD180E) effects a modest improvement in receptor function, either because the longer side chain can more easily reach its αS191 hydrogen bonding partner, or because it fits more poorly in the hydrophobic pocket, destabilizing the closed state. Any mutation that eliminates side chain charge has a significant

[§] The possibility of a salt bridge forming here can be eliminated, given that there are no basic residues in the C loop or in its vicinity.

impact on function, which is expected, given that these mutant side chains are poorer hydrogen bond acceptors and that they experience a much lower energetic solvation benefit upon moving from the hydrophobic pocket into an aqueous environment.

In conclusion, mutant cycle analysis involving a novel backbone mutant has identified an important interaction between an F loop residue that has long been thought to contribute to receptor function and the peptide backbone of loop C. The hydrogen bond between the side chain of γD174/δD180 and the backbone of αS191 likely forms upon agonist binding and is part of the agonist-induced conformational changes that lead to channel opening. Along with contributing new insights into the gating pathway of the nAChR, our results reconcile a long-standing discrepancy between early biochemical studies of the receptor and structural models from the AChBP systems.

2.5 Materials and Methods

Preparation of Unnatural Amino and Hydroxy Acids

All chemical reactions were performed under argon using solvent-column dry solvents{Pangborn, 1996 #22}. Flasks and vials were oven dried at 122°C and cooled in a desiccator box containing anhydrous calcium sulfate. Silica chromatography was carried out in accordance with the methods of Still{Still, 1978 #23}. The preparations of Nha, Akp, and Aah have been described previously{Cashin, 2007 #17; England, 1999 #24; Mu, 2006 #34}.

Synthesis of 2,3-dihydroxypropionate (α-hydroxyserine, Sah)-tRNA

Glycerate, calcium salt dihydrate (286 mg, 2.0 mmol) was measured into a 100 mL round-bottomed flask. Methanol (40 mL) and toluene (10 mL) were added, followed by conc.

hydrochloric acid (1 mL, 12 mmol). The mixture was stirred under reflux for 6 h, at which point the solvent was removed *in vacuo*. This crude residue was then dissolved in dimethylfomamide (6 mL) in a 2-dram vial. *tert*-butyldimethylsilyl chloride (906 mg, 6 mmol) and Imidazole (544 mg, 8 mmol) were then added, and the reaction was stirred at room temperature for 12 h, at which point the reaction was concentrated *in vacuo* to ca. 1 mL, and dichloromethane (10 mL) was added. The precipitate was removed by filtration, and the filtrate was reduced *in vacuo* and purified by flash chromatography on silica (5% ethyl acetate in hexanes) to yield 421 mg (60% over 2 steps) 2,3-di-*tert*-butyldimethylsilyl-glycerate methyl ester. ^{1}H NMR (300 MHz, $CDCl_3$) δ 4.27 (dd, 1H, J = 5.2, 6.2 Hz), 3.80 (dd, 1H, J_{AB} = 9.9 Hz, J_{AX} = 5.2 Hz), 3.73 (dd, 1H, J_{AB} = 9.9 Hz, J_{AX} = 6.6 Hz), 3.70 (s, 3H), 0.88 (s, 9H), 0.85 (s, 9H), 0.07 (s, 3H), 0.05 (s, 3H), 0.03 (s, 3H), 0.02 (s, 3H). ^{13}C NMR (75 MHz, $CDCl_3$) δ 172.71, 74.21, 66.16, 51.99, 26.04, 25.94, 18.57, 18.52, -4.86, -4.87, -5.16, -5.25. LRMS (ES^+) calculated for [$C_{16}H_{36}NaO_4Si_2$] ([M+Na]$^+$) 371.2, found 371.1.

2,3-di-*tert*-butyldimethylsilylglycerate methyl ester (100 mg, 0.29 mmol) was measured into a 2-dram vial. Diethyl ether (3 mL) was added to dissolve the starting material, followed by potassium trimethylsilanolate{Laganis, 1984 #37} (40.7 mg, 0.29 mmol). After 18 h, the potassium salt was isolated by filtration, washed with 2 x 1 mL ether, and dried *in vacuo*. The solid was then resuspended in chloroacetonitrile (3 mL) and allowed to stir at room temperature for 6 h. The reaction was then filtered through a plug of silica to yield the pure product as a colorless liquid: 66.7 mg (62% over 2 steps) 2,3-di-*tert*-butyldimethylsilylglycerate cyanomethyl ester. ^{1}H NMR (300 MHz, $CDCl_3$) δ 4.75 (s, 2H), 4.35 (t, 1H, J = 5.4 Hz), 3.81 (d, 2H, J = 5.4 Hz), 0.90 (s, 9H), 0.87 (s, 9H), 0.10 (s, 3H), 0.08 (s, 3H), 0.06 (s, 3H), 0.05 (s, 3H). ^{13}C NMR (75 MHz, $CDCl_3$) δ 170.82, 114.24, 73.78, 65.92, 48.62, 26.01, 25.87, 18.48, -4.86, -4.90, -5.21, -5.24. HRMS (FAB^+) calculated for [$C_{17}H_{36}NO_4Si_2$] ([M+H]$^+$) 374.2183, found 374.2181.

The transesterification and deprotection of 2,3-di-*tert*-butyldimethylsilylglycerate cyanomethyl ester were performed according to published protocols to yield Sah-tRNA{Nowak, 1998 #35}.

Side chain and backbone mutagenesis

Conventional mutagenesis and unnatural mutagenesis, with the site of interest mutated to either an amber stop codon or a four base frameshift codon (at αS191), were achieved by a standard Stratagene QuikChange protocol. Sequencing through both strands confirmed the presence of the desired mutation. Mouse muscle embryonic nAChR in the pAMV vector was used. All the mutations were made in the presence of a background transmembrane mutation (βL9'S) that lowers whole-cell EC_{50} {Filatov, 1995 #30; Labarca, 1995 #29}. In addition, the α-subunits contain an HA epitope in the M3-M4 cytoplasmic loop for Western blot studies. Control experiments show that this epitope does not detectably alter EC_{50}. mRNA was prepared by in vitro runoff transcription using the Ambion (Austin, TX) T7 mMessage mMachine kit. For conventional mutants, a total of 2.0-4.0 ng of mRNA was injected in a ratio of 2:1:1:1 of α:β:γ:δ. For suppression with unnatural amino and hydroxy acids, a total of 4.0 ng of mRNA was injected in an α:β:γ:δ subunit ratio of 10:1:1:1. Typically, 25 ng of tRNA was injected per oocyte along with mRNA in a ratio of 1:1 with a total volume of 50 nL/cell. As a negative control for suppression, truncated 74-nucleotide tRNA or truncated tRNA ligated to dCA was co injected with mRNA in the same manner as fully charged tRNA. Data from experiments where currents from these negative controls were greater than 10% of the experimental were excluded. Frameshift suppression at αS191 was used for simultaneous incorporation of two unnatural residues{Rodriguez, 2006 #26}.

Electrophysiology

The function of mutant receptors was evaluated using two-electrode voltage clamp. Stage V-VI oocytes of *Xenopus laevis* were employed. Oocyte recordings were made 12-48 h postinjection in two-electrode voltage clamp mode using the OpusXpress 6000A instrument (Axon Instruments, Union City, CA). Oocytes were superfused with a Ca^{2+}-free ND96 solution at flow rates of 1 mL/min before application, 4 mL/min during drug application, and 3 mL/min during wash. Holding potential was -60 mV. Data were sampled at 125 Hz and filtered at 50 Hz. Drug applications were 15 s in duration. Acetylcholine chloride was purchased from Sigma/Aldrich/RBI. Solutions ranging from 0.01 to 5000 µM were prepared in Ca^{2+}-free ND96 from a 1 M stock solution. Dose-response data were obtained for a minimum of 8 concentrations of agonists and for a minimum of five cells. Dose-response relations were fitted to the Hill equation to determine EC_{50} and Hill coefficient values. The dose-response relations of individual oocytes were examined and used to determine outliers. The reported EC_{50} values are from the curve fit of the averaged data.

2.6 References

1. Corringer, P.J., Le Novere, N. & Changeux, J.P. Nicotinic receptors at the amino acid level. Annu Rev Pharmacol Toxicol **40**, 431-58 (2000).
2. Grutter, T. & Changeux, J.P. Nicotinic receptors in wonderland. Trends Biochem Sci **26**, 459-63 (2001).
3. Karlin, A. Emerging structure of the nicotinic acetylcholine receptors. Nat Rev Neurosci **3**, 102-14 (2002).
4. Zhong, W. et al. From ab initio quantum mechanics to molecular neurobiology: a cation-pi binding site in the nicotinic receptor. Proc Natl Acad Sci U S A **95**, 12088-93 (1998).
5. Czajkowski, C. & Karlin, A. Agonist binding site of Torpedo electric tissue nicotinic acetylcholine receptor. A negatively charged region of the delta subunit within 0.9 nm of the alpha subunit binding site disulfide. J Biol Chem **266**, 22603-12 (1991).
6. Czajkowski, C. & Karlin, A. Structure of the nicotinic receptor acetylcholine-binding site. Identification of acidic residues in the delta subunit within 0.9 nm of the 5 alpha subunit-binding. J Biol Chem **270**, 3160-4 (1995).
7. Czajkowski, C., Kaufmann, C. & Karlin, A. Negatively charged amino acid residues in the nicotinic receptor delta subunit that contribute to the binding of acetylcholine. Proc Natl Acad Sci U S A **90**, 6285-9 (1993).
8. Brejc, K. et al. Crystal structure of an ACh-binding protein reveals the ligand-binding domain of nicotinic receptors. Nature **411**, 269-76 (2001).
9. Miyazawa, A., Fujiyoshi, Y., Stowell, M. & Unwin, N. Nicotinic acetylcholine receptor at 4.6 A resolution: transverse tunnels in the channel wall. J Mol Biol **288**, 765-86 (1999).
10. Unwin, N. Refined structure of the nicotinic acetylcholine receptor at 4 angstrom resolution. Journal of Molecular Biology **346**, 967-989 (2005).
11. Akk, G., Zhou, M. & Auerbach, A. A mutational analysis of the acetylcholine receptor channel transmitter binding site. Biophys J **76**, 207-18 (1999).
12. Sine, S.M. et al. Naturally occurring mutations at the acetylcholine receptor binding site independently alter ACh binding and channel gating. J Gen Physiol **120**, 483-96 (2002).
13. Sixma, T.K. & Smit, A.B. Acetylcholine binding protein (AChBP): a secreted glial protein that provides a high-resolution model for the extracellular domain of pentameric ligand-gated ion channels. Annu Rev Biophys Biomol Struct **32**, 311-34 (2003).
14. Shi, J., Koeppe, J.R., Komives, E.A. & Taylor, P. Ligand-induced conformational changes in the acetylcholine-binding protein analyzed by hydrogen-deuterium exchange mass spectrometry. J Biol Chem **281**, 12170-7 (2006).
15. Hansen, S.B. et al. Structures of Aplysia AChBP complexes with nicotinic agonists and antagonists reveal distinctive binding interfaces and conformations. EMBO J **24**, 3635-46 (2005).
16. Hibbs, R.E., Radic, Z., Taylor, P. & Johnson, D.A. Influence of agonists and antagonists on the segmental motion of residues near the agonist binding pocket of the acetylcholine-binding protein. J Biol Chem **281**, 39708-18 (2006).
17. England, P.M., Zhang, Y., Dougherty, D.A. & Lester, H.A. Backbone mutations in transmembrane domains of a ligand-gated ion channel: implications for the mechanism of gating. Cell **96**, 89-98 (1999).
18. Cashin, A.L., Torrice, M.M., McMenimen, K.A., Lester, H.A. & Dougherty, D.A. Chemical-scale studies on the role of a conserved aspartate in preorganizing the agonist binding site of the nicotinic acetylcholine receptor. Biochemistry **46**, 630-9 (2007).

19. Martin, M., Czajkowski, C. & Karlin, A. The contributions of aspartyl residues in the acetylcholine receptor gamma and delta subunits to the binding of agonists and competitive antagonists. J Biol Chem **271**, 13497-503 (1996).
20. Martin, M.D. & Karlin, A. Functional effects on the acetylcholine receptor of multiple mutations of gamma Asp174 and delta Asp180. Biochemistry **36**, 10742-50 (1997).
21. Kash, T.L., Jenkins, A., Kelley, J.C., Trudell, J.R. & Harrison, N.L. Coupling of agonist binding to channel gating in the GABA(A) receptor. Nature **421**, 272-5 (2003).
22. Price, K.L., Millen, K.S. & Lummis, S.C. Transducing agonist binding to channel gating involves different interactions in 5-HT3 and GABAC receptors. J Biol Chem **282**, 25623-30 (2007).
23. Venkatachalan, S.P. & Czajkowski, C. A conserved salt bridge critical for GABAA receptor function and loop C dynamics. Proc Natl Acad Sci U S A (2008).
24. Eisenberg, D. & McLachlan, A.D. Solvation energy in protein folding and binding. Nature **319**, 199-203 (1986).
25. Grosman, C., Zhou, M. & Auerbach, A. Mapping the conformational wave of acetylcholine receptor channel gating. Nature **403**, 773-6 (2000).
26. Pangborn, A.B., Giardello, M.A., Grubbs, R.H., Rosen, R.K. & Timmers, F.J. Safe and convenient procedure for solvent purification. Organometallics **15**, 1518-1520 (1996).
27. Still, W.C., Kahn, M. & Mitra, A. Rapid Chromatographic Technique for Preparative Separations with Moderate Resolution. Journal of Organic Chemistry **43**, 2923-2925 (1978).
28. England, P.M., Lester, H.A. & Dougherty, D.A. Incorporation of esters into proteins: Improved synthesis of hydroxyacyl tRNAs. Tetrahedron Letters **40**, 6189-6192 (1999).
29. Mu, T. in Division of Chemistry and Chemical Engineering 126 (California Institute of Technology, Pasadena, 2006).
30. Laganis, E.D. & Chenard, B.L. METAL SILANOLATES - ORGANIC SOLUBLE EQUIVALENTS FOR O-2. Tetrahedron Letters **25**, 5831-5834 (1984).
31. Nowak, M.W. et al. In vivo incorporation of unnatural amino acids into ion channels in a Xenopus oocyte expression system. Methods Enzymol **293**, 504-529 (1998).
32. Filatov, G.N. & White, M.M. The role of conserved leucines in the M2 domain of the acetylcholine receptor in channel gating. Mol Pharmacol **48**, 379-84 (1995).
33. Labarca, C. et al. Channel gating governed symmetrically by conserved leucine residues in the M2 domain of nicotinic receptors. Nature **376**, 514-6 (1995).
34. Rodriguez, E.A., Lester, H.A. & Dougherty, D.A. In vivo incorporation of multiple unnatural amino acids through nonsense and frameshift suppression. Proc Natl Acad Sci U S A **103**, 8650-5 (2006).

Chapter 3: Probing the Role of Backbone Hydrogen Bonding in a Critical β-sheet of the Extracellular Domain of a Cys-loop Receptor

Reproduced with permission from Kristin Rule Gleitsman, Henry A. Lester, and Dennis A. Dougherty, ChemBioChem **2009**, *10*, 1385-91.

3.1 Abstract

Long-range communication is essential for the function of members of the Cys-loop family of neurotransmitter-gated ion channels. The involvement of the peptide backbone in binding-induced conformational changes that lead to channel gating in these membrane proteins is an interesting, but unresolved issue. To probe the role of the peptide backbone, we have incorporated a series of α-hydroxy acid analogues into the β-sheet rich extracellular domain of the muscle subtype of the nicotinic acetylcholine receptor, the prototypical Cys-loop receptor. Specifically, mutations were made in β-strands 7 and 10 of the α-subunit. A number of single backbone mutations in this region were well tolerated. However, simultaneous introduction of two proximal backbone mutations led to surface-expressed, non-functional receptors. Together, these data suggest that while the receptor is remarkably robust in its ability to tolerate single amide-to-ester mutations throughout these β-strands, more substantial perturbations to this region have a profound effect on the protein. These results support a model in which backbone movements in the outer β-sheet are important for receptor function

3.2 Introduction

An essential feature of allsoteric proteins is that they are innately dynamic molecules, with the Cys-loop superfamily of ligand-gated ion channels providing a classic example. These neurotransmitter receptors are involved in mediating fast synaptic transmission throughout the central and peripheral nervous systems.[1-5] They are among the molecules of learning, memory, and sensory perception, and they are implicated in numerous neurological disorders, including

Alzheimer's disease, Parkinson's disease, and schizophrenia. The muscle subtype of the nicotinic acetylcholine receptor (nAChR) is the prototypical Cys-loop receptor. It is a pentamer of homologous subunits arranged pseudo symmetrically around a central ion-conducting pore. The extracellular domain is largely comprised of β-sheet structure and contains the agonist binding site. The agonist binding site itself is shaped by discontinuous flexible loop regions that meet at the interface between subunits. The primary contributors to the agonist binding site are in the α subunit, with additional contributions from the complementary subunits (γ and δ). The transmembrane domain of each subunit is made up of four membrane-spanning α-helices, with one from each subunit lining the pore. Binding of a small molecule agonist in the extracellular domain triggers a series of conformational changes that leads to the opening of the channel gate some 60 Å away.

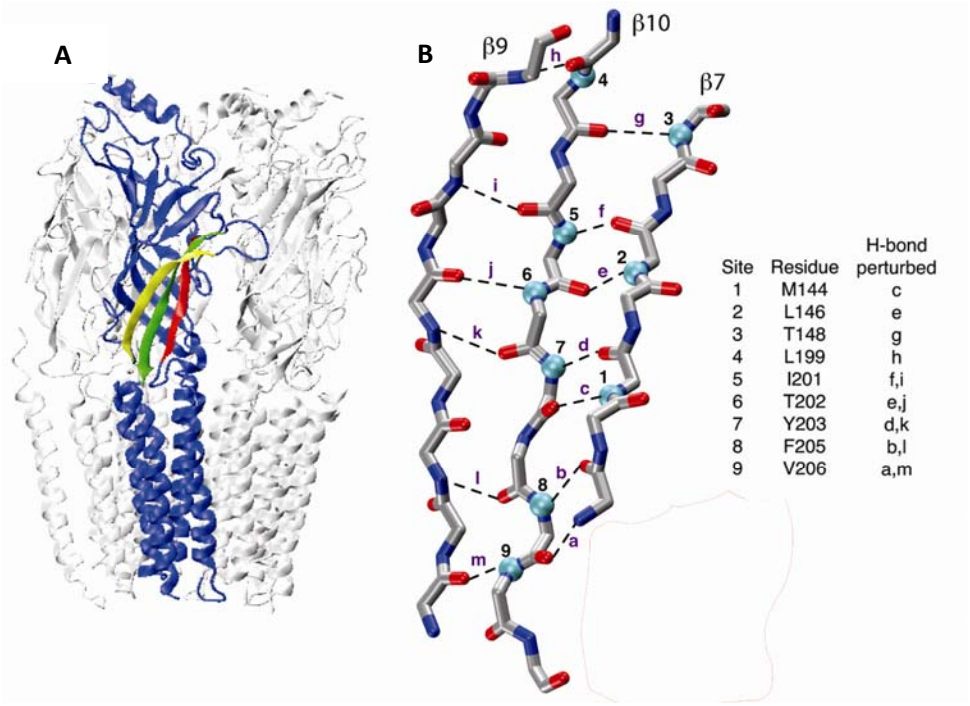

Figure 3.1: Two views of the nAChR. (A) Overall layout of the receptor. One of the five subunits is shown in blue, with α7, α9, and α10 highlighted in red, yellow, and green, respectively. (B) The hydrogen bonding network of the outer β-sheet of the nAChR. Turquoise balls indicate positions at which the backbone NH was mutated to an oxygen. The black dashed lines indicate hydrogen bonds that are completely removed or attenuated due as a result of mutation. Image is based cryo-EM of the full *Torpedo* receptor (2bg9).[6]

Long-range communication is clearly critical in the function of these receptors.[7, 8] Various models for how this communication occurs have been proposed, from specific side chain interactions to more rigid large-scale domain movements.[9-12] Recent linear free energy analysis of the nAChR has given rise to the notion of a "conformational wave"[9] that emanates from the agonist binding site to the gate of the channel in the transmembrane domain. It seems likely that some movement must occur in the immediate region of the binding interaction, with simple side chain movements comprising only a part of the ensuing conformational wave. Significant movements along the peptide backbone may also play a critical role in initiating channel gating.

To investigate the involvement of the peptide backbone in binding-induced conformational changes that lead to channel gating, we have incorporated a series of α-hydroxy acid analogues into the β-sheet rich extracellular domain of the nAChR (Figure 3.1). Upon incorporation of an α-hydroxy acid into a protein, the backbone amide functional group is replaced by an ester, with two major consequences (Figure 3.2). First, the ester bond disrupts the backbone hydrogen bonding pattern associated with β-sheet structure. The ester lacks the NH hydrogen bond donor, and the ester carbonyl is a weaker hydrogen bond acceptor than the amide carbonyl. Previous studies on a small 3-stranded β-sheet protein found that the effect of weakening a hydrogen bond acceptor (the carbonyl) is less destabilizing than removing the hydrogen bond donor (the NH) by about 0.8 kcal/mol.[13] Second, while the *s-trans* planar conformational preference, bond lengths, and bond angles are generally similar to those of amide bonds, the ester bond possesses much greater backbone flexibility due to substantial reduction of the rotation barrier around the C-O versus the C-N single bond.

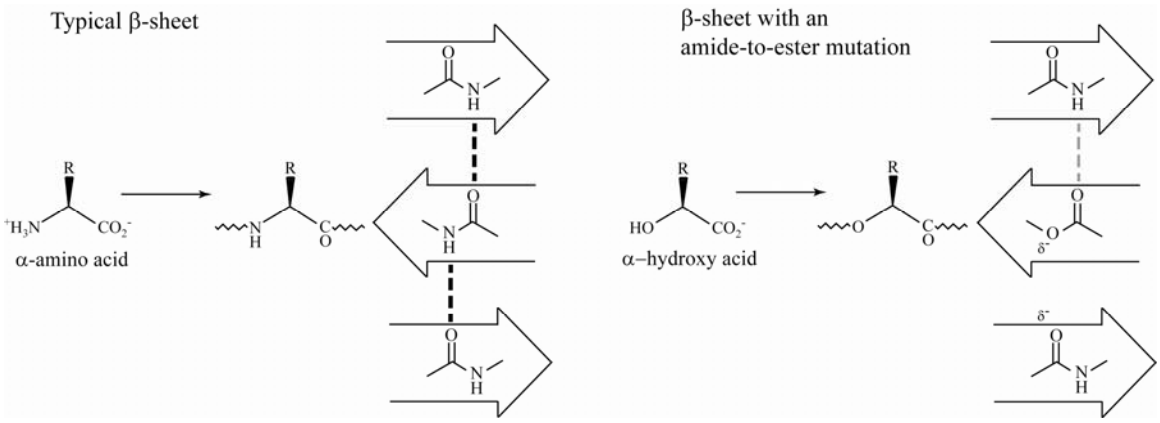

Figure 3.2: Schematic of the backbone amide versus the backbone ester bond in the context of a β-sheet.

In the present work, amide-to-ester mutations were made in two critical α-strands that connect the agonist binding site to the transmembrane region of the receptor (Figure 3.1). To our knowledge, this is the first systematic study of amide-to-ester mutations in a β-sheet of a large allosteric receptor. Specifically, mutations were made in α-strands 7 and 10 (α7 and α10, respectively) of the α-subunit, disrupting the extensive backbone hydrogen bonding network in what has been termed the outer β-sheet of the extracellular domain. The rationale behind studying these strands was two-fold. First, α7 connects the critical cation-π binding residue in loop B (αW149)[14] to the eponymous Cys-loop, which directly contacts the transmembrane region. α10 extends from loop C, which contains two other aromatic binding box residues[15, 16], and connects directly to the first transmembrane helix. Second, recent studies strongly implicate the outer β-sheet in connecting agonist binding to channel gating.[6, 11, 17-19] A study of α7 and α10 in the neuronal α7 nAChR suggests that the rigidity of this region is crucial in transducing channel gating.[18] Furthermore, previous studies show that a triad of residues in this region is important in initiating channel gating.[11] These residues are the C-loop residue αY190, along with αK145 and αD200, on α7 and α10, respectively. Thus, it seemed reasonable to assume that the outer β-sheet was important for connecting agonist binding to channel gating, and that backbone dynamics and hydrogen bonding might be involved. Given that the balance

between rigidity and flexibility is believed to be central to the structure and function of allosteric proteins,[8] involvement of the peptide backbone in mediating allosteric communication in the nAChR would not be surprising. Previous studies of backbone esters in ion channels have focused on the role of backbone flexibility in α-helical domains,[20-22] seeking local movements that directly influence channel gating. Here we hope to better understand how hydrogen bonding in a critical β-sheet region that is distal to the channel gate influences receptor function.

Surprisingly, a number of single backbone mutations in this region were well-tolerated, producing only modest shifts in EC_{50} and wild type-like macroscopic current sizes (I_{max}) in the majority of cases. However, simultaneous introduction of two backbone mutations either in the same α-strand separated by a single amino acid or at amino acids sharing a hydrogen bond between the two α-strands led to surface-expressed, non-functional receptors. Together, these data suggest that while the receptor is remarkably robust in its ability to tolerate single amide-to-ester mutations throughout these α-strands, more substantial perturbations to this region have a profound effect on the protein. Therefore, it would seem that backbone movements in the outer β-sheet are important for receptor function. This adds to a growing body of evidence that points to the importance of this region in mediating the conformational changes that emanate from the agonist binding site to the gate of the channel.

3.3 Results

Single amide-to-ester mutations in α7 and α10 have minimal impact on receptor function

Nine α-hydroxy acids were incorporated into α7 and α10 of the α-subunit extracellular domain, perturbing a total of 13 hydrogen bonds (Figure 3.1). In some cases, the α-hydroxy analogue of the native amino acid was not available. In these instances, conventional mutagenesis was employed to find an alternative amino acid side chain that had both minimal

effect on receptor function and an available α-hydroxy analogue. The effect of the amide-to-ester mutation was then compared to the analogous side chain mutant, instead of the wild-type receptor. Most amide-to-ester mutations produced modest changes in EC_{50} (< 2-fold) (Figure 3.3, Table 3.1). In three cases (αM144, αL199, and αV206) larger, although still not immense, shifts in the 3.5-4-fold range were seen. ACh-induced whole-cell currents of receptors with single α-hydroxy mutations were similar to the currents produced by incorporation of the native amino acid by nonsense suppression.

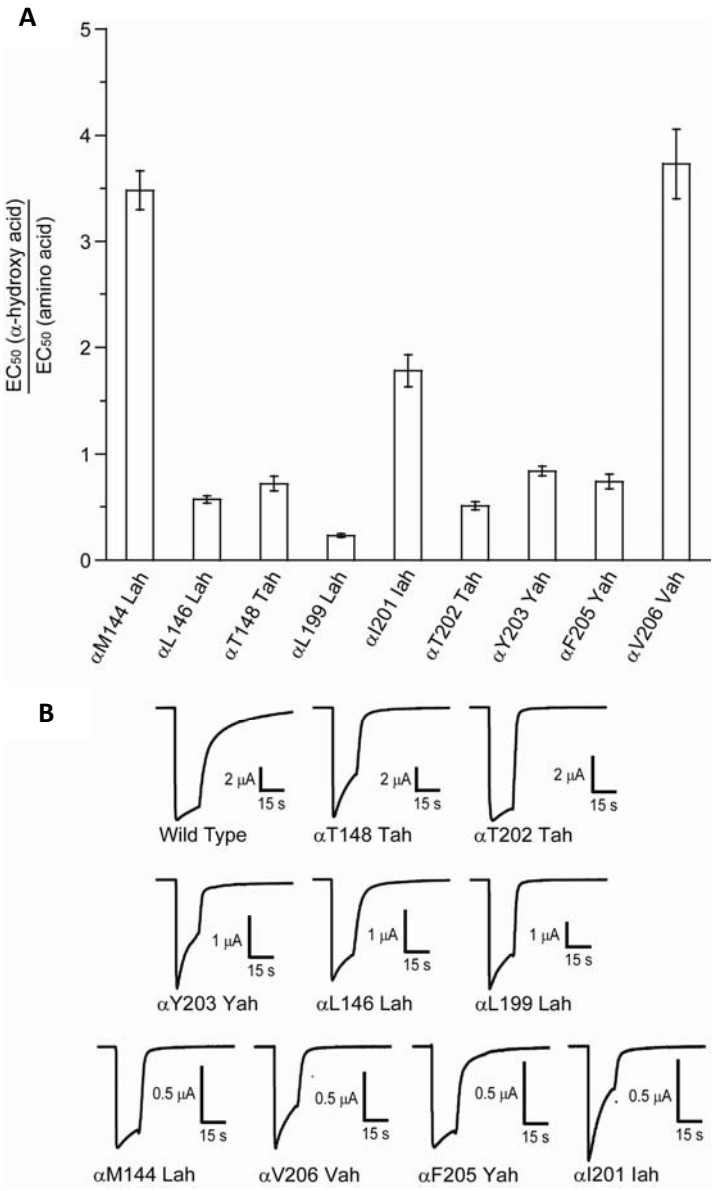

Figure 3.3: Characteristics of nAChR with backbone mutations in β-strands 7 and 10. (A) EC_{50} shifts for backbone mutations made at nine positions in β7and β10. Modest effects on receptor function are seen in all cases. (B) Current traces for backbone mutations made at nine positions in β7and β10.

	EC_{50} (μM)	n_H
WT	46 ± 2	1.8 ± 0.13
αM144Leu	15 ± 0.3	1.7 ± 0.06
αM144Lah	50 ± 0.8	1.7 ± 0.03
αL146Lah	26 ± 0.8	1.3 ± 0.05
αT148Tah	33 ± 3	1.0 ± 0.06
αL199Lah	11 ± 0.5	1.6 ± 0.10
αI201Iah	82 ± 6	1.5 ± 0.12
αT202Tah	24 ± 1	1.4 ± 0.09
αY203Yah	39 ± 0.8	1.9 ± 0.07
αF205Tyr	90 ± 2	1.5 ± 0.05
αF205Yah	67 ±62	1.4 ± 0.13
αV206Vah	170 ± 10	1.9 ± 0.20

Table 3.1: EC_{50} and Hill coefficient (±SEM) values for mutations made in this study.

As EC_{50} is a composite of both binding and gating phenomena, small shifts in EC_{50} may mask a large effect on receptor behavior. Recently, we developed a method to evaluate whether a loss of function (increase in EC_{50}) mutation in the extracellular domain strongly impacts receptor gating (rather than agonist binding).[23] The method, termed ELFCAR (Elucidating Long-range Functional Coupling in Allosteric Receptors), is based on mutant cycle analysis and produces a value for Ω, the coupling between extracellular domain residue and a known gating mutation (in this case βL9'S). This method utilizes whole-cell data to determine whether a mutant that produces a moderate to large increase in EC_{50} has a substantial impact on receptor gating, as indicated by $\Omega>2$. ELFCAR is especially valuable in interpreting moderate increases in EC_{50}, where a dramatic effect on gating might otherwise be missed. An Ω value near one, however, does not preclude a modest effect on gating. The three α-hydroxy mutants in this study that produce increases in EC_{50} – at positions 144, 201, and 206 – all produce an Ω value near one (0.97, 0.65, and 0.69, respectively), suggesting no dramatic impact on receptor gating. This method is not applicable to gain-of-function mutations, so the remaining six

mutants could not be evaluated using ELFCAR. Combined, the data suggest that single α-hydroxy mutations in this region do not substantially impair receptor gating.

Simultaneous incorporation of two α-hydroxy acid mutations in α7 and α10 produces non-functional, surface expressed receptors

The impact of disrupting the polypeptide backbone at more than one location was investigated by simultaneously incorporating two α-hydroxy acids. This was done in two different ways: amide-to-ester mutations were made either in the same α-strand separated by a single amino acid (αM144 and αL146 in α-strand 7), or at amino acids sharing a hydrogen bond between the two α-strands (αL146 and αI201; Figure 3.1). Simultaneous incorporation of the same α-hydroxy (Lah) or amino (Leu, in the case of wild-type recovery) acid was done in both scenarios. This allowed for double suppression using the standard nonsense suppression methodology (see materials and methods). As a large shift in EC_{50} might have been anticipated, the double mutation experiments were carried out in the presence of the αL9'S gating mutation. For mutations that primarily affect binding or have a only moderate effect on channel gating this mutation lowers the EC_{50} by about 40-fold, allowing for reliable EC_{50} measurement of potentially highly deleterious mutations without complications from open channel block at high agonist concentrations.

For both double-mutation (Lah) experiments, no whole-cell current was observed in response to high (>1000 μM) doses of ACh. Wild-type recovery (Leu) by nonsense suppression gave normal whole-cell currents in the range of 5 to 15 μA. Lack of an electrophysiological response can indicate that protein folding, subunit assembly, receptor transport, or receptor function have been impacted.

To determine whether nonfunctional mutant receptors were expressed at the plasma membrane, the localization of these mutant receptors was studied using single molecule Total Internal Reflectance Fluorescence (TIRF) microscopy. Mutant and wild type (recovery by nonsense suppression) receptors were first labelled with biotin conjugated to α-bungarotoxin and subsequently labelled with streptavidin conjugated to the fluorophore Alexa488. Fluorescent puncta corresponding to single receptors were clearly visible on the cell surface (Figure 3.4B). For the double α-hydroxy-containing receptors, the number of puncta was between 50% and 70% of the value seen for wild type receptor (recovery by nonsense suppression) (Figure 3.4B, Table 3.2). Based on previous, extensive studies with this approach,[24] it is clear that double-mutant receptors are being surface expressed at a level such that significant whole-cell current would be observed, if the receptors were functional. That is, the calculated expected whole-cell currents from the α-hydroxy double-mutant receptors based on puncta density are on the order of 3 to 5 μA (Table 3.2). Since we can easily detect this magnitude of ACh-induced current, our results clearly show that non-functional receptors have been expressed on the oocyte surface. The calculated expected whole cell currents from the wild-type receptors based on puncta density are on the order of 6 to 7 μA, in agreement with the electrophysiological data.

αI201L146	# Puncta/ image frame	Calculated current size (μA)
Leu	265 ± 36	7.5 ± 1.0
Lah	179 ± 33	5.1 ± 0.9
76mer	51 ± 10	1.4 ± 0.3
uninjected	27 ± 5	0.8 ± 0.2
αL146M144		
Leu	214 ± 15	6.1 ± 0.4
Lah	121 ± 4	3.4 ± 0.1
76mer	56 ± 5	1.6 ± 0.1
Uninjected	37 ± 4	1.0 ± 0.1

Table 3.2: Puncta densities and corresponding estimated current sizes from TIRF microscopy experiments. 76mer refers to unaminoacylated tRNA.

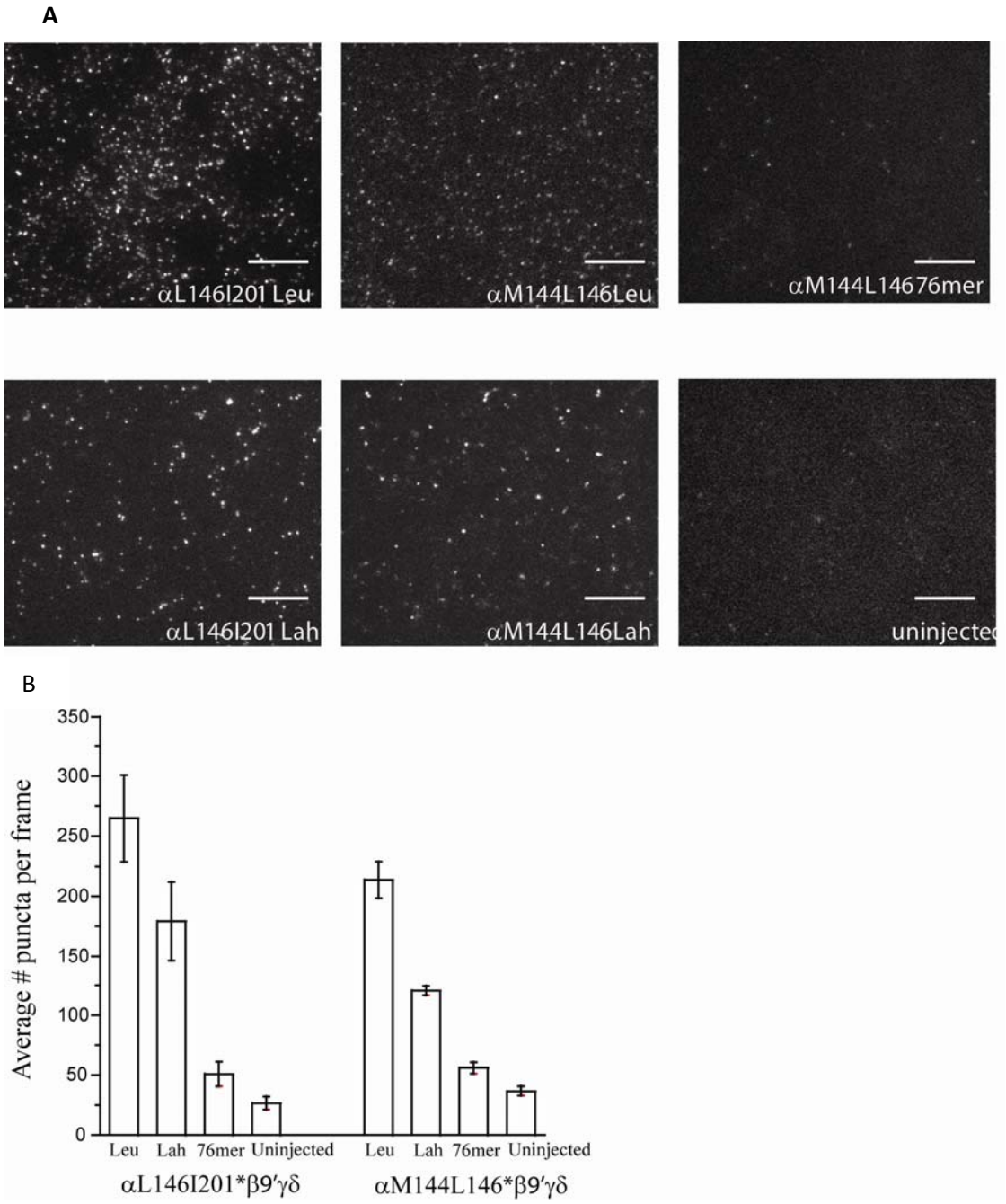

Figure 3.4: Analysis of non-functional nAChRs containing two amide-to-ester mutations by TIRF microscopy. (A) Puncta density for receptors labeled with Leu refers to recovery of the wild-type peptide backbone by nonsense suppression; Lah refers to incorporation of leucine α-hydroxy; and 76mer indicates the negative control experiment (coinjection of mRNA with a tRNA molecule that has not been charged with an amino or hydroxy acid). The puncta density for both Leu and Lah are significantly higher than for either the 76mer or uninjected oocyte controls (t-test values for Lah vs. 76mer are: P=0.0009 (L146I120); P<0.0001 (L146M144); for Lah vs. uninjected: P= 0.0003 (L146I120); P< 0.0001 (L146M144). Data are compiled from ≥6 non-overlapping images from ≥2 oocytes. (B) Representative TIRF images corresponding to the data in (A). Scale bars represent 6 μm.

Note that α-bungarotoxin is a potent inhibitor of the nAChR that binds tightly in the same region[25] as ACh and requires properly folded receptor for tight binding. Thus, successful α-bungarotoxin binding indicates that the overall structure of the extracellular domain and binding site were not grossly perturbed. These results indicate that simultaneous incorporation of two α-hydroxy mutations in this region leads to nonfunctional, surface-expressed receptors.

3.4 Discussion

The α-sandwich structure comprised of "inner" and "outer" β-sheets – first revealed in the AChBP structure[14,15] and later confirmed in images of the full nAChR[6, 26] – is accepted to be a critical structural feature of Cys-loop receptors. In the present work, we have probed the robustness of this structure by selectively removing/weakening backbone hydrogen bonds that define the structure, using backbone ester substitution. The remarkable generality of nonsense suppression techniques for incorporating unnatural residues into receptors and channels expressed in *Xenopus* oocytes makes this study possible. One could have imagined several outcomes for such experiments. If movement within the sheets is critical to receptor function, backbone mutations could facilitate receptor gating, perhaps even creating constitutively active receptors. Alternatively, if an intact β-sandwich is essential for receptor function, backbone mutations could disable the receptor.

Here we have focused on the outer β-sheet of the extracellular domain, and in particular on α7 and α10, which have been proposed to play key roles in receptor function. Perhaps surprisingly, individual amide-to-ester mutations throughout both strands resulted in functional receptors with only modest changes in EC_{50}. Evidently, the outer β-sheet is relatively

robust, and the receptor can absorb the loss of a single hydrogen bond in this region. Interestingly, however, simultaneous replacement of two nearby residues with their α-hydroxy analogues produced surface-expressed but non-functional receptors. Using receptor labelling with fluorescent α-bungarotoxin, and single-molecule imaging by TIRF microscopy, we demonstrate that the number of double-mutant receptors expressed on the oocyte is more than adequate to produce measurable currents, if the receptors were functional. Tight binding by α-bungarotoxin requires proper folding in the region of the agonist binding site, which is quite near the mutations considered here. In fact, in the α-bungarotoxin-bound crystal structure of the α1-subunit,[27] residues at the top of both α7 and α10 are in close proximity to the bound α-bungarotoxin molecule. Successful binding of α-bungarotoxin to the double mutant receptors, as detected by TIRF microscopy, strongly suggests that the structure of this region is not greatly perturbed.

The implication is that the crucial outer β-sheet of the nAChR is not overly fragile – it can tolerate the disruption caused by a single backbone substitution – but it must be intact for receptor function, and apparently two proximal backbone mutations are too disruptive. Folding, assembly, and transport to the cell surface, however, can still occur in the double mutants discussed here.

These results can be understood in the context of emerging models of the conformational changes in the extracellular domain that lead to receptor activation. Recent MD simulations[19, 28] have pointed to a pivotal role for β10 in communicating the inward motion of the agonist binding site-shaping C-loop to the motions of the transmembrane domain that eventually produce channel opening. The proposed upward and outward motion allows αR209 on β10 to approach αE45 on the β2-β3 linker, resulting in an interaction between these two

residues; an interaction that was previously concluded to be important for coupling agonist binding and channel gating based on mutant cycle analysis of single channel data.

β7 likewise harbors a residue, αK145, that has been implicated in connecting agonist binding with channel gating. When agonist binds and the C-loop closes in, a salt bridge between αK145 on β7 and αD200 on β10 breaks, and αK145 forms a hydrogen bond with αY190 on the C-loop.[10] This electrostatic rearrangement was proposed to initiate conformational changes that contribute to opening of the central ion-conducting pore.

Studies of engineered disulfide linkages between β7 and β10 in the α7 nAChR also suggest that the outer β-sheet plays a role in transmitting agonist binding-induced conformational changes to the channel gate.[17] Specifically, in the background of a non-desensitizing mutation, one engineered disulfide-containing receptor could be activated by divalent cations alone, which normally play a role as allosteric modulators. This implies that reduced mobility in the outer β-sheet of these receptors results in a lower barrier to channel activation. These and other researchers[16] have suggested that this β-sheet may act as a lever, where binding at one end tilts the lever resulting in a movement at the other, transmembrane-adjacent, end. A certain amount of rigidity in this region seems to be fundamental to normal receptor function.

Using this lever analogy, our results suggest that two or more nearby α-hydroxy acid mutations lead to a more flexible and thus ineffective lever that is unable to communicate agonist binding events to the transmembrane region of the receptor. Thus, disruption of hydrogen bonding in the outer β-sheet would seem to interrupt the conformational wave that connects the agonist binding-induced motions of the C-loop to the subsequent motions of the transmembrane region.

It is also possible that the loss of hydrogen bonding between these strands could lead to misalignment of the binding box residues, impairing agonist binding to the receptor. However, it seems less likely that the binding region of the receptor is grossly malformed, since α-bungarotoxin is still able to bind to the mutant receptors.

In conclusion, we find that the network of hydrogen bonds formed in the outer β-sheet of the nAChR is fairly robust, tolerating single amide-to-ester mutations throughout. However, eliminating two proximal hydrogen bonds completely destroys receptor function, adding further support to gating models that ascribe important roles to these β-strands of the nAChR extracellular domain.

3.5 Materials and Methods

Unnatural Hydroxy Acid Suppression

Synthetic α-hydroxy acids were conjugated to the dinucleotide dCA and ligated to truncated 74-nucleotide tRNA as previously described.[29] Typically, 25 ng of tRNA was injected per oocyte along with mRNA in a total volume of 50 nL/cell. mRNA was prepared by in vitro runoff transcription using the Ambion (Austin, TX) T7 mMessage mMachine kit. The site of interest was mutated to the amber stop codon by standard means, verified by sequencing through both strands. Mouse muscle embryonic nAChR in the pAMV vector was used. A total of 4.0 ng of mRNA was injected in an α:β:γ:δ subunit ratio of 10:1:1:1. The ratio of tRNA to mRNA was typically 1:1. In addition, the α-subunits contain an HA epitope in the M3-M4 cytoplasmic loop for Western blot studies. Control experiments show that this epitope does not detectably alter EC_{50}. As a negative control for suppression, truncated 74-nucleotide tRNA or truncated tRNA ligated to dCA to give a 76mer was co injected with mRNA in the same manner as fully charged tRNA. Data from experiments where currents from these negative controls was greater

than 10% of the experimental were excluded. The positive control for suppression involved wild-type recovery by co-injection with 74-nucleotide tRNA ligated to wild type amino acid. For suppression at multiple sites, the tRNA:mRNA ratio was increased to 2:1.

Electrophysiology

Stage V-VI oocytes of *Xenopus laevis* were employed. Oocyte recordings were made 12-48 h post-injection in two-electrode voltage clamp mode using the OpusXpress 6000A instrument (Axon Instruments, Union City, CA). Oocytes were superfused with a Ca^{2+}-free ND96 solution at flow rates of 1 mL/min before application, (15 second) 4 mL/min during drug application, and 3 mL/min during wash. Holding potentials were -60 mV. Data were sampled at 125 Hz and filtered at 50 Hz. Acetylcholine chloride was purchased from Sigma/Aldrich/RBI. Solutions ranging from 0.01 to 5000 mM were prepared in Ca^{2+}-free ND96 from a 1 M stock solution. Dose-response data were obtained for a minimum of 8 concentrations of agonists and for a minimum of five cells. Dose-response relations were fitted to the Hill equation to determine EC_{50} and Hill coefficient values. The dose-response relations of individual oocytes were examined and used to determine outliers. The reported EC_{50} values are from the curve fit of the averaged data.

Total Internal Reflection Fluorescence Microscopy

Xenopus oocytes were prepared for single molecule TIRF microscopy as follows. 24-48 hours after injection of mRNA and tRNA, oocytes were incubated in a 0.5 ng/µL solution of biotin conjugated to α-bungarotoxin (Molecular Probes, Invitrogen, Eugene, OR) for 4- 12 hours. This was followed by two wash steps with a 5 mg/mL bovine serum albumin solution and one wash with Ca^{2+}-free ND96. Subsequently, oocytes were incubated in a 0.2 ng/µL solution streptavidin conjugated to the fluorophore Alexa488 (Molecular Probes, Invitrogen, Eugene, OR)

for 15- 30 minutes, followed by two additional wash steps each with BSA and Ca^{2+}-free ND96. The vitelline membrane of labeled oocytes was removed with forceps following a 5-10 minute incubation in a hypertonic solution (220 mM sodium aspartate, 10 mM HEPES, 10 mM EDTA, 2 mM MgCl2, pH 7.38). Devitellinized oocytes were transferred to an imaging chamber with a clean glass coverslip mounted on the microscope stage with the animal pole oriented toward the coverslip. The TIRF microscope used to collect the data consists of a Melles-Griot Argon (Ar) ion laser coupled to a fiber optic that extends to an Olympus TIRF illuminator adapted to a standard inverted IX-71 Olympus microscope (Center Valley, PA). A wavelength of 488 nm was used to excite and detect the Alexa488 fluorophores, by using the Z488 filter cube from Chroma Technology Corporation (Rockingham, VT). A 100X 1.45 NA Olympus TIRF objective was used. Images were captured with a Photometrics Cascade front illuminated CCD camera from Princeton Instruments (Trenton, NJ). Andor iQ from Andor Technology (South Windsor, CT) was used to acquire the data. The data were subsequently processed and analyzed with ImageJ (National Institutes of Health). Puncta were manually counted and densities from ≥6 images and ≥2 oocytes were compiled and averaged. Expected current sizes were calculated as (#puncta/image frame area)*average oocyte area*single channel conductance.

Acknowledgements

We thank Dr. Rigo Pantoja for advice and assistance with TIRF measurements. This work was supported by the NIH (NS 34407; NS 11756). K. R. G. was partially supported by an NSF Graduate Research Fellowship.

3.6 References

1. Corringer, P.J., Le Novere, N. & Changeux, J.P. Nicotinic receptors at the amino acid level. *Annu Rev Pharmacol Toxicol* **40**, 431-58 (2000).
2. Grutter, T. & Changeux, J.P. Nicotinic receptors in wonderland. *Trends Biochem Sci* **26**, 459-63 (2001).
3. Connolly, C.N. & Wafford, K.A. The Cys-loop superfamily of ligand-gated ion channels: the impact of receptor structure on function. *Biochemical Society Transactions* **32**, 529-534 (2004).
4. Lester, H.A., Dibas, M.I., Dahan, D.S., Leite, J.F. & Dougherty, D.A. Cys-loop receptors: new twists and turns. *Trends in Neurosciences* **27**, 329-336 (2004).
5. Sine, S.M. & Engel, A.G. Recent advances in Cys-loop receptor structure and function. *Nature* **440**, 448-455 (2006).
6. Unwin, N. Refined structure of the nicotinic acetylcholine receptor at 4 angstrom resolution. *Journal of Molecular Biology* **346**, 967-989 (2005).
7. Changeux, J.P. & Edelstein, S.J. Allosteric mechanisms of signal transduction. *Science* **308**, 1424-1428 (2005).
8. Cui, Q. & Karplus, M. Allostery and cooperativity revisited. *Protein Sci* **17**, 1295-307 (2008).
9. Grosman, C., Zhou, M. & Auerbach, A. Mapping the conformational wave of acetylcholine receptor channel gating. *Nature* **403**, 773-6 (2000).
10. Lee, W.Y. & Sine, S.M. Principal pathway coupling agonist binding to channel gating in nicotinic receptors. *Nature* **438**, 243-7 (2005).
11. Mukhtasimova, N., Free, C. & Sine, S.M. Initial coupling of binding to gating mediated by conserved residues in the muscle nicotinic receptor. *J Gen Physiol* **126**, 23-39 (2005).
12. Xiu, X., Hanek, A.P., Wang, J., Lester, H.A. & Dougherty, D.A. A unified view of the role of electrostatic interactions in modulating the gating of Cys loop receptors. *J Biol Chem* **280**, 41655-66 (2005).
13. Deechongkit, S., Dawson, P.E. & Kelly, J.W. Toward assessing the position-dependent contributions of backbone hydrogen bonding to beta-sheet folding thermodynamics employing amide-to-ester perturbations. *J Am Chem Soc* **126**, 16762-71 (2004).
14. Zhong, W. et al. From ab initio quantum mechanics to molecular neurobiology: a cation-pi binding site in the nicotinic receptor. *Proc Natl Acad Sci U S A* **95**, 12088-93 (1998).
15. Brejc, K. et al. Crystal structure of an ACh-binding protein reveals the ligand-binding domain of nicotinic receptors. *Nature* **411**, 269-76 (2001).
16. Sixma, T.K. & Smit, A.B. Acetylcholine binding protein (AChBP): a secreted glial protein that provides a high-resolution model for the extracellular domain of pentameric ligand-gated ion channels. *Annu Rev Biophys Biomol Struct* **32**, 311-34 (2003).
17. Law, R.J., Henchman, R.H. & McCammon, J.A. A gating mechanism proposed from a simulation of a human alpha7 nicotinic acetylcholine receptor. *Proc Natl Acad Sci U S A* **102**, 6813-8 (2005).
18. McLaughlin, J.T., Fu, J., Sproul, A.D. & Rosenberg, R.L. Role of the outer beta-sheet in divalent cation modulation of alpha7 nicotinic receptors. *Mol Pharmacol* **70**, 16-22 (2006).
19. Yi, M., Tjong, H. & Zhou, H.X. Spontaneous conformational change and toxin binding in alpha7 acetylcholine receptor: insight into channel activation and inhibition. *Proc Natl Acad Sci U S A* **105**, 8280-5 (2008).
20. England, P.M., Zhang, Y., Dougherty, D.A. & Lester, H.A. Backbone mutations in transmembrane domains of a ligand-gated ion channel: implications for the mechanism of gating. *Cell* **96**, 89-98 (1999).

21. Lu, T. et al. Probing ion permeation and gating in a K+ channel with backbone mutations in the selectivity filter. *Nat Neurosci* **4**, 239-46 (2001).
22. Nagaoka, Y., Shang, L., Banerjee, A., Bayley, H. & Tucker, S.J. Peptide backbone mutagenesis of putative gating hinges in a potassium ion channel. *Chembiochem* **9**, 1725-8 (2008).
23. Gleitsman, K.R., Shanata, J.A., Frazier, S.J., Lester, H.A. & Dougherty, D.A. Long-range coupling in an allosteric receptor revealed by mutant cycle analysis. *Biophys J* **96**, 3168-78 (2009).
24. Pantoja, R., Rodriguez, E.A., Dibas, M.I., Dougherty, D.A. & Lester, H.A. Single-molecule imaging of a fluorescent unnatural amino acid incorporated into nicotinic receptors. *Biophys J* **96**, 226-37 (2009).
25. Nirthanan, S. & Gwee, M.C. Three-finger alpha-neurotoxins and the nicotinic acetylcholine receptor, forty years on. *J Pharmacol Sci* **94**, 1-17 (2004).
26. Miyazawa, A., Fujiyoshi, Y. & Unwin, N. Structure and gating mechanism of the acetylcholine receptor pore. *Nature* **423**, 949-55 (2003).
27. Dellisanti, C.D., Yao, Y., Stroud, J.C., Wang, Z.Z. & Chen, L. Crystal structure of the extracellular domain of nAChR alpha1 bound to alpha-bungarotoxin at 1.94 A resolution. *Nat Neurosci* **10**, 953-62 (2007).
28. Cheng, X., Wang, H., Grant, B., Sine, S.M. & McCammon, J.A. Targeted molecular dynamics study of C-loop closure and channel gating in nicotinic receptors. *PLoS Comput Biol* **2**, e134 (2006).
29. Nowak, M.W. et al. In vivo incorporation of unnatural amino acids into ion channels in Xenopus oocyte expression system. *Methods Enzymol* **293**, 504-29 (1998).

Chapter 4: Long-Range Coupling in an Allosteric Receptor Revealed by Mutant Cycle Analysis

Reproduced with permission from Kristin Rule Gleitsman, Jai A.P. Shanata, Shawnalea J. Frazier, Henry A. Lester, and Dennis A. Dougherty. Biophys. J. **2009**, *96*, 3168-3178.

4.1 Abstract

The functional coupling of residues that are far apart in space is the quintessential property of allosteric proteins. For example, in Cys-loop receptors the gating of an intrinsic ion channel is allosterically regulated by the binding of small molecule neurotransmitters 50-60 Å from the channel gate. Some residues near the binding site must have as their primary function the communication of the binding event to the gating region. These gating pathway residues are essential to function, but their identification and characterization can be challenging. The present work introduces a simple strategy, derived from mutant cycle analysis, for identifying gating pathway residues using macroscopic measurements alone. In the exemplar Cys-loop receptor, the nicotinic acetylcholine receptor, a well-characterized reporter mutation (βL9'S) known to impact gating was combined with mutations of target residues in the ligand-binding domain hypothesized or previously found to be functionally significant. A mutant cycle analysis of the macroscopic EC_{50} measurements can then provide insights into the role of the target residue. This new method - **e**lucidating **l**ong-range **f**unctional **c**oupling in **a**llosteric **r**eceptors (ELFCAR) - can be applied to a number of reporter mutations in a wide variety of receptors to identify both previously characterized and novel mutations that impact the gating pathway. We support our interpretation of macroscopic data with single-channel studies. ELFCAR should be broadly applicable to determining functional roles of residues in allosteric receptors.

4.2 Introduction

Cys-loop receptors mediate fast synaptic transmission throughout the central and peripheral nervous systems.[2-5] These pentameric, ligand-gated ion channels are prototypical allosteric receptors,[6] in that the activation (gating) of an intrinsic ion channel is allosterically regulated by the binding of small molecule neurotransmitters (acetylcholine (ACh), serotonin, GABA, or glycine). While valuable structural insights for Cys-loop receptors have appeared in recent years,[1, 7] detailed conformational mechanisms linking neurotransmitter binding to channel gating remain elusive.

Structurally, Cys-loop receptors have two principal functional domains (Figure 4.1). The extracellular domain, rich in β-sheet structure, contains the agonist binding sites. Each subunit also contains a transmembrane domain comprised of four membrane-spanning helices, one of which (M2) lines the ion channel. While the precise location of the channel gate has been debated, the consensus positions it at or below the middle of the M2 helix. This puts the channel gate some 50-60 Å away from the agonist binding sites. Neurotransmitter binding events must therefore be communicated over this distance to the channel gate.

In terms of function, such a clear demarcation of domains is less evident. For a given residue, if a mutation at the site leads to a change in receptor function, this could be because the binding of agonist or the gating of the channel (or both) has changed. It seems safe to say that residues in the middle of the transmembrane domain do not contribute directly to agonist binding, and so residues in the transmembrane domain that contribute to function are typically described as “gating” residues. In contrast, one expects to find residues in the extracellular domain with varying functional roles. Some residues will primarily facilitate agonist binding, either by directly contacting the agonist or by refining the shape or electronic properties of the

agonist binding site. However, to achieve the long-range communication that is fundamental to Cys-loop receptor function, other extracellular domain residues must be involved in communicating the binding event to the channel gate, serving an instrumental role in the gating pathway. These gating pathway residues are in some ways the most interesting, but their identification and characterization can be challenging.

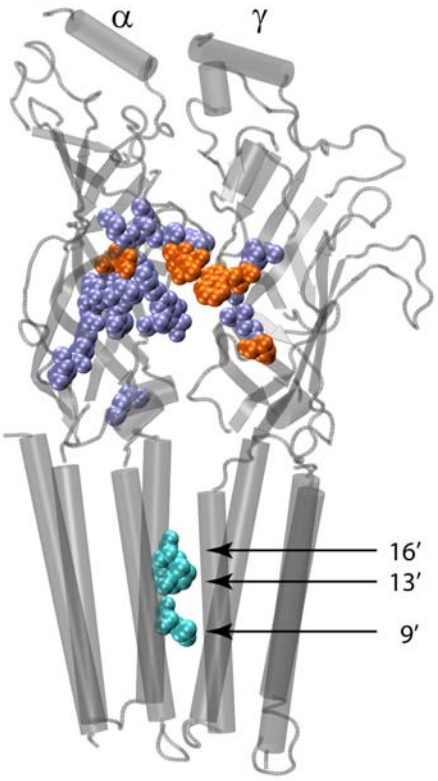

Figure 4.1: . Residues considered here. Shown are two adjacent subunits of the cryo-EM structure of the *Torpedo* nAChR (pdb 2BG9).[1] The reporter residues in the transmembrane domain are shown as cyan and are labeled. Residues in the extracellular domain are in two classes: those with no long-range coupling (purple) and the five residues that show significant long-range coupling (orange). One non-coupling residue (γE168) is not defined in the EM structure and so is not shown.

One strategy for determining whether a given residue primarily contributes to agonist binding or channel gating involves single-channel recording on appropriate mutants, followed by kinetic analysis. However, in some Cys-loop receptors (such as 5-HT_3 [8]), single-channel conductances are too small for reliable kinetic analyses;[9, 10] in many other Cys-loop receptors, single-channel kinetics are complex or nonstationary, again vitiating single-channel kinetic

analysis.[11, 12] Also, in other ion channels[13] and in allosteric receptors in general, single-channel studies are often not possible.

A more broadly applicable approach, allowing one to efficiently evaluate a number of mutants in search of unusual behavior, is to measure macroscopic currents across multiple concentrations. This produces the EC_{50} value, the concentration that induces half-maximal current in response to applied agonist, along with comparative measurements of maximal agonist-induced currents. In the case of ligand-gated ion channels, EC_{50} is a composite value, being responsive to both changes in agonist binding and channel gating behaviors. As such, it can be challenging to interpret shifts in EC_{50}. Here we describe an approach to use the readily obtained EC_{50} values to identify residues that substantially impacting receptor gating. We refer to the method as ELFCAR (**e**lucidating **l**ong-range **f**unctional **c**oupling of **a**llosteric **r**eceptors). The basic tool involves mutant cycle analysis of EC_{50} values for distant pairs of mutation sites. Complementary observations concerning mutational effects on receptor efficacy and the effects of partial agonists support the basic methodology. Thus, ELFCAR provides an efficient strategy for identification of key gating pathway residues that may otherwise evade detection, without performing single-channel studies.

Key to the approach is the definitive feature of allosteric proteins –action at a distance. When a mutation in the transmembrane domain that is unambiguously associated with channel gating is paired with various mutations in the extracellular domain, the observation of non-multiplicative EC_{50} shifts for the two mutations signals a functional coupling between the two residues, and thus identifies the extracellular domain mutation as influencing gating. We show that this behavior derives from the typical allosteric kinetic scheme for Cys-loop receptors, suggesting the approach could provide a general probe of allosteric receptors.

4.3 Results

The prototypical and most-studied Cys-loop receptor, the muscle nicotinic acetylcholine receptor (nAChR), was used in this study. It is important to appreciate that the method is directly applicable to other Cys-loop receptors, and, in favorable cases, to other allosteric proteins as well. Here we have employed the muscle-type nAChR as a well-established system that allows us to evaluate the methodology.

The muscle nAChR is a heteropentamer with subunit composition ($\alpha_2\beta\gamma\delta$).Two non-equivalent binding sites are located in the extracellular domain at the αδ and αγ subunit interfaces. Nearly all Cys-loop receptors, including all nAChRs, contain a conserved leucine residue in the hydrophobic, pore-lining M2 helix of each subunit (Figure 4.1). Mutating this residue, termed L9', to serine lowers the EC_{50}.[14, 15] Structural studies place L9' near the middle of the M2 helix, in the region of the occlusion of the closed channel, and while it can be debated whether L9' constitutes a literal gate of the channel, there can be no doubt that it is a crucial gating residue. In the present work, the L9'S mutation in the β subunit was used as a *reporter* to evaluate mutations of residues in the extracellular domain that may function as binding residues or as gating pathway residues.

βL9'S as a reporter of functional role for extracellular residues

Agonist occupancy at both binding sites is required for efficient opening of the channel pore. Scheme 4.1 shows a simplified kinetic model for activating the nAChR, leading to an expression for EC_{50} (Eq. 4.1),[16] where A is the agonist; R^C and R^O denote the closed and open states of the receptor; k_1 and k_{-1} are forward and reverse rate constants for agonist binding; K_D is the dissociation constant for the agonist; and Θ is the gating equilibrium constant, given by the

ratio of the channel opening rate, β, to the channel closing rate, α. It is well understood that the actual kinetic model for the nAChR is likely more complicated, and that different Cys-loop receptors may show kinetic schemes that differ in detail. In addition, a strong gating mutation could enable spontaneous openings of the channel when no agonist is bound. This could compromise the kinetic model discussed here. However, the βL9'S mutation alone does not lead to extensive spontaneous openings, and the types of mutations emphasized here, if they impact gating at all, discourage channel opening (decrease Θ), suggesting that spontaneous openings will not produce a major perturbation to the system. Scheme 4.1 is typical for an allosteric receptor, capturing the essence of the situation: function depends on binding of an allosteric effector as well as signal transduction (gating). For ligand-gated ion channels, this means that EC_{50} depends on both K_D and Θ, where Θ is a measure of receptor efficacy. The graphical representation of the relationship between EC_{50} and Θ, based on Eq. 4.1, is shown in Figure 4.2. Simulations of more complex kinetic schemes produce qualitatively similar plots. For full agonists – that is, those that produce a large Θ - the plot is linear with a negative slope. We will refer to this as the "high slope" region of the plot. For smaller values of Θ - such as would be associated with partial agonism - the plot approaches an asymptote. We will refer to this as the "plateau" region.[17]

$$A + R^C \underset{k_{-1}}{\overset{2k_1}{\rightleftharpoons}} A + AR^C \underset{2k_{-1}}{\overset{k_1}{\rightleftharpoons}} A_2R^C \underset{\alpha}{\overset{\beta}{\rightleftharpoons}} A_2R^O$$

Scheme 4.1

where, $K_D = k_{-1}/k_1$ and $\Theta = \beta/\alpha$

$$EC_{50} = \frac{K_D}{(\Theta + 2)^{1/2} - 1} \qquad (4.1)$$

A defining feature of allosteric proteins is that an allosteric effector shifts the equilibrium between two states, historically termed tensed and relaxed. However, binding of the allosteric effector itself does not define the exact state as tensed or relaxed, rather it produces a shift in the equilibrium *distribution* between these states. Consequently, once the allosteric signal is saturated, this equilibrium distribution depends only on the equilibrium constant governing tensed-relaxed interconversion. In the case of ligand-gated ion channels, such as the nAChR studied here, different allosteric effectors—i.e., different ligands for ligand-gated ion channels—produce different closed-open equilibria, characterized by Θ. Thus, while full agonists (Θ >>1) cause the channel to be mostly open when agonist is bound, partial agonists influence this allosteric transition to a lesser extent, resulting in a smaller perturbation of the gating equilibrium. It is the varying extent to which ligand binding can bias the equilibrium that produces the general shape of the relationship between EC_{50} (function) and Θ, seen in Figure 4.2.

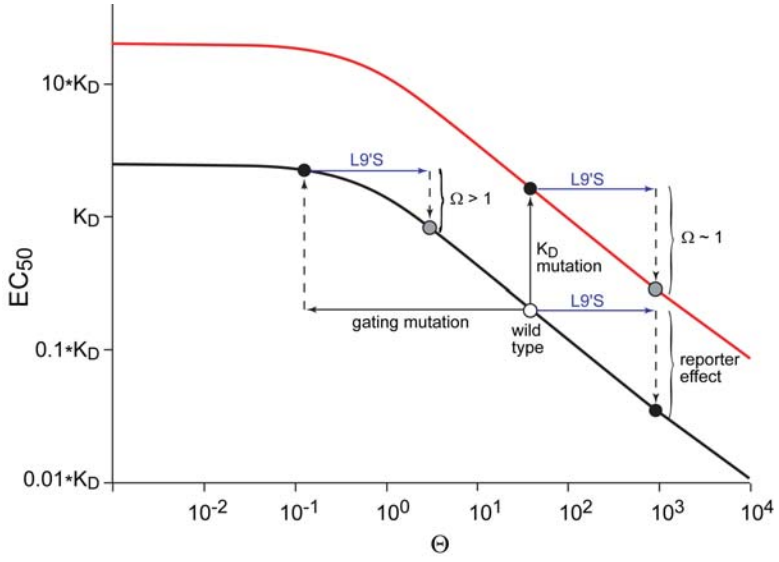

Figure 4.2: Black line: the relationship between EC_{50} and Θ, as given in Eq. (4.1). Red line: the same equation, but with a larger K_D. For both plots, in the negative slope region changes in Θ produce significant changes in EC_{50}, as shown when the reported effect is added to the wild type receptor. However, when beginning with Θ in the low slope region, a much smaller shift in EC_{50} occurs for equivalent shifts in Θ.

Previous studies[15, 18-20] have shown that polar mutations at L9' substantially increase Θ, causing a corresponding drop in EC_{50}. Our goal was to determine whether it was possible to use a *reporter* mutation such as βL9'S to evaluate whether the shift in EC_{50} from mutation at a *target* residue is primarily a result of changes in binding (K_D) or gating (Θ). Consider such a target mutation in the extracellular domain that only increases K_D, i.e., a pure binding mutation. This has the effect of raising the EC_{50} versus Θ curve, but maintaining its shape (Figure 4.2, red line). Addition of the βL9'S mutation then causes a comparable increase in Θ, lowering EC_{50} by the same factor as in the wild type. The pairing of an extracellular domain binding mutation with the reporter transmembrane domain mutation results in a multiplicative shift in EC_{50}; the two mutations are independent.

Now, consider the consequences of an extracellular domain target mutation that affects gating, and not binding. Deleterious mutations (increase in EC_{50}) will cause a drop in Θ, and if the effect is large enough, the agonist employed will now be a partial agonist. The EC_{50} vs. Θ relationship for this mutant will now lie in the plateau region of Figure 4.2. As a result, the subsequent increase in Θ caused by adding the βL9'S mutation will induce a much smaller drop in EC_{50}. The pairing of these mutations will no longer give a multiplicative shift in EC_{50}, and therefore the two mutations are functionally coupled. Thus, the βL9'S gating mutation acts as a reporter to identify a target mutation that is substantially loss of function (decreasing Θ). It is clear from Figure 4.2 that a gain of function gating mutation (lower EC_{50}; increasing Θ) will still be in the high slope region and so will be additive with the βL9'S mutation. This method cannot detect gain of function gating mutations.

For many mutations in the extracellular domain, the βL9'S mutation is indeed multiplicative, producing a consistent 40-fold shift to lower EC_{50} (Table 4.1).[15, 21, 22] We now report the first examples of mutations closely associated with the agonist binding site for which the effect of βL9'S is substantially less than 40-fold, indicating non-multiplicative behavior (Figure 4.1). Four of these are conventional mutants: αY190F, γD174NδD180N, γW55YδW57Y and αD200N. Others have probed these sites, and they are generally considered to primarily influence gating.[23-29] As such, these studies validate the ELFCAR method. The fifth, a novel mutant, replaces αS191 with its α-hydroxy analogue, which we abbreviate Sah (for serine α-hydroxy), converting the backbone amide that links αY190 and αS191 to a backbone ester.[30, 31]

Mutant cycle analysis suggests long-range coupling

The typical way to analyze a system in which two mutations are evaluated, both individually and in tandem, is by mutant cycle analysis (Figure 4.3). Briefly, if a mutation at one site has no structural or energetic impact at a second site, then the effect of simultaneous mutations at both sites will simply be multiplicative (Figure 4.3). In the parlance of mutant cycle analysis, the coupling parameter, Ω, will be unity. In contrast, if two residues interact, the simultaneous mutation at both sites will lead to an effect that is either greater or less than the product of their individual effects, producing an Ω value that significantly deviates from unity. This approach has been broadly applied to a wide range of systems, including Cys-loop receptors, where several investigators have used mutant cycle analysis of EC_{50} values to determine functional coupling between neighboring residues of the extracellular domain.[32-34]

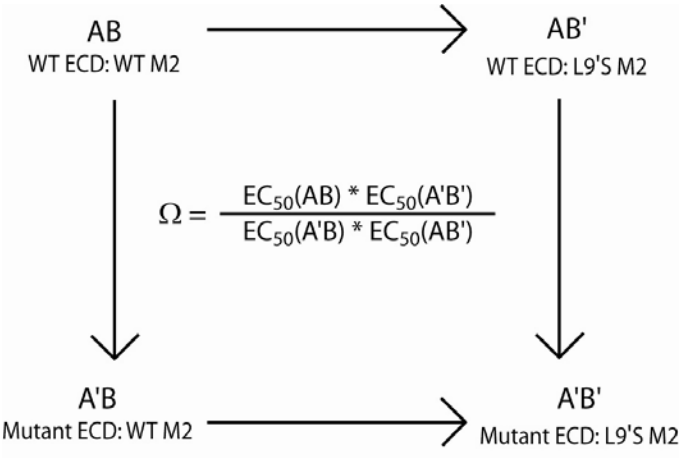

Figure 4.3: Scheme for double mutant cycle analysis where A and B represent amino acid positions and A' and B' represent mutations at these sites. The coupling parameter, Ω, is calculated from the given equation.

As could be anticipated from the EC_{50} values in Table 4.1, the vast majority of mutations made in the extracellular domain of the nAChR produce an Ω for coupling to βL9'S of ~ 1, indicating the functional independence of these residues. However, the five mutations noted above - αY190F, γD174NδD180N, γW55YδW57Y, αD200N, and αS191Sah - produced larger Ω values. We consider a value of Ω > 2 to signify a meaningful coupling (Figure4.4).

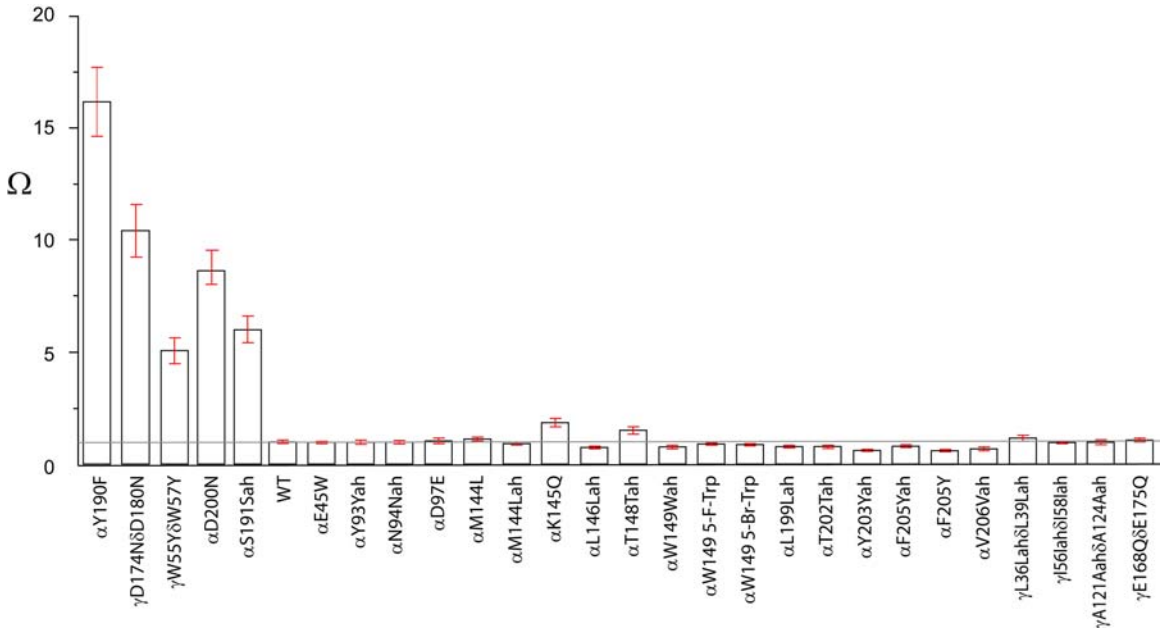

Figure 4.4: Values of Ω (coupling to βL9'S) for mutations considered here. The standard 40-fold shift expected for a βL9'S mutation produces an Ω value of one (horizontal line). 5-F-Trp is 5-fluorotryptophan and 5-Br-Trp is 5-bromotryptophan. For α-hydroxy acids (Yah, Nah, Lah, Tah, Wah, Vah, Iah, and Aah), a 3-letter abbreviation is used: the 1-letter code for the parent amino acid is followed by ah; thus Yah is the α-hydroxy acid of tyrosine.

Phenomenologically, this establishes a long-range coupling between these extracellular domain sites and the βL9' site, as one would expect for an allosteric receptor. Typically, an Ω that deviates significantly from a value of 1 is interpreted to indicate a direct interaction between the residues, such as a hydrogen bond or a salt bridge. In the present case, though, such a direct interaction is clearly impossible. We feel the interpretation of Figure 4.2 is much more palatable. Significant coupling is seen because both the βL9'S mutation and the particular extracellular domain mutation disrupt the gating pathway.

Single-channel recording supports whole-cell mutant cycle analysis conclusions

The most convincing way to evaluate the impact of a particularly interesting mutation is by single-channel analysis. To test our interpretation of the mutant cycle analyses using EC_{50} values, we chose three extracellular domain mutants which ELFCAR identified as gating pathway residues (αY190F, γD174NδD180N, and γW55YδW57Y), for single-channel studies. From these recordings, the open probability in the patch, NP_{open} was obtained. N is the number of channels in the patch, which often cannot be precisely determined. P_{open} is derived from Scheme 4.1 and depends only on Θ at equivalent points on the dose-response relation. The NP_{open} measurements reported were obtained using the macroscopic EC_{50} concentration of ACh, and thus represent $0.5(NP_{open,max})$. Each of the three target mutations produces a very large decrease in NP_{open} (Figure 4.5; Table 4.2) compared to the wild type value of ~0.5 (data not shown); they are substantially deleterious gating pathway mutations. Also consistent with the model, adding the βL9'S mutation substantially increases NP_{open}. The single-channel analysis thus supports the interpretation of the macroscopic EC_{50} data.

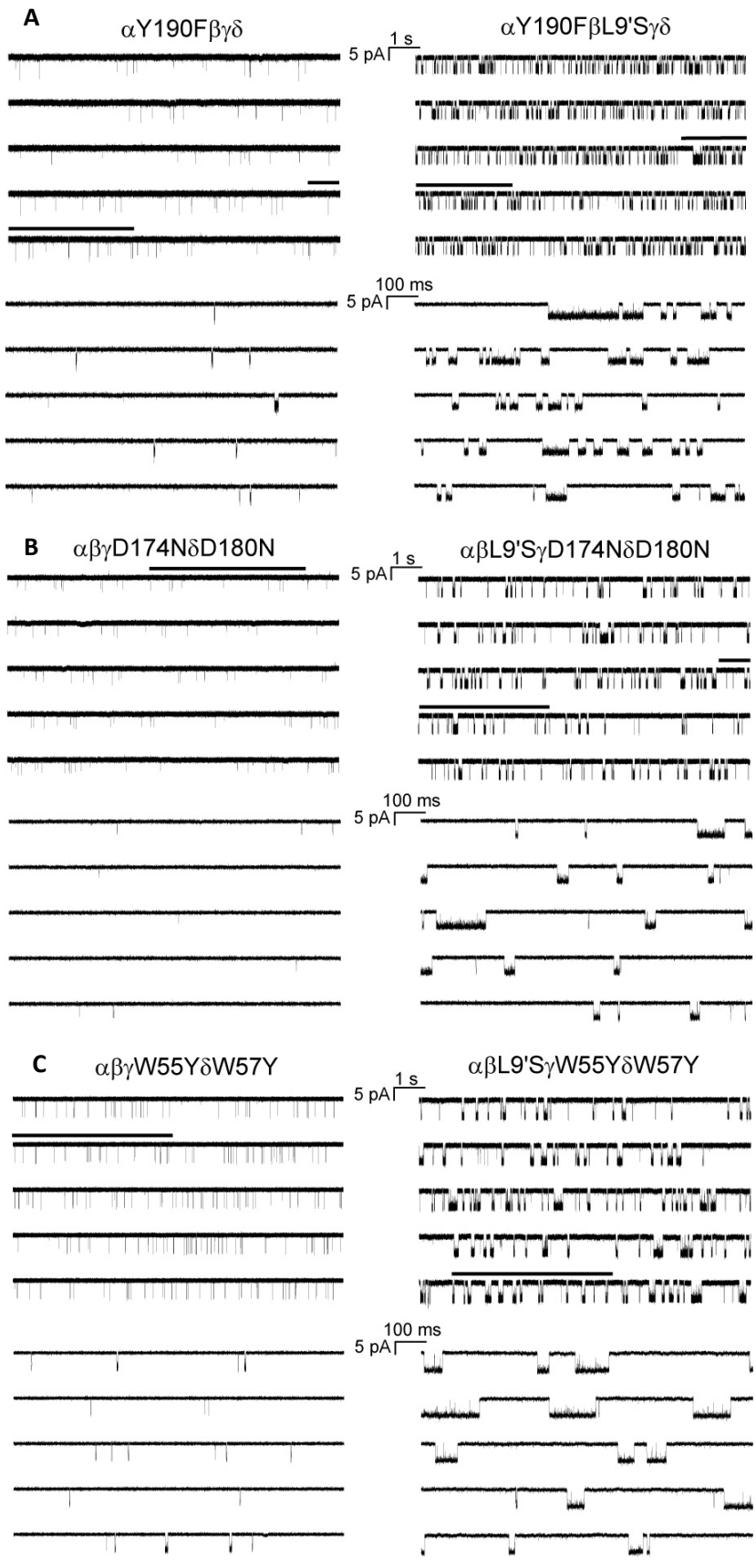

Figure 4.5: Single-channel currents for select mutants. In each case, ACh is applied at the macroscopic EC_{50} value (Table 4.1), and the left panel has no reporter mutation while the right panel is for receptors with the βL9'S reporter mutation. For each of the 6 receptors, the lower trace (5s) depicts an expansion of the section of the upper trace indicated with a line. Records were obtained in the cell-attached configuration with a pipette potential of + 100 mV and are shown at 5 kHz bandwidth. Channel openings are shown as downward deflections.
(A) αY190F.
(B) γD174NδD180N.
(C) γW55YδW57Y.

Other reporter mutations support gating pathway assignments

An implication of this experimental strategy is that other residues in the transmembrane domain that substantially increase Θ could act as reporters for extracellular domain residues; we are not limited to the β subunit or the well-characterized L9' position. To test this notion, L9'S mutations were made in the α, γ, and δ subunits, and two other Ser mutations were made in the M2 helix of the α subunit at positions V13' and L16' (Figure 4.1). All of these mutations lower EC_{50} significantly, and all positions are confidently ascribed to be gating residues. As shown in Figure 6, the extracellular domain mutations that give significant Ω values with βL9'S also show significant Ω values with L9'S mutations present in the other subunits. Recalling that there are two α subunits, we find that there is a general coupling parameter sequence of $\beta \approx \delta > \alpha > \gamma$. Thus, subtle asymmetries between subunits exist regarding the L9' residues' contribution to gating, which are also reflected in the EC_{50} values of the various L9'S mutants (Table 4.1). If one considers positions other than 9', all the mutated gating pathway residues again produce meaningful Ω values, and the magnitude of their effect is consistently α9' > α16' > α13' (Figure 4.6).

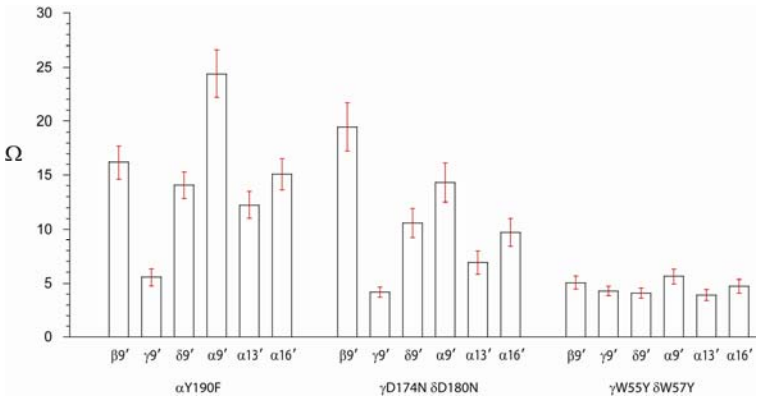

Figure 4.6: Values of Ω for various reporter mutations. For each of the three extracellular domain mutations, results for six different reporter mutations are shown. Reporter mutations are identified by their location, in each case, the mutation is of a hydrophobic residue to serine.

The reporter mutation βL9'S systematically increases I_{max} for gating pathway residues

This interpretation of the mutant cycle analysis data predicts other behaviors for extracellular gating pathway residues. For example, to produce a significant mutant cycle analysis coupling to L9' ($\Omega > 2$), the mutation in the extracellular domain must convert ACh to a partial agonist, such that the target mutation is now in the plateau region of Figure 4.2. Due to this decrease in Θ, the maximal current observed in response to saturating concentrations of ACh (I_{max}) should diminish. In general, interpreting differences in I_{max} can be challenging due to variations in whole-cell current among oocytes, which can stem from a variety of sources that may or may not relate to the actual mutation in question. However, use of a reporter mutation can assist in the interpretation of I_{max} differences. For mutations that render ACh a partial agonist, increasing efficacy through a reporter mutation produces a significant systematic increase in I_{max}. We find that these increases are larger and more consistent than the typical variability in I_{max} in conventional mutagenesis studies. Thus, if a receptor with a target mutation shows a large increase in mean I_{max} on introduction of a reporter mutation, the mutation likely affects gating. This is shown in Figure 4.7 for mutations with large Ω values, along with several examples with Ω near one. Recovery of I_{max} by introduction of the reporter mutation confirms the gating pathway residue assignments made by mutant cycle analysis. Moreover, the single-channel observations support this interpretation, in that the increase in NP_{open} is the microscopic correlate of the macroscopic observation of recovery of I_{max} (Table 4.2).

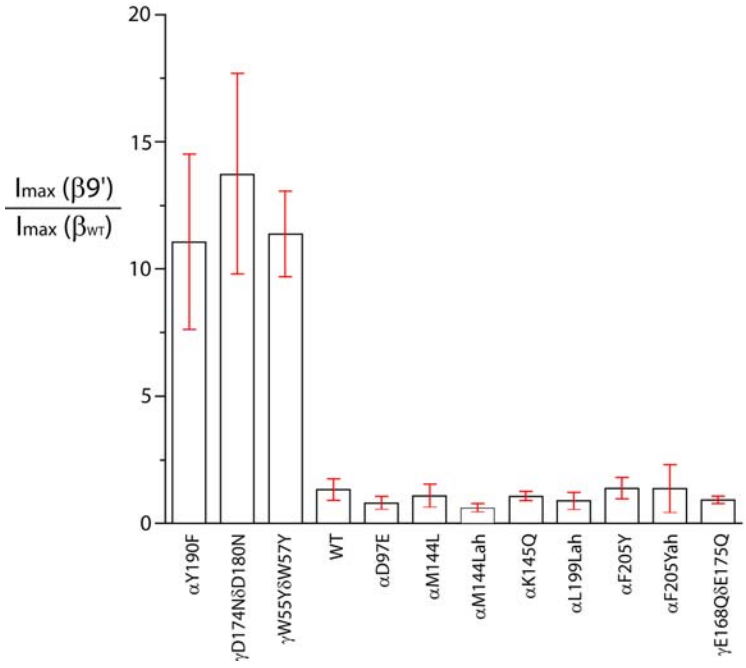

Figure 4.7: Variation in I_{max} in response to introduction of a βL9'S reporter mutation.

Experiments with the partial agonist succinylcholine support gating pathway assignments

Given the argument that a substantially deleterious mutation of a gating pathway residue converts the full agonist ACh to a partial agonist, which manifests as a diminished I_{max}, it is interesting to consider the behavior of an inherent partial agonist, such as succinylcholine (SuCh).[35] The relative efficacy, ε, of a partial agonist can be defined as the ratio of the maximal current elicited by a partial agonist (PA) to the maximal current elicited by a full agonist (FA; Eq. 4.2). At saturating doses of agonist, all the receptors are presumed to be in a diliganded state (A_2R), meaning that differences in I_{max} for the two agonists are due to differences in the probability that a single channel is open when the binding equilibrium is saturated, $P_{open,max}$. For wild type muscle nAChR, SuCh is a partial agonist with ~4% efficacy relative to ACh.

$$\varepsilon = \frac{I_{max,PA}}{I_{max,FA}} = \frac{P_{open,max,PA}}{P_{open,max,FA}}, \quad P_{open,max} = \frac{\beta}{\alpha+\beta} = \frac{\Theta}{\Theta+1} \tag{4.2}$$

In the presence of an αL9'S mutation alone, SuCh becomes a full agonist. Three of the five gating pathway residues were characterized using the partial agonist SuCh. Unlike what is observed for binding mutations, when αY190F, γD174NδD180N, and γW55YδW57Y contained a L→S mutation at either the 9' (α or β), 13' (α), or 16' (α) site, the recovery of SuCh toward full agonism is blocked. As before, the magnitude of the effect follows the trend α9' > α16' > α13' (data not shown). This is interpreted as further evidence that mutation of these extracellular domain residues drastically impairs normal gating function. Note that the efficacies of SuCh for the gating pathway mutants without the L9'S reporter mutation are not dramatically different from that of wild type (0.04 ± 0.02 for wild type, 0.04 ± 0.01 for αY190F, 0.02 ± 0.01 for γD174NδD180N, and 0.01 ± 0.0009 for γW55YδW57Y). This again highlights how the use of a reporter mutation can uncover important aspects of receptor function that might otherwise be missed.

4.4 Discussion

In the present work we propose that appropriately designed double mutant studies can provide valuable insights into the mechanism of action of an allosteric receptor. We begin with a mutation at a site whose function is unambiguous. Here, this reporter residue can be one of several sites in the transmembrane region of a ligand-gated ion channel, far removed from the agonist binding site. It is assumed that mutations at this site primarily, if not exclusively, perturb the gating of the receptor, and this view is supported by detailed studies of the reporter mutations. A second site, the target site, can then be probed by combining mutations there with a reporter mutation. Here we consider a number of target sites that are far removed from the reporter residue. Analysis of the results can proceed along several lines. The classical tool is a mutant cycle analysis. Indeed we find that, while most pairings of remote residues produce

independent behavior ($\Omega \sim 1$), for select target residues a mutant cycle analysis produces strong coupling parameters. Typically, such coupling is interpreted to indicate a direct interaction between the residues. However, in all cases here the residues are much too far apart to accommodate a direct structural interaction. As such, we have an allosteric coupling between remote residues, which manifests in a mutant cycle analysis just as if the two were structurally coupled. Of course, such action at a distance is the definitive feature of an allosteric system, but there are few cases where such pairwise interactions have been seen. Since the reporter mutation influences gating, coupling requires that the target residue also impact gating, allowing an apparent long-range interaction to be revealed in the mutant cycle analysis. We have labeled such residues as being on the "gating pathway," with the understanding that any mutation that preferentially stabilizes one state of the receptor could produce a positive result in ELFCAR, regardless of its location in the receptor. The particular residues studied here, however, do lie in regions of the receptor that have been considered to be part of the primary structural transduction from binding site to channel gate.

A less phenomenological analysis can be made with reference to Figure 4.2. The key here is that if the mutation at the target site perturbs gating by decreasing Θ, moving the system to the left along the EC_{50} vs. Θ curve, and, if the effect is large enough, the system will now be in the plateau region. Then, when the reporter mutation is added, its effect on EC_{50} will be diminished relative to what is seen in the receptor that is wild type at the target site. To be informative, the mutation at the target site must be loss of function (diminished Θ) and must have a substantial effect on gating. If Θ is diminished only slightly by the target mutation, or if Θ is increased (gain of function) the system will remain in the region of high slope, and the reporter mutation will have its normal effect. Also, when we do see significant coupling, that

does not rule out the possibility that K_D has changed in addition to Θ; ELFCAR can only establish that a significant decrease in Θ has occurred. At the same time, when a target mutation produces a large shift in EC_{50} but a conventional 40-fold additional shift on adding the βL9'S reporter mutation, it is tempting to conclude that the target mutation exclusively impacted K_D. However, changes in Θ that are significant but not large enough to move the system into the plateau region of Figure 4.2 could be involved in addition to or instead of a K_D change. For example, the K145Q mutation has been reported to impact gating,[26] but without moving Θ into the plateau region. In the present work, K145Q shows a marginal functional coupling with L9'S, with an Ω value near the cutoff for significance (1.9 ± 0.2). As such, ELFCAR is best suited to identifying mutations that strongly perturb gating (Ω>2); negative results should be interpreted cautiously. Note that in receptors for which the wild type Θ is smaller than in the muscle-type nAChR, ELFCAR would be expected to be more sensitive to small changes in Θ.

Several additional observations support our analysis of the results seen here. First, in a typical mutant cycle analysis, Ω values less than 1 can be observed and are functionally significant. However, in the present context, the model of Figure 2 allows only for $\Omega > 1$, which is consistent with our data. Importantly, three mutations shown here to impact gating by the ELFCAR approach have been confirmed to be gating mutations by single-channel analyses. The single-channel values we report are NP_{open}. The true probability that a single channel is open at these concentrations, P_{open}, is increased by a factor of N, where N is the number of channels in the patch. Because the measured probability that the channel is open is very low ($\leq$2%) for the gating pathway mutations without the reporter mutation, the number of channels in the patch cannot be exactly determined. However, if there are actually multiple channels in these patches, our NP_{open} values would be overestimates of P_{open}. The measured NP_{open} values are substantially

diminished upon addition of each of the three target residues we tested (αY190F, γD174NδD180N, and γW55YδW57Y), such that the modest perturbation of EC_{50} associated with the target mutations can be primarily ascribed to dramatic changes in the gating pathway. Other single-channel studies of residues considered here are also consistent with our findings.

Other observations support our general model. If a target mutation substantially reduces Θ, then ACh should become a partial agonist at the receptor. This should lead to reduced maximal currents from whole-cell recordings, and just such an effect is seen. Also, an inherent partial agonist should be sensitive to the consequences of the target mutation, and we find that is indeed the case for SuCh.

It is interesting to consider the residues that have been probed here; Figure 4.1 highlights them all. The considerable distance between the reporter residues and the target residues is clear from this image. Concerning the target residues, those with no strong coupling (purple) are dispersed throughout the extracellular domain, and, although only five have been identified so far, the same is true of the gating pathway residues (orange). There is no simple pattern that distinguishes the two classes.

The agonist binding site of the nAChR is an "aromatic box," shaped by five, conserved aromatic residues: αY93 (A), αW149 (B), αY190 (C1), αY198 (C2) and γW55/δW57 (D).[7, 36] The letter designations signify the "loop" of the extracellular domain that contains the particular residue[37]. Since all the natural agonists of Cys-loop receptors have a cationic group, the presence of the aromatic box suggested that a cation-π interaction contributes to agonist binding.[38, 39] Indeed, αW149 (B) and the aligning residues have been shown to contribute to agonist binding through a cation-π interaction in both the nAChR and the 5-HT_3 receptors.[22, 40] We find Ω~1, consistent with a binding role for this residue. Note that subtle mutations have

been employed at this site, taking advantage of the power of unnatural amino acid mutagenesis.

We cannot rule out the possibility that more disruptive mutations at this and other sites would impact receptor gating. Indeed, the αW149F mutation has been probed, and it impacts both binding and gating.[41] Most of the mutations in Table 4.1 are, by conventional standards, relatively subtle, and we would argue that some caution must by employed in interpreting the consequences of more severe mutations.

The residue analogous to αY198 (C2) has been shown to bind serotonin through a cation-π interaction in the MOD-1 receptor[42]. Previous studies in the nAChR show that mutations at this site exhibit normal coupling to L9'S mutations.[43] Single-channel studies of the αY198F mutant indicate only modest changes in gating[24] that would be outside the limits of detection for ELFCAR.

The residue αY93 (A) has been extensively probed. In the $GABA_A$ receptor the analogous residue makes a cation-π binding interaction to the native agonist.[44] In the nAChR, side chain mutations at this site strongly impact channel gating. However, the mutation studied here – αY93Yah – is a *backbone* mutation. Our finding of Ω~1 indicates no strong perturbation of gating by a backbone mutation in this region. This conclusion is supported by the similar result at the adjacent residue (αN94Nah).

The remaining two box residues, αY190 (C1) and γW55/δW57 (D), have never been shown to make a cation-π interaction with an agonist. Both are clearly assigned as gating pathway residues according to the ELFCAR method. αY190 has been extensively studied. That αY190F strongly impacts gating is unambiguously established by the single-channel records of Figure 4.5A. Other workers have also found strong perturbations to gating for mutations at this site .[25, 26] Some studies have also found a contribution to binding, but, as discussed above, the

present work does not address this issue. The important point is that the finding of a large Ω value in ELFCAR is fully supported by single channel studies. In addition, a backbone mutation at the adjacent residue, αS191Sah, also produces a large Ω value in ELFCAR. We have recently shown that this residue makes a strong hydrogen bond to a side chain from the complementary subunit (γ/δ), and that the hydrogen bond contributes significantly to gating.[45] Most gating models for the nAChR invoke considerable movement of loop C,[7, 46, 47] and the finding of large Ω values for these two loop C residues is consistent with these models.

The final binding box residue, γW55/δW57 (D), shows a large Ω value for the Tyr mutant. Our single-channel studies (Figure 4.5C) clearly establish an impact on gating for this mutation. Previous single-channel studies of the Phe mutant show a small effect on binding (3.4 fold) and a very large effect on gating (50-fold),[48] consistent with the present results. There is reason to anticipate that loop D may also undergo significant rearrangements during gating. In Unwin's image of the *Torpedo* nAChR,[1] with no agonist bound, TrpD is flipped out away from the box that is so well formed in AChBP (with or without agonist bound). This again suggests that movement of TrpD occurs on ligand binding, consistent with it being a gating pathway residue.

The fifth gating pathway residue we identified, αD200, is not part of the aromatic binding box, but appears to lie outside the box. However, it is part of a triad of residues that includes αY190 and αK145 and that has been suggested to undergo significant rearrangement on gating.[26] Previous single-channel studies have shown that mutation at this site perturbs gating.[23, 26] As such, the large Ω seen here with ELFCAR is fully consistent with other studies.

In the present work, we have developed an efficient strategy for identifying mutations that impact receptor function by significantly impeding the gating pathway. The method involves combining mutations of extracellular domain residues proposed to be functionally

important with a known gating pathway (reporter) mutation. For interesting sites, ELFCAR can provide guidance for more focused, advanced studies, such as detailed unnatural amino acid mutagenesis of putative binding residues or single-channel analysis, where possible, for gating residues.

The kinetic model of Scheme 4.1 refers to the nAChR, but it contains the essential features of any allosteric system. There is a binding interaction with an allosteric effector and an intrinsic conformational change associated with the signaling event. The former is a bimolecular association, and so is saturable at high ligand concentration. However, the conformational change is unimolecular, and so it is an intrinsic property of the system. It is the combination of these two processes that produces the curvature of Figure 4.2 and thus allows for the specific application of mutant cycle analysis presented here. As such, we anticipate that the same approach could be applied to other allosteric systems, allowing a facile means to identify the roles of particular residues in a complex protein system. Thus, while this study has focused exclusively on a single Cys-loop receptor, we believe the approach is broadly applicable to other Cys-loop receptors and to allosteric receptors in general. Certainly, comparable reporter residues can be found in the other Cys-loop receptors; the L9' residue is highly conserved and it seems likely to play an important gating role throughout the family. We emphasize that, although all members of the Cys-loop family are genetic orthologs, functional paralogs, and structural homologs, there is growing evidence that the detailed mechanisms of action will vary from system to system.[39] Thus, the present approach, based on the readily obtained EC_{50} measure, offers a robust and efficient way to search for such variations in gating mechanism.

Target Mutation	WT EC_{50}	EC_{50} with Reporter Mutation	Ratio	Ω
		βL9'S		
wild type	46	1.2	38	1.00
γD174NδD180N	590	160	3.7	11
αY190F	1200	520	2.3	17
γW55YδW57Y	180	24	7.5	5.1
αD200N	130	29	4.5	8.6
αS191Sah	300	50	6.0	6.4
αE45W	120	3	40	0.96
αY93Yah	39	1	39	0.98
αN94Nah	87	2.2	40	0.97
αD97E	3.3	0.09	37	1.0
αM144L	15	0.37	41	0.95
αM144Lah	50.4	1.3	39	0.99
αK145Q	170	8.1	21	1.8
αL146Lah	26	0.5*	52	0.74
αT148Tah	33	1.3	25	1.5
αW149Wah	36	0.72	50	0.77
αW149 5-F-Trp	200	4.7	43	0.90
αW149 5-Br-	88	2	44	0.87
αL199Lah	11	0.18	61	0.63
αT202Tah	24	0.48	50	0.77
αY203Yah	39	0.62	63	0.61
αF205Yah	67	1.4	48	0.80
αF205Y	90	1.5	60	0.64
αV206Vah	170	3.1	55	0.70
γL36δL39Lah	28	0.63	44	0.86
γI56δI58Iah	33	0.83	40	0.96
γA121δA124Aah	25	0.66	38	1.0
γE168QδE175Q	42	1.2	35	1.1
		γL9'S		
wild type	46	4.5	10	1.0
γD174NδD180N	590	244	2	4.2
αY190F	1200	650	2	5.5
γW55YδW57Y	180	74	2	4.2
		δL9'S		
wild type	46	1	46	1.0
γD174NδD180N	590	140	4	11
αY190F	1200	370	3	14
γW55YδW57Y	180	16	11	4.1
		αL9'S		
wild type	46	0.35	131	1.0
γD174NδD180N	590	65	9	14
αY190F	1200	223	5	24
γW55YδW57Y	180	7.5	24	5.5
		αV13'S		
wild type	46	0.1	460	1.0
γD174NδD180N	590	8.9	66	7
αY190F	1200	32	38	12
γW55YδW57Y	180	1.5	120	3.8
		αL16'S		
wild type	46	0.47	98	1.0
γD174NδD180N	590	59	10	10
αY190F	1200	190	6	15
γW55YδW57Y	180	8.5	21	4.6

Table 4.1: EC_{50} values with and without βL9'S reporter mutation for coupled and non-coupled residues. Values for the 3 coupled residues are also given for reporter mutations in all other subunits (γ, δ, and α) and positions (9', 13', and 16'). The ratio of EC_{50}s: target/(target with reporter) and resultant calculated Ω values are also reported. The standard error for all EC_{50} values was <10%, except for *, which had standard error of 20%. Data at sites α148(51), α149(24), and αS191(47) have been reported previously

Mutant	Ω	I_{max} ratio	NP_{open}	NP_{open} βL9'S
αY190F	17	11	0.0026 ± 0.0006	0.18 ± 0.04
γD174NδD180N	11	13	0.0007 ± 0.0005	0.08 ± 0.06
γW55YδW57Y	5	12	0.018 ± 0.005	0.26 ± 0.06

Table 4.2: Coupling parameter, Ω, and I_{max} ratio from whole-cell data. NP_{open} values (± SEM) at respective macroscopic EC_{50} values (Table 4.1).

4.5 Materials and Methods

Site-Directed Mutagenesis

Fetal mouse muscle nicotinic acetylcholine receptor (nAChR) α, β, γ, δ subunits were utilized in the experiments. Each subunit was expressed in pAMV vectors. Mutations were made at the site of interest using a standard Stratagene QuikChange protocol. For the incorporation of unnatural residues, the site of interest was mutated to the amber stop codon. In addition, the α subunits contain an HA epitope in the M3-M4 cytoplasmic loop for Western blot studies. Control experiments show that this epitope does not detectably alter EC_{50}. Primers were designed to fulfill the established criteria and were ordered from Integral DNA technologies. Polymerase chain reaction (PCR) reactions were carried out using a high fidelity Pfu DNA polymerase, and a 10 minute extension time was used in each thermocycle. Annealing temperatures were modified as required for successful incorporation of the mutation. DpN1 digestion was used to eliminate methylated template DNA from the PCR products. Following PCR purification (Qiagen standard protocol), amplification of the PCR product was conducted by electroporation with Super Competent Top 10 *E. coli* followed by 12 h of growth on agar/LB/ampicillin plates. Single colonies were selected and amplified in liquid LB/ampicillin

culture. The DNA was isolated from the bacteria (Qiagen, miniprep kit), and sequenced to verify the successful incorporation of the mutation at the selected site.

The circular bacterial plasmid of the mutation-containing DNA was linearized using a Not1 restriction enzyme. Linearized plasmids were used as the DNA template for *in vitro* transcription using T7 mMessage mMachine enzyme kits (Ambion) to make mRNA. Quantification of mRNA was determined using a NanoDrop spectrophotometer (NanoDrop Technologies, Thermo Scientific, Wilmington, DE).

For conventional mutations, the stoichiometry of subunits was 2:1:1:1 of α:β:γ:δ by mass with a total mRNA concentration of ~2 μg/μL. For unnatural mutations,[49] a total of 40 ng of mRNA in a 10:1:1:1 α:β:γ:δ subunit ratio was coinjected with the synthetic α-hydroxy acids conjugated to the dinucleotide dCA and ligated to truncated 74-nucleotide tRNA as previously described. Ratios of mRNA to tRNA were typically 1:1.

Stage V-VI oocytes of *Xenopus laevis* (Nasco, Fort Atkinson, WI) were injected with 50 nL of the mRNA or mRNA/tRNA mixture and subsequently incubated for a period of 12- 36 h, depending on the mutation site. The oocytes were incubated in culture media containing 1-2% horse serum at 18 ˚C.

Whole-cell electrophysiology

Whole-cell electrophysiological recordings were performed on injected *Xenopus laevis* oocytes after 12 - 36 h incubation. Recording was done in two-electrode voltage clamp mode using the OpusXpress 6000A (Axon Instruments, Union City, CA). Oocytes were superfused with Ca^{2+}-free ND96 solution (in mM: 96 NaCl, 2 KCl, 1 $MgCl_2$, 5 HEPES) at flow rates of 4 mL/min during drug application (15 s) and 3 mL/min during wash (130 s). Macroscopic agonist-induced

currents were recorded in response to bath application of the indicated agonist concentrations at -60 mV or -80 mV. Data were sampled at 125 Hz and filtered at 50 Hz. ACh chloride and SuCh chloride were purchased from Sigma/Aldrich/RBI (St. Louis, MO). Agonist solutions ranging from 0.0100 to 5000 μM were prepared in Ca^{2+}-free ND96 from a 1 M stock solution. Dose-response relations were constructed for each mutation using data from $\geq$5 oocytes. Dose-response relations were fitted to the Hill equation (Eq. 4.3) to determine the EC_{50} and the Hill coefficient.

$$I/I_{max} = 1/(1+(EC_{50}/[A])^{n_H}) \quad (4.3)$$

where I is the current for agonist concentration [A], I_{max} is the maximum current, EC_{50} is the concentration to elicit half maximal response, and n_H is the Hill coefficient. The dose-response relations of individual oocytes were examined and used to determine outliers. The reported EC_{50} values are from the curve fit of the averaged data.

Single-channel characterization of selected gating pathway residue mutants

Single-channel recording was performed in the cell-attached configuration on devitellinized oocytes 24-60 h after injection at 20 ± 3°C with an applied pipette potential of +100 mV, as described previously.[50] Pipettes were fabricated from thick-walled (I.D. = 0.80 mm, O.D. = 1.60 mm) KG-33 glass (Garner Glass Company, Claremont, CA) and coated with Sylgard (World Precision Instruments, Sarasota, FL); they had resistances of 8-25 MΩ. The bath solution contained, in mM, 120 KCl, 5 HEPES, 1 $MgCl_2$, 2 $CaCl_2$, pH = 7.4, so that the transmembrane potential of the patch was -100 mV and the reversal potential for agonist-induced currents was ~0 mV. The pipette solution contained, in mM, 100 KCl, 10 HEPES, 1 $MgCl_2$, 10 K_2EGTA, pH = 7.4 and was supplemented with the indicated concentrations of ACh using a 1 M stock solution.

Prior to single-channel recording, whole-cell expression levels were determined with 100-1000 μM ACh doses using the whole-cell recording conditions on each mutant. When whole-cell expression exceeded ~300 nA for receptors with the target mutation alone and ~3 μA for receptors with both a target mutation and a reporter mutation, oocytes were typically incubated 4-10 additional h prior to single-channel recording. Data were collected using a GeneClamp 500B amplifier (Axon Instruments, Union City, CA) with a CV-5 GU headstage at full bandwidth (4-pole Bessel, -3 dB, 50 kHz). The signal was then low-pass filtered (8-pole Bessel, -3 dB, 20 kHz) and sampled with a Digidata 1320A and Clampex 9.2 (Axon Instruments, Union City, CA) at 50 or 100 kHz. Only recordings that showed no simultaneous activations were included in NP_{open} analysis. In this manner ≥3 patches at EC_{50} were analyzed for all mutants, except for the αβγD174NδD180N and αβL9'SγD174NδD180N mutants for which 2 patches each were obtained. Data were filtered offline (Gaussian, -3 dB, 5 kHz) and electrical interference at harmonics of 60 Hz was removed, if necessary. Event transitions were detected with Clampfit 9.2 (single-channel search). A dead time, t_d, of 40 μs was applied to all events. The time-average probability that exactly one channel in the patch is open (NP_{open}) was calculated as the total open time divided by the total closed time.

Acknowledgements

We thank B.N. Cohen for advice on single-channel recording and analysis. This work was supported by the NIH (NS 34407; NS 11756). J.A.P.S. was partially supported by an NRSA training grant. K.R.G. was partially supported by an NSF Graduate Research Fellowship.

4.6 References

1. Unwin, N. Refined structure of the nicotinic acetylcholine receptor at 4 angstrom resolution. *Journal of Molecular Biology* **346**, 967-989 (2005).
2. Connolly, C.N. & Wafford, K.A. The Cys-loop superfamily of ligand-gated ion channels: the impact of receptor structure on function. *Biochemical Society Transactions* **32**, 529-534 (2004).
3. Grutter, T. & Changeux, J.P. Nicotinic receptors in wonderland. *Trends Biochem Sci* **26**, 459-63 (2001).
4. Lester, H.A., Dibas, M.I., Dahan, D.S., Leite, J.F. & Dougherty, D.A. Cys-loop receptors: new twists and turns. *Trends in Neurosciences* **27**, 329-336 (2004).
5. Sine, S.M. & Engel, A.G. Recent advances in Cys-loop receptor structure and function. *Nature* **440**, 448-455 (2006).
6. Changeux, J.P. & Edelstein, S.J. Allosteric mechanisms of signal transduction. *Science* **308**, 1424-1428 (2005).
7. Sixma, T.K. & Smit, A.B. Acetylcholine binding protein (AChBP): a secreted glial protein that provides a high-resolution model for the extracellular domain of pentameric ligand-gated ion channels. *Annu Rev Biophys Biomol Struct* **32**, 311-34 (2003).
8. Peters, J.A., Hales, T.G. & Lambert, J.J. Molecular determinants of single-channel conductance and ion selectivity in the Cys-loop family: insights from the 5-HT3 receptor. *Trends Pharmacol Sci* **26**, 587-94 (2005).
9. Chang, Y. & Weiss, D.S. Channel opening locks agonist onto the GABAC receptor. *Nat Neurosci* **2**, 219-25 (1999).
10. Davies, P.A. et al. The 5-HT3B subunit is a major determinant of serotonin-receptor function. *Nature* **397**, 359-63 (1999).
11. Keramidas, A. & Harrison, N.L. Agonist-dependent single channel current and gating in alpha4beta2delta and alpha1beta2gamma2S GABAA receptors. *J Gen Physiol* **131**, 163-81 (2008).
12. Legendre, P. The glycinergic inhibitory synapse. *Cell Mol Life Sci* **58**, 760-93 (2001).
13. Li, G. & Niu, L. How fast does the G1uR1Q(flip) channel open? *Journal of Biological Chemistry* **279**, 3990-3997 (2004).
14. Filatov, G.N. & White, M.M. The role of conserved leucines in the M2 domain of the acetylcholine receptor in channel gating. *Mol Pharmacol* **48**, 379-84 (1995).
15. Labarca, C. et al. Channel gating governed symmetrically by conserved leucine residues in the M2 domain of nicotinic receptors. *Nature* **376**, 514-6 (1995).
16. Kalbaugh, T.L. Ligand-binding residues integrate affinity and efficacy in the NMDA receptor. *Molecular pharmacology* **66**, 209-219 (2004).
17. Edelstein, S.J., Schaad, O. & Changeux, J.P. Single binding versus single channel recordings: a new approach to study ionotropic receptors. *Biochemistry* **36**, 13755-60 (1997).
18. Mitra, A., Cymes, G.D. & Auerbach, A. Dynamics of the acetylcholine receptor pore at the gating transition state. *Proc Natl Acad Sci U S A* **102**, 15069-74 (2005).
19. Kosolapov, A.V., Filatov, G.N. & White, M.M. Acetylcholine receptor gating is influenced by the polarity of amino acids at position 9' in the M2 domain. *J Membr Biol* **174**, 191-7 (2000).
20. Sigurdson, W., Chen, J., Akabas, M., Karlin, A. & Auerbach, A. Single-Channel Kinetic-Analysis of Mouse Achr M2 Mutants Alpha-L251c and Alpha-S248c. *Biophysical Journal* **66**, A212-A212 (1994).

21. Kearney, P.C. et al. Dose-response relations for unnatural amino acids at the agonist binding site of the nicotinic acetylcholine receptor: tests with novel side chains and with several agonists. *Mol Pharmacol* **50**, 1401-12 (1996).
22. Zhong, W. et al. From ab initio quantum mechanics to molecular neurobiology: a cation-pi binding site in the nicotinic receptor. *Proc Natl Acad Sci U S A* **95**, 12088-93 (1998).
23. Akk, G., Sine, S. & Auerbach, A. Binding sites contribute unequally to the gating of mouse nicotinic alpha D200N acetylcholine receptors. *J Physiol* **496 (Pt 1)**, 185-96 (1996).
24. Akk, G., Zhou, M. & Auerbach, A. A mutational analysis of the acetylcholine receptor channel transmitter binding site. *Biophys J* **76**, 207-18 (1999).
25. Chen, J., Zhang, Y., Akk, G., Sine, S. & Auerbach, A. Activation kinetics of recombinant mouse nicotinic acetylcholine receptors: mutations of alpha-subunit tyrosine 190 affect both binding and gating. *Biophys J* **69**, 849-59 (1995).
26. Mukhtasimova, N., Free, C. & Sine, S.M. Initial coupling of binding to gating mediated by conserved residues in the muscle nicotinic receptor. *J Gen Physiol* **126**, 23-39 (2005).
27. O'Leary, M.E. & White, M.M. Mutational analysis of ligand-induced activation of the Torpedo acetylcholine receptor. *J Biol Chem* **267**, 8360-5 (1992).
28. Sine, S.M. et al. Naturally occurring mutations at the acetylcholine receptor binding site independently alter ACh binding and channel gating. *J Gen Physiol* **120**, 483-96 (2002).
29. Xie, Y. & Cohen, J.B. Contributions of Torpedo nicotinic acetylcholine receptor gamma Trp-55 and delta Trp-57 to agonist and competitive antagonist function. *J Biol Chem* **276**, 2417-26 (2001).
30. Chapman, E., Thorson, J.S. & Schultz, P.G. Mutational Analysis of Backbone Hydrogen Bonds in Staphylococcal nuclease. *J. Am. Chem. Soc.* **119**, 7151-7152 (1997).
31. England, P.M., Zhang, Y., Dougherty, D.A. & Lester, H.A. Backbone mutations in transmembrane domains of a ligand-gated ion channel: implications for the mechanism of gating. *Cell* **96**, 89-98. (1999).
32. Kash, T.L., Jenkins, A., Kelley, J.C., Trudell, J.R. & Harrison, N.L. Coupling of agonist binding to channel gating in the GABA(A) receptor. *Nature* **421**, 272-5 (2003).
33. Price, K.L., Millen, K.S. & Lummis, S.C. Transducing agonist binding to channel gating involves different interactions in 5-HT3 and GABAC receptors. *J Biol Chem* **282**, 25623-30 (2007).
34. Venkatachalan, S.P. & Czajkowski, C. A conserved salt bridge critical for GABAA receptor function and loop C dynamics. *Proc Natl Acad Sci U S A* **105**, 13604-9 (2008).
35. Xiu, X., Hanek, A.P., Wang, J., Lester, H.A. & Dougherty, D.A. A unified view of the role of electrostatic interactions in modulating the gating of Cys loop receptors. *J Biol Chem* **280**, 41655-66 (2005).
36. Brejc, K. et al. Crystal structure of an ACh-binding protein reveals the ligand-binding domain of nicotinic receptors. *Nature* **411**, 269-76 (2001).
37. Corringer, P.J., Le Novere, N. & Changeux, J.P. Nicotinic receptors at the amino acid level. *Annu Rev Pharmacol Toxicol* **40**, 431-58 (2000).
38. Dougherty, D.A. & Stauffer, D.A. Acetylcholine binding by a synthetic receptor. Implications for biological recognition. *Science* **250**, 1558-1560 (1990).
39. Dougherty, D.A. Cys-loop neuroreceptors: structure to the rescue? *Chem Rev* **108**, 1642-53 (2008).
40. Beene, D.L. et al. Cation-pi interactions in ligand recognition by serotonergic (5-HT3A) and nicotinic acetylcholine receptors: The anomalous binding properties of nicotine. *Biochemistry* **41**, 10262-10269 (2002).
41. Akk, G. Aromatics at the murine nicotinic receptor agonist binding site: mutational analysis of the alphaY93 and alphaW149 residues. *J Physiol* **535**, 729-40 (2001).

42. Mu, T.W., Lester, H.A. & Dougherty, D.A. Different binding orientations for the same agonist at homologous receptors: a lock and key or a simple wedge? *J Am Chem Soc* **125**, 6850-1 (2003).
43. Kearney, P.C., Zhang, H., Zhong, W., Dougherty, D.A. & Lester, H.A. Determinants of nicotinic receptor gating in natural and unnatural side chain structures at the M2 9' position. *Neuron* **17**, 1221-9 (1996).
44. Padgett, C.L., Hanek, A.P., Lester, H.A., Dougherty, D.A. & Lummis, S.C.R. Unnatural amino acid mutagenesis of the GABA(A) receptor binding site residues reveals a novel cation-pi interaction between GABA and beta(2)Tyr97. *Journal of Neuroscience* **27**, 886-892 (2007).
45. Gleitsman, K.R., Kedrowski, S.M.A., Lester, H.A. & Dougherty, D.A. An Intersubunit Hydrogen Bond in the Nicotinic Acetylcholine Receptor that Contributes to Channel Gating *J Biol Chem* **283**, 35638-43 (2008).
46. Gao, F. et al. Agonist-mediated conformational changes in acetylcholine-binding protein revealed by simulation and intrinsic tryptophan fluorescence. *J Biol Chem* **280**, 8443-51 (2005).
47. Miyazawa, A., Fujiyoshi, Y. & Unwin, N. Structure and gating mechanism of the acetylcholine receptor pore. *Nature* **423**, 949-55 (2003).
48. Akk, G. Contributions of the non-alpha subunit residues (loop D) to agonist binding and channel gating in the muscle nicotinic acetylcholine receptor. *J Physiol* **544**, 695-705 (2002).
49. Nowak, M.W. et al. *In vivo* incorporation of unnatural amino acids into ion channels in a *Xenopus* oocyte expression system. *Methods Enzymol* **293**, 504-529 (1998).
50. Hamill, O.P., Marty, A., Neher, E., Sakmann, B. & Sigworth, F.J. Improved patch-clamp techniques for high resolution current recording from cells and cell-free membrane patches. *Pflugers Arch.* **391**, 85-100 (1981).

Chapter 5: Probing the Role of the Peptide Backbone in the Aromatic Binding Box of the nAChR

5.1 Introduction

The residues that are involved in agonist-binding in the nicotinic acetylcholine receptor (nAChR) have been known for over two decades.[1] Even before any structural data were available, researchers had identified several key aromatic residues important to agonist binding. These amino acids include αY93, αW149, αY190, αY198, and γW55 and δW57. The AChBP crystal structure confirmed the importance of these residues and indicated they form a box like configuration around the agonist.[2] This "aromatic binding box" is shown in Figure 5.1. The recent crystal structures of AChBP with and without agonist bound and decades of careful biochemical studies have yielded a substantial amount of information about the interactions between nAChR and agonist.

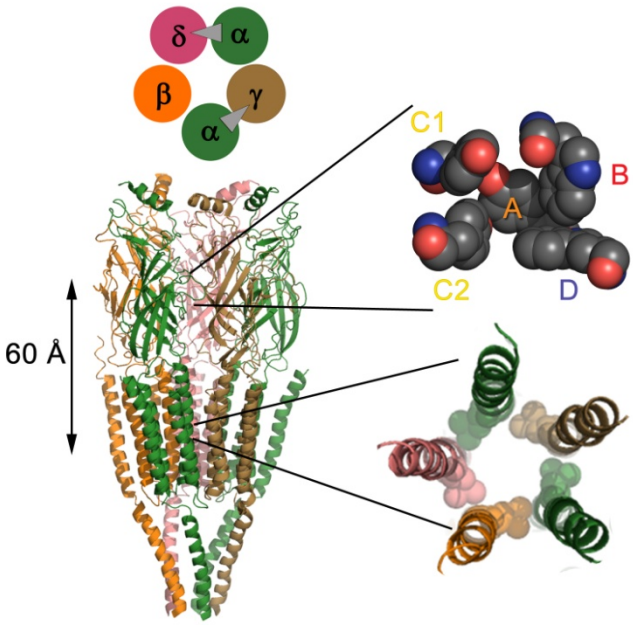

Figure 5.1: Overall structure of the muscle nAChR. The location of the aromatic binding box (upper right) and the putative channel gate (lower right) are indicated.

Considerably less is known about how the conformational changes that accompany binding interface with channel gating. Single channel electrophysiology of the nAChR coupled

with linear free energy analysis has inspired the idea that a "conformational wave," a series of progressive conformational changes originating at the binding site and terminating at the channel gate, is responsible for coupling agonist binding to channel opening.[3, 4] Linear free energy analysis indicates that blocks of residues encompassing the agonist binding site move early in the gating transition, that is, the motions that initiate the conformational wave originate in the vicinity of aromatic binding box. In further support of this idea, the side chains of three residues near the acetylcholine binding site, αY190, αD200, and αK145, have been shown to influence gating and are proposed to initiate the allosteric cascade that links binding to gating.[5] In addition to the importance of specific side chains present near the binding site, significant movement along the protein backbone is probably necessary to propagate the conformational changes that result in channel gating.

To interrogate the role of the peptide backbone in the agonist binding site in initiating the gating cascade, ten individual ester mutations were made to the backbone of the aromatic box residues and their i+1 neighbors. Combined, these mutations disrupted the hydrogen bonding ability at all non-carbon backbone positions of the aromatic box residues; the ester mutation at the box residue directly eliminates a hydrogen bond donor and the ester mutation at the i+1 residue decreases the hydrogen bonding ability of the adjacent carbonyl (of the box residue). In addition, the incorporation of a backbone ester endows a greater amount of backbone flexibility by removing the pronounced amide resonance. The conjugation of the H-N-C=O moiety in amides leads to a significantly higher barrier to interconversion between the trans and cis isomers, although the trans preferences in esters is stronger than in amides for steric reasons. Thus, if backbone motions in the aromatic binding box are important for

initiating the conformational changes that transduce agonist binding into channel opening, ester incorporation at these sites will significantly impact receptor function.

5.2 Results and Discussion

5.2.1 α-Hydroxy Incorporation at Aromatic Box Residues in the Primary Subunit.

Ester mutations were made at the aromatic box residues, αY93, αW149, αY190, αY198, and their i +1 neighbors, αN94, αT150, αS191, αL199, in the primary binding subunit. One ester mutation, at αS191, led to a severe loss of function and an impairment of channel gating. The backbone NH at this residue was found to make an important intersubunit hydrogen bond and is discussed in detail in Chapter 2. However, the majority of the α-hydroxy mutations at these sites produced very little effect on receptor function (less than 2-fold change in EC_{50}, Figure 5.2 and Table 5.1). Two sites, αT150 and αL199, had intermediate effects on receptor function, producing approximately 5-fold shifts in EC_{50} values. An ELFCAR analysis[6] (see Chapter 4) revealed that, with the exception of the αS191Sah mutation, the loss-of-function mutants had normal Ω-values, indicating that ester incorporation does not severely impair the gating behavior of these receptors.

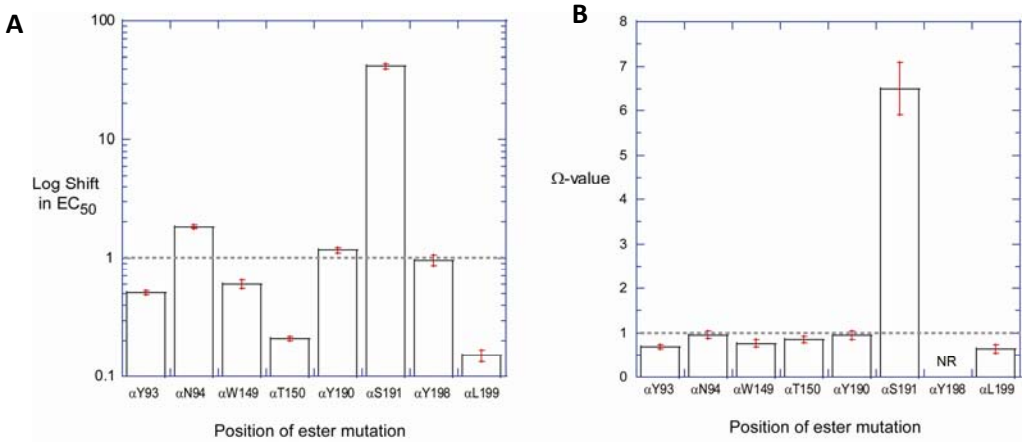

Figure 5.2: A) The log fold shifts in EC_{50} values for α-hydroxy mutations in the α-subunit. B) The corresponding Ω-values for these mutations.

Table 5.1: Fold shifts in EC_{50} values and Ω-values for backbone ester mutations in the α-subunit

Position of ester mutation	EC_{50} Shift	Ω-value
αY93	0.51 ± 0.02	0.69 ± 0.05
αN94	1.8 ± 0.07	0.96 ± 0.08
αW149	0.60 ± 0.05	0.77 ± 0.08
αT150	0.21 ± 0.009	0.86 ± 0.08
αY190	1.2 ± 0.07	0.95 ± 0.09
αS191	42 ± 2	6.5 ± 0.6
αY198	0.96 ± 0.1	NR
αL199	0.15 ± 0.02	0.64 ± 0.09

The αT50Tah mutation has been studied previously.[7, 8] Originally the backbone NH of this residue combined with the backbone NH of neighboring αW149 was proposed to interact with a critical aspartate residue (αD89) to promote an efficient interaction between αW149 and agonist.[9] However, experimental work does not corroborate this hypothesis. Instead, αT150 and αW149 backbone amides seem to belong to a network of redundant hydrogen bonds in this region that hold the side chain of αW149 in place for agonist binding.[8]

An approximately five fold decrease in EC_{50} was observed for the α-hydroxy mutant of αL199, indicating a moderate gain-of-function. None of the existing structures (Torpedo cryo-EM,[10] AChBP crystal structures,[11] or the α_1 mm nAChR crystal structure[12]) show any hydrogen bonds to the backbone NH of αL199. A further analysis of the hydrogen bonds to the protein backbone at αL199 in a 7 ns MD simulation of a homology model of the muscle nAChR extracellular domain (see Chapter 6) further shows very little hydrogen bonding to the NH throughout the trajectory (Figure 5.3A).

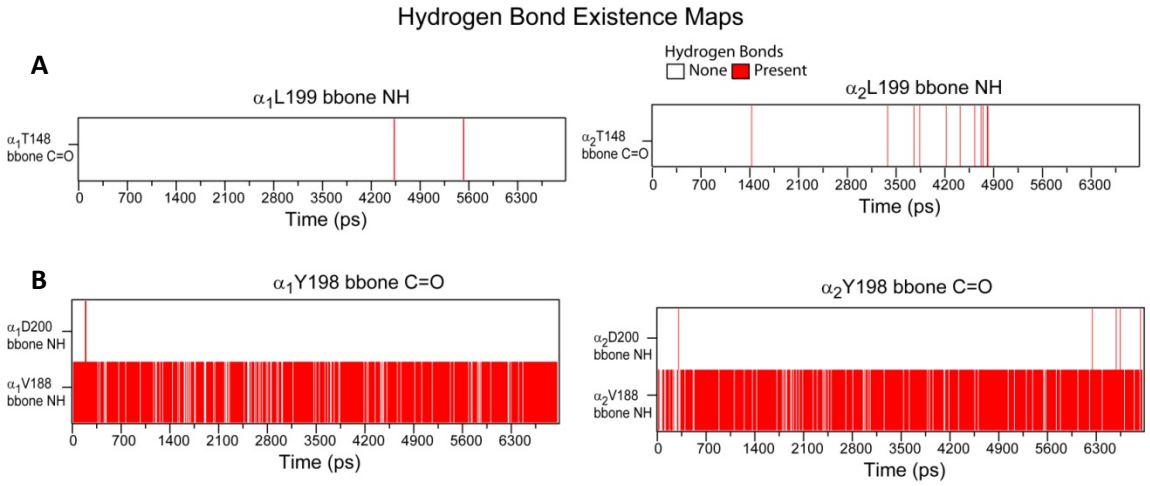

Figure 5.3: Hydrogen bond analysis of the moieties affected by the backbone ester mutation at αL199in the αγ (left) and αδ (right) binding sites. A) Hydrogen bonds formed with the αL199 NH. B) Hydrogen bonds formed with the αY198 cabonyl.

Replacing the backbone NH with an oxygen diminishes the hydrogen bonding ability of the neighboring carbonyl, in this case, the C=O group on αY198. Examining the hydrogen bonding pattern of this moiety reveals a hydrogen bond to the backbone NH of αV188 that is present throughout the 7 ns simulation (Figure 5.3B). This hydrogen bond is between the two β-sheets flanking the C-loop and may provide some structural rigidity to this region of the protein. Therefore, the weakening of this hydrogen bond, combined with increased backbone flexibility at αL199, may result in greater C-loop mobility. Numerous studies implicate the closure of the C-loop upon agonist binding in early transduction of the signal from agonist binding to channel pore opening.[6, 13, 14] A plausible model posits that the inward motion of the C-loop pulls at the flanking β-sheets (β7β10), changing crucial interactions between the interfacial residues of the extracellular and transmembrane domains. The putative increased ability of the C-loop to undergo this inward motion as a result of the increased backbone flexibility endowed by the αL199Lah mutation would thus make the receptor easier to open, leading to the observed gain-of-function behavior. As this mutation leads to a decrease in the EC_{50} value, the ELFCAR

analysis[6] is unable to detect whether a significant change in gating underlies the macroscopic phenotype.

5.2.2 Biphasic Behavior of Complementary Binding Site Ester Mutations

5.2.2.1 Whole-Cell Electrophysiological Characterization of the Biphasic Phenotype

Mutating the aromatic box residue contributed by the complementary binding subunit, γW55/δW57, to its analogous α-hydroxy acid leads to anomalous receptor behavior. Simultaneous ester incorporation at these sites alone leads to an unremarkable ~2-fold shift in EC_{50} (Figure 5.4A). However, in the presence of the L9'S pore mutation in any subunit, a two-component (biphasic) dose-response relation was observed (Figure 4B). Moreover, the macroscopic behavior was dramatically different when the binding sites were mutated individually. Mutating the δ-subunit alone (in conjunction with the βL9'S pore mutation) gave a monophasic dose-response curve with an EC_{50} value that is consistent with the typical 40-fold decrease observed with the βL9'S mutation. An ester mutation at this position in the γ-subunit, however, exhibited biphasic behavior, similar to that observed for the double binding site mutant receptor (Figure 5.4C).

One potential explanation for this behavior is that the ester mutation in the non-α aromatic binding box residue prevents proper subunit assembly. For example, if the γW55Wah subunit is inefficiently expressed or incorporated into the pentameric receptor, the δW57Wah subunit could act as a replacement. This would lead to both α_2β9'γ55Wah δ57Wah and α_2 β9'$(\delta 57Wah)_2$ receptors, with this mixed population giving rise to the observed biphasic behavior. Poor incorporation efficiency has been demonstrated to produce multicomponent

dose-response relations[15] and both γ-less and δ-less mouse muscle nAChRs have been observed.[16, 17]

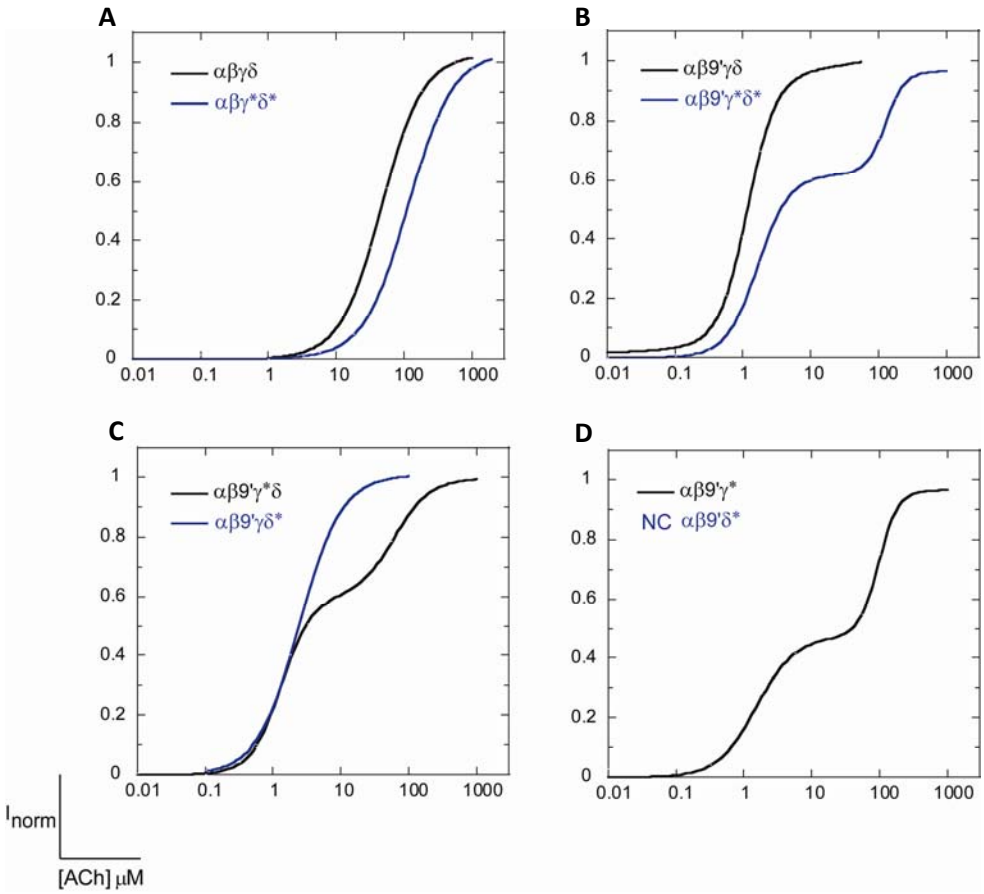

Figure 5.4: Dose-response relations of the wild-type and backbone ester mutations at γW55/δW57. A) No L9'S pore mutation. WT is in black, ester mutant is in blue. B) βL9'S pore mutation. WT is in black. Ester mutant is in blue. C) Differential effects of ester incorporation in only one subunit. γ-only is in black, δ-only is in blue. D) Subunit omission. The black curve is the δ-less receptor with the ester mutation in γ and the βL9'S pore mutation. No currents were observed for the ester-containing γ-less receptors.

Subunit-less experiments, in which the mRNA for either the γ or the δ-subunits was omitted, were performed to examine the issue of subunit incorporation. The γ-less receptors did not express, while the δ-less receptors produced biphasic dose-response behavior (Figure 5.4D). While the ability of δ-less receptors to express supports the inefficient incorporation hypothesis, the fact that these receptors themselves produce biphasic dose-response relations does not. No obvious stochiometic mixture for two δ-less receptors could retain two functional

binding sites, as the mouse muscle β-subunit is not known to function as a binding subunit. These data thus beg the question: can the observed biphasic behavior arise from a homogeneous receptor population?

5.2.2.2 Biphasic Behavior is Theoretically Possible From a Single Receptor Population

Cys-loop ligand-gated ion channels function by allosteric transitions between various closed (non-conducting) and open (ion conducting) states.[4, 18, 19] In principle, these transitions may occur with or without the binding of agonist, although spontaneous (agonist-free) openings occur with very low probability. In the case of the muscle nAChR, the binding of two molecules of agonist are required for efficient channel opening (Figure 5.5). Once agonist binds to the receptor, it induces conformational changes of the receptor from a resting state (closed channel) to an activated state (open channel). Activation may be followed by the return to the resting state following agonist dissociation or by a transition to an agonist-bound desensitized state (closed channel). Because the diliganded open state is strongly energetically preferred over the diliganded closed state, the open state of the receptor has a much higher affinity for agonists than the closed state of the receptor (nanomolar versus micromolar). This ensures two things; first, that once two molecules of agonist bind, the receptor opens quickly, and second, that if the receptor opens with only one molecule of agonist bound (monoliganded opening), the second molecule of agonist rapidly binds to produce the energetically favorable diliganded open state.

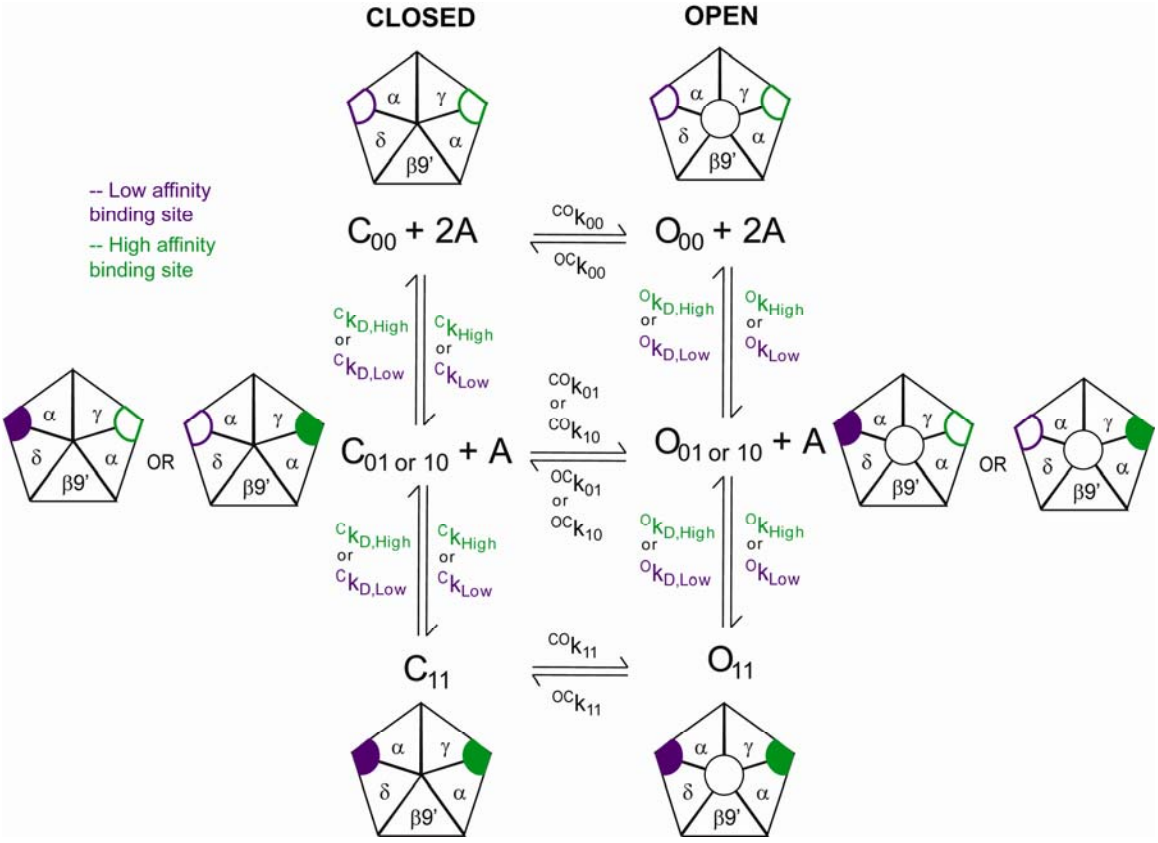

Figure 5.5: Basic kinetic scheme for the muscle nAChR. Moving from left to right represents a channel opening event. Moving from top to bottom represents a ligand-binding event. Purple and green are used to denote the nonequivalent low and high affinity acetylcholine binding sites, resprectively.

The kinetics of these allosteric transitions are governed by rate constants related to the energy barriers between allosteric states. These parameters determine the probability with which any individual ion channel will be found in a given conformation at any instant in time. These rate constants include (1) on and off rate constants for agonist binding, (2) rates constants for the transition from the resting to activated state, and (3) rate constants for transitions out of the activated state to the desensitized or resting states. A full complement of rate constants permits a complete description of the system and allows for the prediction of ion channel behavior both on the single channel and macroscopic levels.

In order to determine if biphasic dose-response behavior can arise simply by varying the rate constants in the standard kinetic model of the muscle nAChR, we employed the program STOIC (Simulations of Transient Openings of Ionotropic-receptor Channels).[20] This program employs a kinetic-based Monod-Wyman-Changeux allosteric model based on linear free energy relations to describe the effects of ligand binding events on interconversions between closed, open, and desensitized conformations of a single channel. Ensemble averages of these single channel simulations can be used to generate macroscopic dose-response data and thus EC_{50} values. The kinetic scheme for STOIC allows the user to control the on and off rates for agonist binding, as well as interconversion rates among resting, activated, and desensitized states. STOIC also allows for non-equivalent binding sites, which is crucial in modeling a receptor that displays differential behavior at each binding site.

Before using STOIC to simulate the mutant dose-response behavior, wild-type behavior was modeled using reported rates from experimental single-channel studies, where available (Table 5.2). These rates provided a starting point for lengthy, but non-exhaustive, efforts to determine the rates constants responsible for inducing a change from a monophasic to biphasic dose-response curve. The successful generation of a two-component dose-response relation based on adjusting the kinetic parameters within the standard model for receptor action means that the observed biphasic behavior of the γ55Wahδ57Wah receptors could be produced by a single receptor population.

A number of biphasic dose-response curves were produced with a variety of combinations of kinetic parameters. However, there was a consistent trend in the equilibrium dissociation constants when comparing the monophasic and biphasic curves: the affinity of the low affinity binding site for agonist in the open state is *less* than the affinity of the high affinity

binding site for agonist in the closed state (Table 5.2). Stated otherwise, the monoliganded open state (low affinity site occupied) has become an energetically favorable state, leading to monoliganded openings making a significant contribution to the overall open state of the receptor. This suggests monoliganded openings as a possible origin for biphasic dose-response behavior arising from a single, homogenous receptor population.

		monophasic	monophasic	**biphasic**	**biphasic**	monophasic	monophasic
		WT	**αβ9'γδ**				
(s^{-1})	$^{c}k_{High}$	1.00E+08	1.00E+08	1.00E+08	1.00E+08	1.00E+08	1.00E+08
	$^{c}k_{D,High}$	5200	235	50	553.15	10000	553.15
	$^{c}k_{Low}$	1.00E+08	1.00E+08	1.00E+08	1.00E+08	1.00E+08	1.00E+08
	$^{c}k_{D,Low}$	1.04E+05	1175.00	8.00E+05	8.00E+05	8.00E+05	8.00E+05
($M^{-1}s^{-1}$)	$^{o}k_{High}$	1.00E+08	1.00E+08	1.00E+08	1.00E+08	1.00E+08	1.00E+08
	$^{o}k_{D,High}$	1.6	0.35	1.2381	1.2381	1.2381	1.2381
	$^{o}k_{Low}$	1.00E+08	1.00E+08	1.00E+08	1.00E+08	1.00E+08	1.00E+08
	$^{o}k_{D,Low}$	32	1.75	6500	30000	6500	100
	$^{c}Kd_{eq,High}$	5.20E-05	2.35E-06	5.00E -07	5.53E -06	1.00E-04	5.53E-06
	$^{c}Kd_{eq,Low}$	1.04E-03	1.175E-05	8.00E-03	8.00E-03	8.00E-03	8.00E-03
	fold affinity	20	5	**16000**	**1446**	**80**	**1446**
	$^{o}Kd_{eq,High}$	1.60E-08	3.50E-09	1.24E-08	1.24E-08	1.24E-08	1.24E-08
	$^{o}Kd_{eq,Low}$	3.20E-07	1.75E-08	6.50E -05	3.00E -04	6.50E-05	1.00E-06
	fold affinity	20	5	**5250**	**24231**	**5250**	**81**

Table 5.2: Parameters used in STOIC simulations.

5.2.2.3 Anomalous receptors display normal receptor stochiometry

To experimentally probe for correct subunit assembly, single molecule photobleaching experiments were undertaken. For these experiments, EGFP was inserted into the M3-M4 linker of the β- and γ-subunits. These EGFP-containing proteins were then further fluorescently

labeled using the competitive antagonist α-bungarotoxin monoconjugated to the Alex488 fluorophore.

Photobleaching of a single fluorescent molecule is a discrete process. A stepwise decrease in fluorescence intensity results for a protein-ligand complex containing several fluorescent molecules, with the number of observed photobleaching steps corresponding to the number of fluorescent moieties in the complex. In principle, the number of photobleaching steps would exactly equal the number of fluorescent molecules. In reality, however, a distribution of photobleaching steps is observed. This distribution reflects a number of contributing phenomena. First, due to the experimental set up, a subset of fluorescent molecules will photobleach prior to image acquisition. Second, a significant percentage (~20%) of "fluorescent" proteins are nonfluorescent. Thirdly, incomplete labeling of the receptors with α-bungarotoxin and/or imperfectly labeled αBtxA488 reagent reduces the number of observed photobleaching steps. Finally, more than the anticipated number of photobleaching steps is occasionally observed due to either the colocalization of two receptors or an αBtx labeled with more than one Alexa488 molecule. Therefore, in addition to counting the number and distribution of photobleaching steps, comparing the distribution of photobleaching steps between the wild-type and mutant proteins is necessary to assess differences in receptor subunit composition.

To confirm normal receptor assembly, three sets of experiments were performed. In the first, the β-subunit was tagged with EGFP, and the receptor was labeled with αBtxA488. Both WT and mutant receptors bearing an EGFP containing β-subunit and labeled with αBtxAlexa488 displayed puncta with 1 (29%, 25%, respectively), 2 (46%, 38%), 3 (24%, 28%), and 4-6 (7%, 9%) photobleaching steps (Figure 5.6A). This confirmed the incorporation of the β-

subunit into the mutant receptors, however, it could not distinguish whether the mutant receptors contained two different binding sites (e.g., one αγ and one αδ) or two αδ or two αγ. Therefore, a subsequent experiment was needed to confirm that we were not observing γ-less or δ-less receptors.

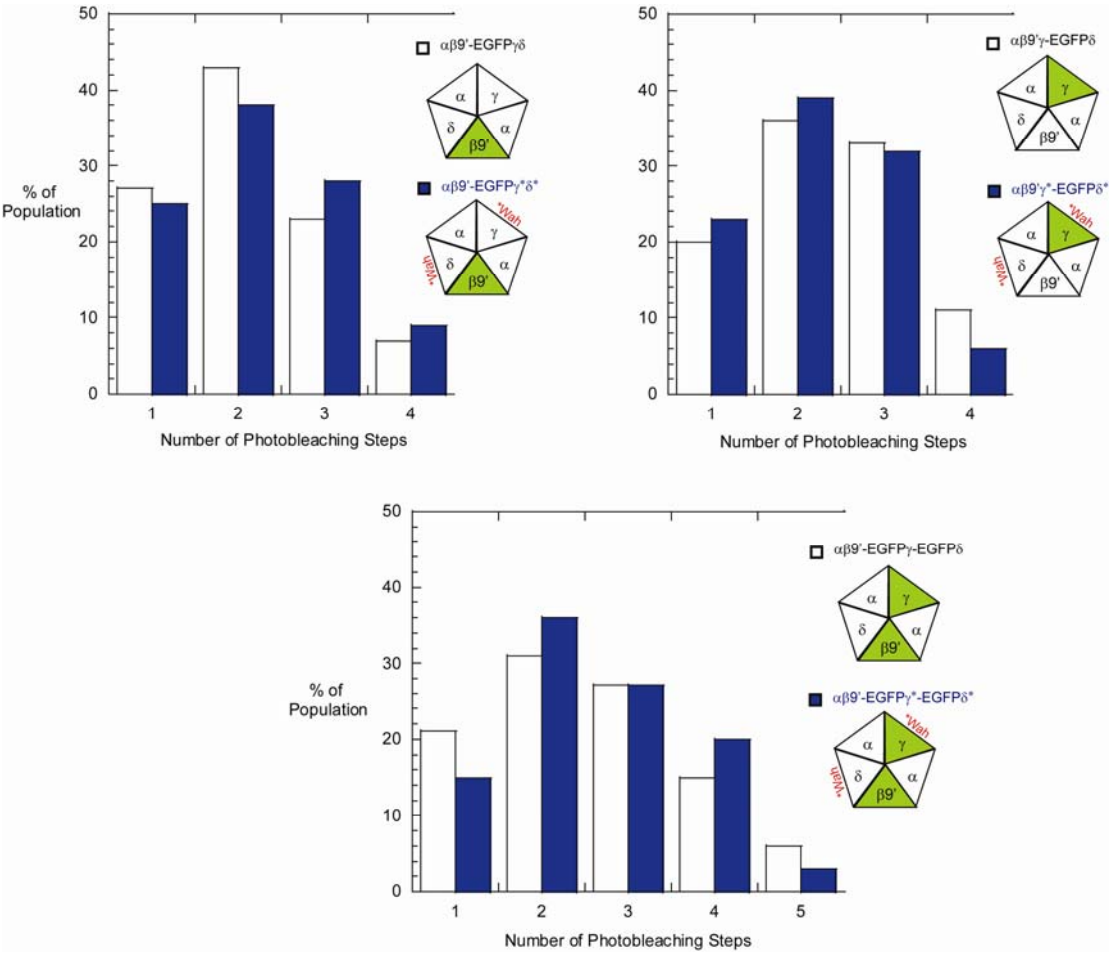

Figure 5.6: Photobleaching histograms. White and blue bars represent the wild-type and double ester-containing receptors, respectively. In all cases, receptors were labeled with αBtxA488. A) β9'-EGFP B) γ-EGFP C) β9'-EGFP and γ-EGFP.

An EGFP-tagged γ-subunit labeled with αBtxAlexa488 is used to probe whether the γ-subunit is normally assembled into the receptor. Three photobleaching steps would indicate that the fluorescently labeled γ-subunit is assembled correctly in the receptor. Alternatively, four photobleaching steps would be seen if there are two αγ binding sites and only two

photobleaching steps would be observed if there are two αδ binding sites. By comparing the photobleaching profiles of the αβ9'γ55Wahδ57Wah mutants with that of wild type receptors, it was possible to determine that these receptors were assembled normally. Both wild type and mutant receptors bearing an EGFP containing γ-subunit and labeled with αBtxAlexa488 displayed puncta with 1 (13%, 26%, respectively), 2 (23%, 44%), 3 (21%, 36%), and 4-6 (7%, 7%) photobleaching steps (Figure 5.6B).

An additional experiment was done wherein EGFP-bearing β and γ subunits were expressed and subsequently labeled with αBtxAlexa488. WT-like photobleaching profiles with a maximum of four photobleaching steps were observed, confirming correct receptor assembly. In this case, the photobleaching profiles were as follows: 21%, 15% displayed one photobleaching step, 31%, 36% showed two photobleaching steps, 27%, 27% displayed three photobleaching steps, 15%, 20% had four photobleaching steps, and 6%,3% had five or more photobleaching steps for WT and mutant receptors, respectively (Figure 5.6C).

Overall, the distribution of photobleaching steps of the mutant receptors is consistent with that of the WT receptors, confirming a stochiometric subunit population similar to that of the wild-type receptors. These data do not rule out heterogeneity in the receptor population, but do strongly suggest a receptor population that is homogeneous with respect to subunit composition.

5.2.2.4 Biphasic behavior: novel phenomenon or experimental artifact?

Typically a biphasic dose-response curve is indicative of a mixed population of receptors. Through kinetic modeling it was shown that this behavior can theoretically be produced by a single population of receptors. However, an alternative possibility is that one of the

components is the result of re-aminoacylation of the suppressor tRNA (see also Chapter 1). Based on the original data set collected, several lines of evidence would suggest against this.

Two types of control experiments are used to detect re-aminoacylation, as described in Chapter 1. The first involves co-injecting uncharged suppressor tRNA along with the mRNA containing the stop codon at the site(s) of interest. This control typically yielded no detectable currents and in no case gave current sizes above 10% of the experimental response, where Wah-tRNA or Trp-tRNA was co-injected. On a single day, currents from the re-aminoacylation control produced currents from which a reliable dose-response relation could be constructed, giving an EC_{50} value of 480 μM. The average current size of such control experiments was approximately 160 nA, while the experimental data displayed currents in the tens of microamperes range. The second control involves the recovery of the wild-type phenotype by co-injecting the natural amino acid appended to the suppressor tRNA with the mutant mRNA. Robust currents of a similar size of the Wah-tRNA experimental work were observed, but no biphasic behavior was observed. Robust current sizes and monophasic dose-response relations were also observed for the incorporation of both Tyr and Yah at γW55 and δW57. If one of the components of the biphasic dose-response were a result of re-aminoacylation, then this component should have also been present in other suppression experiments.

In addition to the control experiments, two other experimental results strongly suggest that re-aminoacylation did not lead to the originally observed two-component dose response. First, the dose-response relations for partial agonists epibatidine and succinylcholine for the αβ9γW55WahδW57Wah receptors are monophasic (Figure 5.7). Importantly, the monophasic behavior of these partial agonists was observed on the same day as biphasic behavior was observed for acetylcholine. Second, the differential behavior of the two binding sites provides

some support for the idea that the biphasic phenomenon is not a result of re-aminoacylation. However, differential incorporation of the re-aminoacylated amino acid at the two binding sites might also explain this behavior.

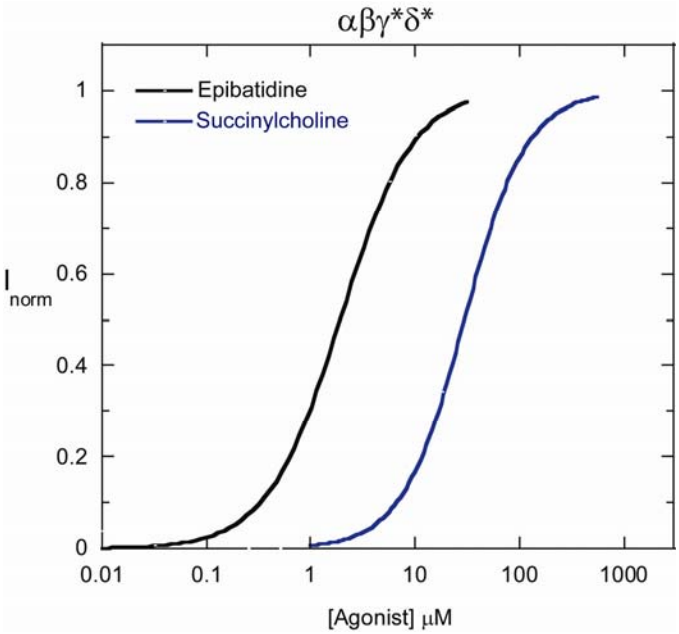

Figure 5.7: Dose-response curves of αβ9'γ55Wahδ57Wah receptors for partial agonists epibatidine and succinylcholine.

The experiments listed above were conducted between the spring of 2006 and the spring of 2008. Upon encountering expression problems in the summer of 2008, the mutant mRNA was re-made and tryptophan α-hydroxy was re-synthesized, at which point it was discovered that the original stock had been racemic. Both racemic and S-Wah were synthesized and shown to produce similar shifts in EC_{50}. However, at this point the biphasic dose-response behavior was no longer observed. In addition, significant current from the 76mer control was observed. Although the appearance of 76mer current did not correspond to the observation of biphasic dose-response behavior, it did raise concerns that the original biphasic data was a result of a mixed receptor population. Without being able to reproduce the biphasic behavior, it is impossible to draw any conclusions from the original data det.

5.3 Materials and Methods

5.3.1 Whole-cell Electrophysiology and data analysis

Electrophysiological measurements were carried out 18-72 hours post-microinjection. Macroscopic measurements were performed with a two-electrode voltage-clamp circuit using an OpusXpress (Axon Instruments, Foster City, CA). Oocytes were bathed in the extracellular recording solution Ca^{2+} -free ND96 (96 mM NaCl, 2 mM KCl, 1 mM $MgCl_2$ ($6H_2O$, 5 mM HEPES, pH 7.4). ACh-induced currents were recorded in response to bath application of acetylcholine (flow rate of 4 mL/min for 15 seconds) at a holding potential of -60 mV. Data were sampled at 125 Hz and filtered at 50 Hz. Individual dose-response data were fit to the Hill equation (Equation 1) where I is the current, Imax is maximal current, [A] is agonist concentration, EC_{50} is the concentration to elicit a half-maximal response, and n is the Hill coefficient.

$$y = I_{\max} * \frac{[A]^n}{[A]^n + EC_{50}^n} \tag{5.1}$$

Biphasic dose-response data were fit with a two component Hill equation (Equation 2) where c1 is the weighted value corresponding to the lower EC_{50} component.

$$y = I_{\max} * \left[c_1 * \frac{[A]^{n1}}{[A]^{n1} + EC_{50,1}^{n1}} + (1 - c_1) * \frac{[A]^{n2}}{[A]^{n2} + EC_{50,2}^{n2}} \right] \tag{5.2}$$

Macroscopic data represent measurements obtained from 5-27 individual oocytes.

5.3.2 STOIC

The STOIC simulation program is designed to run in the MATLAB environment. STOIC is available upon request via the internet at

<http://www.unige.ch/sciences/biochemie/Edelstein/research.html>. The parameters used in this model are given in the Results and Discussion section.

5.3.3 Single-molecule labeling and TIRF microscopy

GFP-tagged subunits were created using an integration of PCR fragments technique, which does not require the use of restriction enzymes. Forward and reverse primers for pEGFP-N1 vector (Clontech; excitation maximum = 488 nm; emission maximum = 507 nm) were designed with 5' overhangs of 24 nucleotides corresponding to the eight amino acid residues immediately before and after the desired insertion site of the nAChR subunit (after position P350 in β and L351 in γ). A GFP fragment with overhangs was amplified by 30 cycles of PCR and purified by extraction from a 1% agarose gel using a QIAquick gel extraction kit (Qiagen). Concentration of purified GFP fragment with overhangs was quantified using a NanoDrop spectrophotometer (NanoDrop Technologies). The GFP fragment was then inserted into the appropriate nAChR subunit vector with a 5:1 mass ratio of insert:destination vector by 18 cycles of PCR. GFP-tagged nAChR subunit DNA was obtained by DpnI digest and transformed using Blue Top10 cells by electroporation. Colonies were picked and the complete EGFP inserted nAChR subunit DNA was identified by DNA sequencing.

Xenopus oocytes were prepared for imaging by TIRF microscopy by first stripping the vitalline membrane with forceps, following immersion in a hypertonic solution (220 mM NaAspartate, 10 mM HEPES, 10 mM EDTA, 2 mM MgCl2, pH 7.38) for five to ten minutes. The oocytes were subsequently placed, animal pole down, on a clean glass coverslip in an imaging chamber on the microscope stage. The room was cooled to 15- 20 C to both minimize drift and maintain the health and mechanical stability of the oocytes. The TIRF microscope was a Melles-Griot Argon (Ar) ion laser connected via a fiber optic to an Olympus TIRF illuminator adapted to

a standard inverted IX-71 Olympus microscope (Center Valley, PA). An excitation wavelength of 488 nm was selected to excite and detect the Alexa488 and eGFP fluorophores using a Z488 filter cube from Chroma Technology Corporation (Rockingham, VT). Time-lapse images were captured over a period of 5- 20 minutes using a Photometrics Cascade front illuminated CCD camera from Princeton Instruments (Trenton, NJ). Data were acquired on Slidebook from Intelligent Imaging Innovations Inc (Santa Monica, CA) and then analyzed using ImageJ (National Institutes of Health), Clampfit 9.2 (Axon Instruments, Foster City, CA), and Origin 7.0 (OriginLab, Northhampton, MA).

Analysis was performed by examining the fluorescence profiles of puncta imaged over several minutes. Puncta that did not result in discrete photobleaching steps during the acquisition were excluded from analysis. In addition, the analysis was limited to cases where fewer than 0.3 puncta/μm^2 were observed in order to avoid excess co-localization of receptors within a diffraction-limited spot.

5.4 References

1. Changeux, J.P. & Edelstein, S.J. Nicotinic Acetylcholine Receptors: From Molecular Biology to Cognition (Odile Jacob, New York, 2005).
2. Brejc, K. et al. Crystal structure of an ACh-binding protein reveals the ligand-binding domain of nicotinic receptors. *Nature* **411**, 269-76 (2001).
3. Auerbach, A. Life at the top: the transition state of AChR gating. *Sci STKE* **2003**, re11 (2003).
4. Colquhoun, D. From shut to open: what can we learn from linear free energy relationships? *Biophys J* **89**, 3673-5 (2005).
5. Sine, S.M. & Engel, A.G. Recent advances in Cys-loop receptor structure and function. *Nature* **440**, 448-55 (2006).
6. Gleitsman, K.R., Lester, H.A. & Dougherty, D.A. Probing the role of backbone hydrogen bonding in a critical beta sheet of the extracellular domain of a cys-loop receptor. *Chembiochem* **10**, 1385-91 (2009).
7. Cashin, A.L., Petersson, E.J., Lester, H.A. & Dougherty, D.A. Using physical chemistry to differentiate nicotinic from cholinergic agonists at the nicotinic acetylcholine receptor. *J Am Chem Soc* **127**, 350-6 (2005).
8. Cashin, A.L., Torrice, M.M., McMenimen, K.A., Lester, H.A. & Dougherty, D.A. Chemical-scale studies on the role of a conserved aspartate in preorganizing the agonist binding site of the nicotinic acetylcholine receptor. *Biochemistry* **46**, 630-9 (2007).
9. Lee, W.Y. & Sine, S.M. Invariant aspartic Acid in muscle nicotinic receptor contributes selectively to the kinetics of agonist binding. *J Gen Physiol* **124**, 555-67 (2004).
10. Unwin, N. Refined structure of the nicotinic acetylcholine receptor at 4A resolution. *J Mol Biol* **346**, 967-89 (2005).
11. Rucktooa, P., Smit, A.B. & Sixma, T.K. Insight in nAChR subtype selectivity from AChBP crystal structures. *Biochem Pharmacol* **78**, 777-87 (2009).
12. Dellisanti, C.D., Yao, Y., Stroud, J.C., Wang, Z.Z. & Chen, L. Crystal structure of the extracellular domain of nAChR alpha1 bound to alpha-bungarotoxin at 1.94 A resolution. *Nat Neurosci* **10**, 953-62 (2007).
13. Law, R.J., Henchman, R.H. & McCammon, J.A. A gating mechanism proposed from a simulation of a human alpha7 nicotinic acetylcholine receptor. *Proc Natl Acad Sci U S A* **102**, 6813-8 (2005).
14. McLaughlin, J.T., Fu, J., Sproul, A.D. & Rosenberg, R.L. Role of the outer beta-sheet in divalent cation modulation of alpha7 nicotinic receptors. *Mol Pharmacol* **70**, 16-22 (2006).
15. Covernton, P.J. & Connolly, J.G. Multiple components in the agonist concentration-response relationships of neuronal nicotinic acetylcholine receptors. *J Neurosci Methods* **96**, 63-70 (2000).
16. Charnet, P., Labarca, C. & Lester, H.A. Structure of the gamma-less nicotinic acetylcholine receptor: learning from omission. *Mol Pharmacol* **41**, 708-17 (1992).
17. Francis, M.M. & Papke, R.L. Muscle-type nicotinic acetylcholine receptor delta subunit determines sensitivity to noncompetitive inhibitors, while gamma subunit regulates divalent permeability. *Neuropharmacology* **35**, 1547-56 (1996).

18. Colquhoun, D. Binding, gating, affinity and efficacy: the interpretation of structure-activity relationships for agonists and of the effects of mutating receptors. *Br J Pharmacol* **125**, 924-47 (1998).
19. Jackson, M.B. Perfection of a synaptic receptor: kinetics and energetics of the acetylcholine receptor. *Proc Natl Acad Sci U S A* **86**, 2199-203 (1989).
20. Edelstein, S.J., Schaad, O., Henry, E., Bertrand, D. & Changeux, J.P. A kinetic mechanism for nicotinic acetylcholine receptors based on multiple allosteric transitions. *Biol Cybern* **75**, 361-79 (1996).

Chapter 6: Studies of α-Hydroxy Acid Incorporation *In Silico*

6.1 Introduction

Using unnatural amino acid mutagenesis, we have gained atomic-level manipulation of protein structure. Our ability to interpret the impact of our mutations is greatly aided by structural models of the neuroreceptors we study. Although recent progress in the determination of three-dimensional structures of ion channels provides a wealth of information, a full understanding of the structure-function relationship for a protein requires insight into dynamic properties as well as static structure. Combining atomic resolution structures with highly sophisticated computational approaches provides a virtual route to understanding experimental results, developing models of protein function, and making predictions that can be tested in the laboratory. Arguably, all-atom molecular dynamics simulations offer the most complete computational approach to study complex biological molecules. This approach consists of constructing an atomic model of the macromolecular system, representing the microscopic forces with a potential function, and integrating Newton's second law of motion "F=ma" to generate a trajectory. The result is essentially a movie showing the dynamic motions of the system as a function of time.

Standard molecular dynamics simulation packages offer parameters capturing the relevant physical characteristics of twenty standard amino acids. Absent, however, are parameters for unnatural amino and α-hydroxy acids. The goal of our study was therefore to develop parameters to describe backbone esters and to apply these in a molecular dynamics simulation to understand the impact of a particular ester mutation in the aromatic binding box.

6.2 Results and Discussion

6.2.1 Homology Modeling

Homology models of the extracellular domain of the mouse muscle nAChR were constructed based on the crystal structure of the acetylcholine binding protein (AChBP, PDB: 1I9B[1]) using the Modeller software package.[2, 3] This process began by aligning the sequence of the mouse muscle extracellular domain with that of the Lymnaea stagnalis AChBP.[1] After several initial alignments using TCoffee[4] produced unsatisfactory homology models, an alignment based on experimental work was used.[5] Using Lysine scanning mutagenesis, Sine et al. were able to distinguish core hydrophobic from surface hydrophilic orientations of residue side chains and use this information to align residues in AChR subunits with equivalent residues in the homologous AChBP. The Modeller program was used to generate several homology models, which were evaluated based on the following criteria: appropriate secondary structural elements, the residue positions in the highly conserved aromatic box and the F-loop, and discrete optimized protein energy (DOPE) scores.[6]

DOPE is an atomic distance-dependent statistical, or "knowledge-based," potential optimized for model assessment. This scoring potential was used to evaluate the overall quality of the initial homology models as a whole, as well as to look at the models on a residue-by-residue basis. This latter method was useful in identifying potentially problematic regions in the homology models, marked by high DOPE scores, for further optimization. Comparing the DOPE profiles of the homology models to that of the original template also proved a useful evaluation criterion (Figure 6.1).

One region that was consistently problematic was the F-loop. The F-loop in the complementary binding subunits is much longer than that in AChBP, leading to considerable variation in this region of the homology models. Numerous subsequent loop refinements were therefore used on this region. Evaluation of the position of the F-loop was based on distances between the vicinal disulfide in the C-loop and γD174/δD180, which is known to be within 9 Å based on several cross-linking studies.[7-9] The selected homology model (model 8, Figure 6.1), after loop minimization, served as the starting structure both in its unmodified form and with the backbone ester replacing the amide in residues γW55 and δW57 (see Chapter 5).

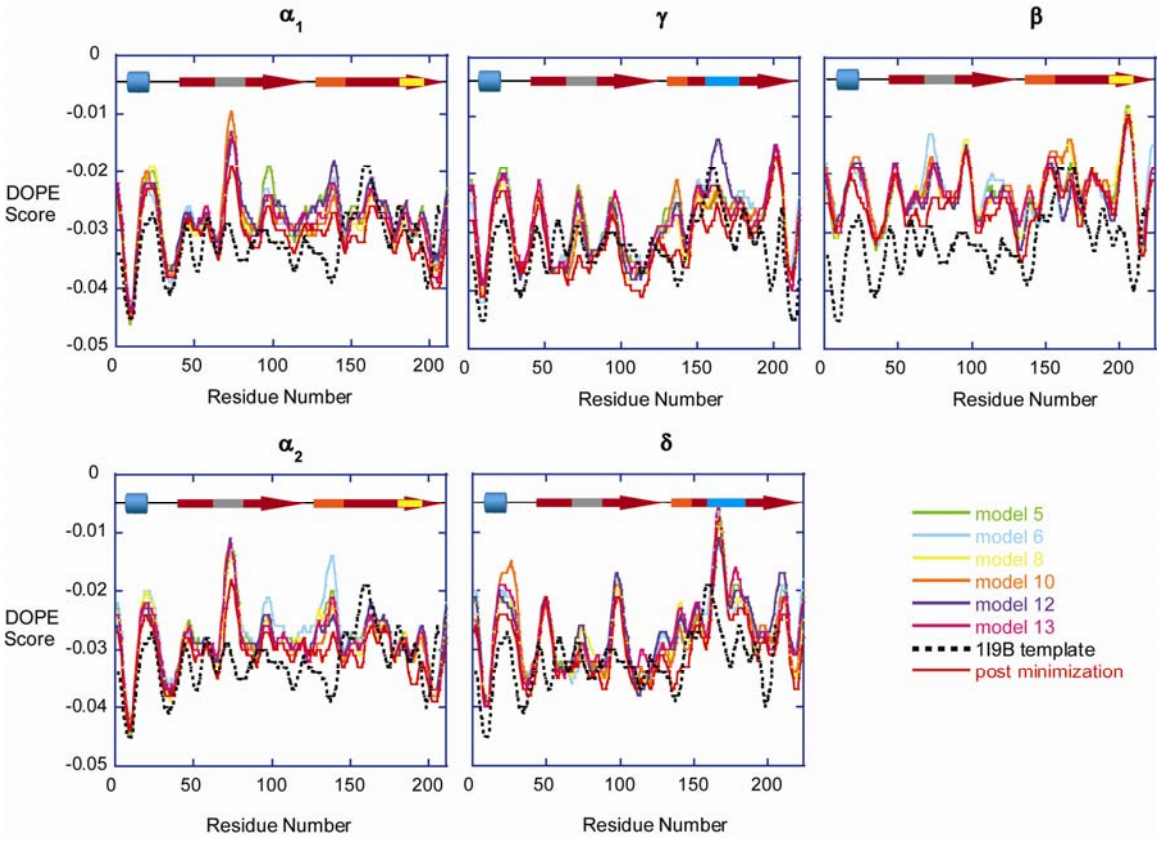

Figure 6.1: DOPE profiles for selected homology models. The protein secondary structure is highlighted above each profile. The red arrows denote β-sheets 1-6 and 7-10, respectively. The α_1 helix is designated as a blue cylinder and the MIR is shown in grey. The Cys, C-, and F-loops are represented as orange, yellow, and cyan bars, respectively.

6.2.2 Ester parameterization

To create the ester-containing protein, Pymol[10] was used to replace the backbone NH at position γW55 and δW57 with an oxygen. This structure was imported into the GROMACS simulation program and the parameters for the backbone ester were manually adjusted. The ester parameters were derived from charges in 1-lauroyl-glycerol and similar molecules in the GROMACS forcefield. In order to correctly parameterize the bond between the backbone oxygen and the i-1 carbonyl, these residues were effectively unified to create one set of parameters describing the backbone ester. These parameters were tested by comparing the behavior of a model VWL tripeptide to an analogous molecule containing a backbone ester in the middle residue. Similar behavior was observed in terms of both structure and energy, as shown in Figure 6.2.

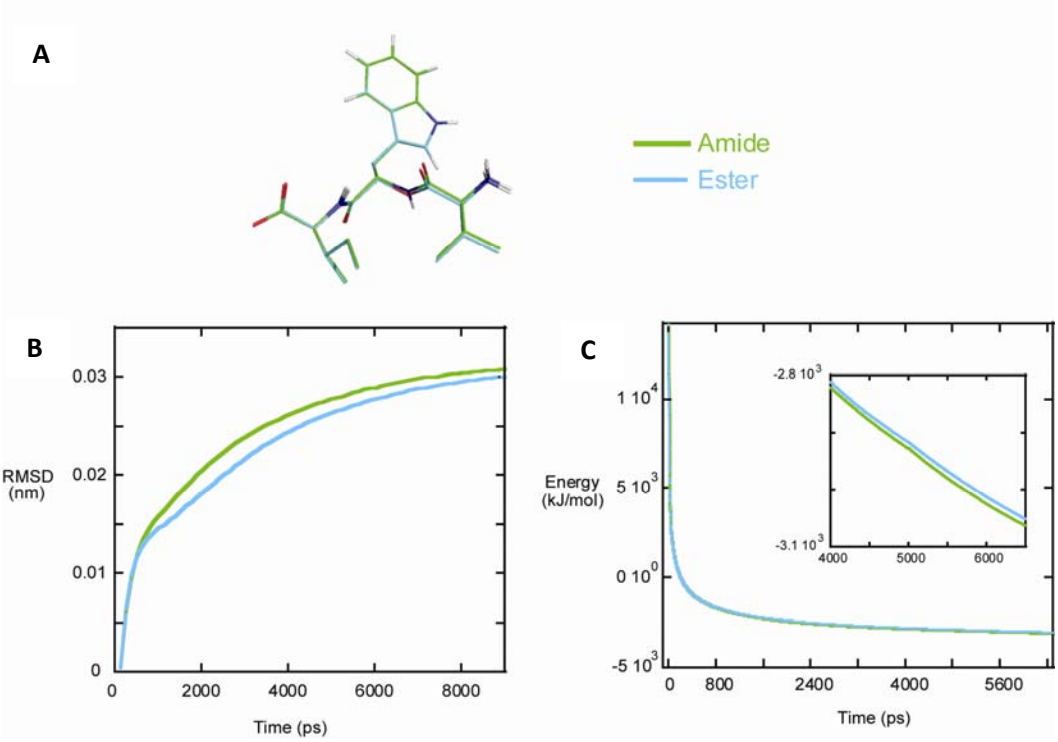

Figure 6.2: A) Structures of the amide and ester model tripeptide at the end of the minimization runs. B) The RMSD profiles of the model tripeptides. C) The energy profiles of the model tripeptides. The inset shows the energy minimization for the final 2500 ps.

6.2.3 Molecular Dynamics Simulations

The unmodified and ester-containing proteins were converted to GROMACS format and subsequently placed into a periodic box with 7 Å gaps between the protein and the box edge. Explicit solvation was added with SPC water molecules. Physiological conditions were simulation by adding sodium and chloride ions to the box at a molarity of 150 mM, with excess sodium ions to neutralize the charge of the protein. After an initial set of minimizations, unrestrained MD simulations of both the unmodified and ester-containing proteins were run to 6950 ps (see methods). The resulting trajectories were then analyzed.

6.2.3.1 Structural Analysis of MD Trajectories

Root mean-square fluctuation (RMSF) provides information about the residue mobility relative to the average structure, analogous to crystallographic B-factors. An RMSF analysis of the trajectories produced RMSF profiles and B-factors that were mapped onto the structure. This analysis shows that the ester-containing protein (<RMSF> = 0.19 nm) is moderately more mobile than the wild-type protein (<RMSF> = 0.16 nm). Examining each subunit individually reveals the greatest amount of mobility in the α subunit at the α/γ interface of the ester-containing protein. Some of the largest differences in RMSF values of individual residues between the WT and ester-modified proteins are seen in the γ-subunit, notably in the F-loop region (Figure 6.3).

The most and least mobile regions are qualitatively similar to those seen in other simulations of nAChRs,[11-15] as well as in the AChBP crystal structures.[16, 17] These regions include the MIR, the Cys-loop, the C-loop and the F-loop.

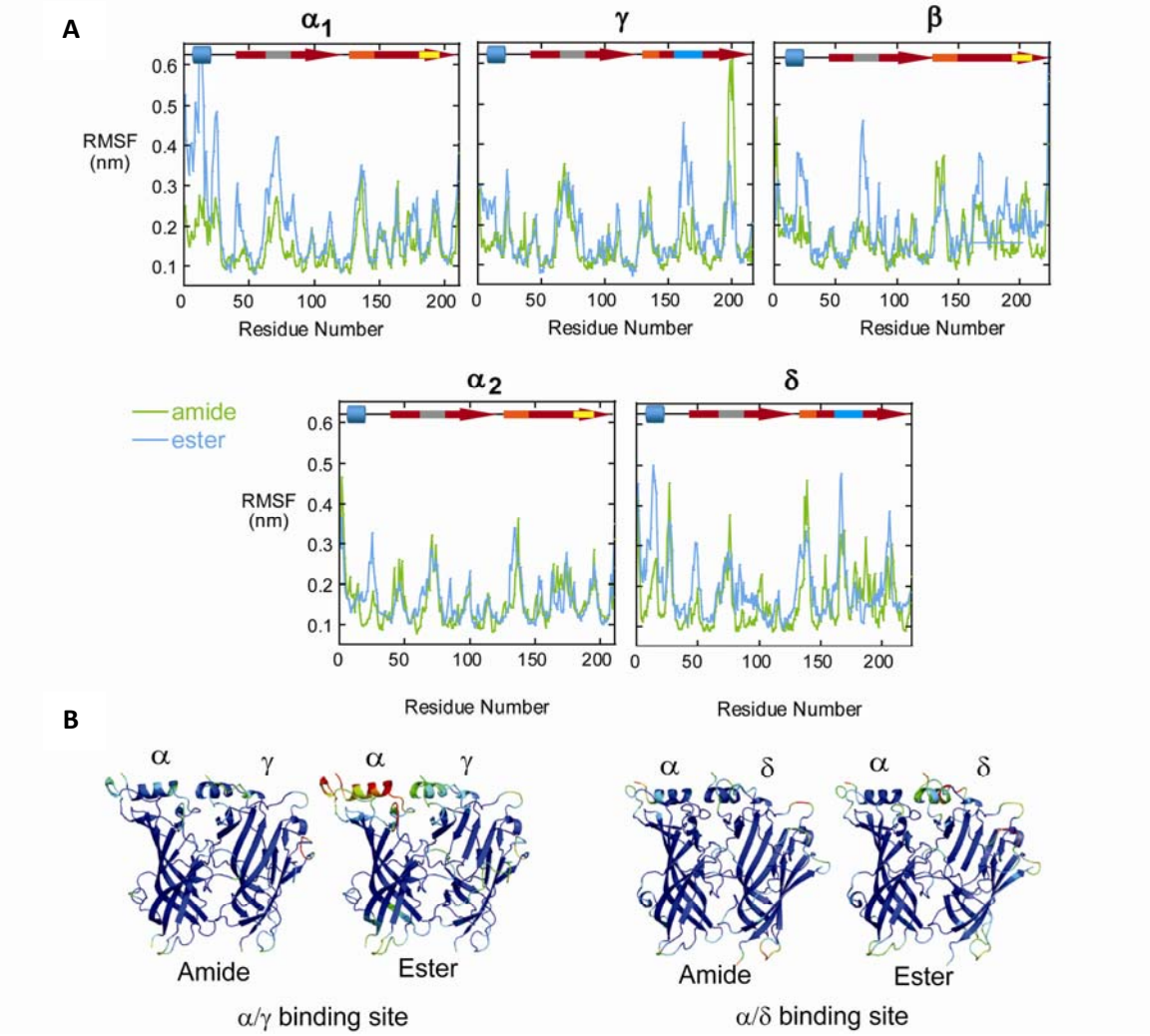

Figure 6.3: A) RMSF profiles of the WT and ester-containing proteins. The protein secondary structure is highlighted above each profile. The red arrows denote β-sheets 1-6 and 7-10, respectively. The α_1 helix is designated as a blue cylinder and the MIR is shown in grey. The Cys, C-, and F-loops are represented as orange, yellow, and cyan bars, respectively. B) The computed B-factor values color coded onto the receptor structure, with red corresponding to the most mobile region and blue corresponding to the most stable region.

The increased residue fluctuations in the ester-containing protein revealed by the RMSF analysis is further shown in the overall root mean-square deviation (RMSD) of the protein. The RMSD is used to compare the spatial deviation between structures in time and the original structure (at time = 0 ps). This can provide a sense of the overall structural stability of the simulated protein. As shown in Figure 6.4, the overall protein RMSD is higher in the ester-containing protein than in the WT protein.

Examination of the movement of the aromatic box residues reveals more divergent behavior between the ester-containing and wild-type proteins for the α/γ binding site than the α/δ binding site (Figure 6.4). Further analysis reveals additional asymmetry between the two binding sites.

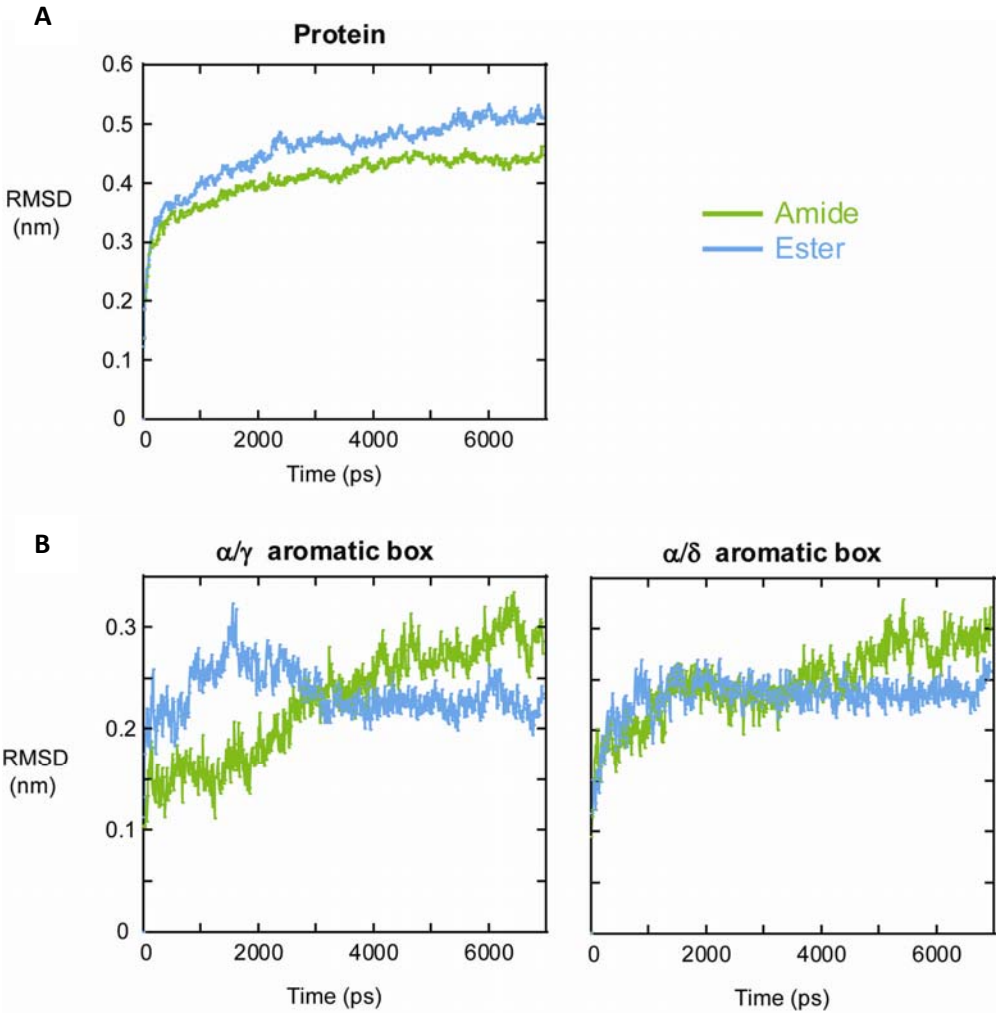

Figure 6.4: RMSD Profiles. A) The entire protein. B) The α/γ and α/δ aromatic boxes.

Looking at the side chain plane angles provides a sense of the organization of the aromatic box residues during the course of the simulation. In particular, motions of other box residues relative to the mutated box residue, γW55/δW57, were analyzed (Figure 6.5). Consistent with the box RMSDs, the plane angle fluctuations were more similar in the α/δ

binding site than the α/γ binding site, although similar conformations are sampled by the wild-type and ester-containing proteins. This is perhaps best illustrated in the plane angles between αY93 and γW55. An abrupt change in plane angle from ~150° to ~50° is seen in the ester-containing protein at about 1200 ps, corresponding to the flipping of the aromatic face of the αY93 side chain relative to γW55. This side chain flipping motion is also observed in the wild-type simulation at a later point in the simulation, around 4000 ps.

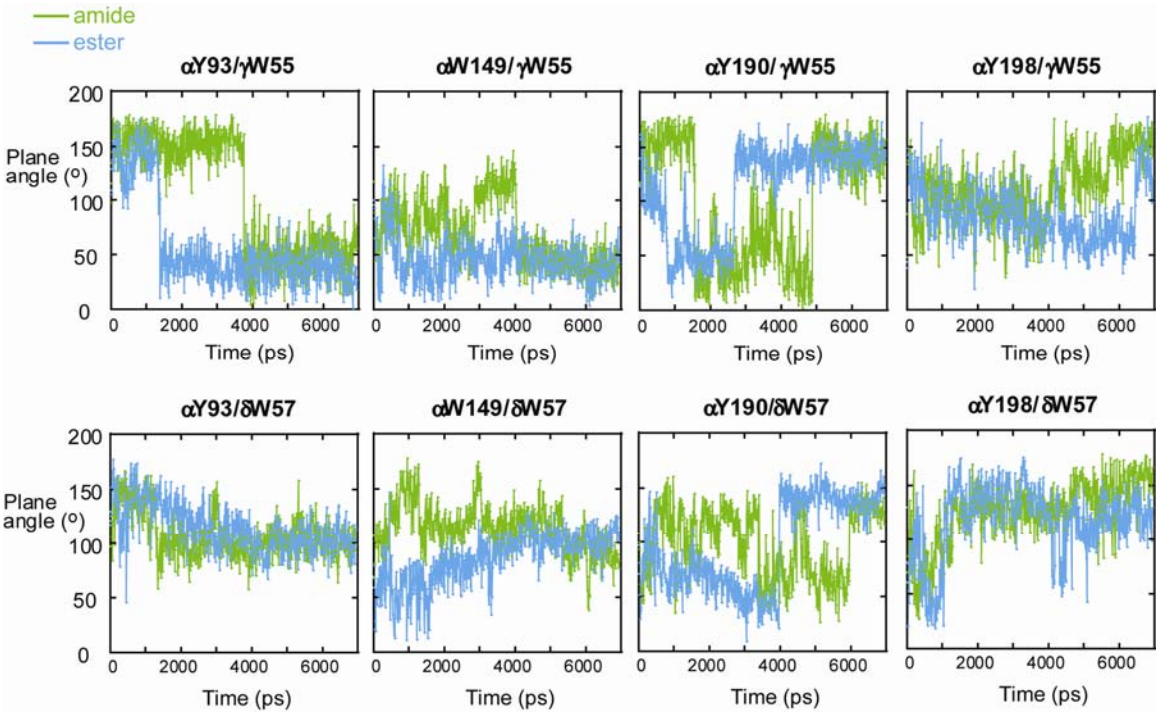

Figure 6.5: Sidechain plane angle fluctuations of the aromatic box residues.

One of the most striking differences between the unmodified and ester-containing proteins was in the behavior of the C-loop. A visual inspection of the trajectories reveals that the C-loop in the ester-containing receptor moves downward, while that of the wild-type protein more nearly remains in its original position (Figure 6.6). This motion occurs within the first several hundred picoseconds of the simulation. In addition, this motion is more pronounced in the α/γ binding site than in the α/δ binding site.

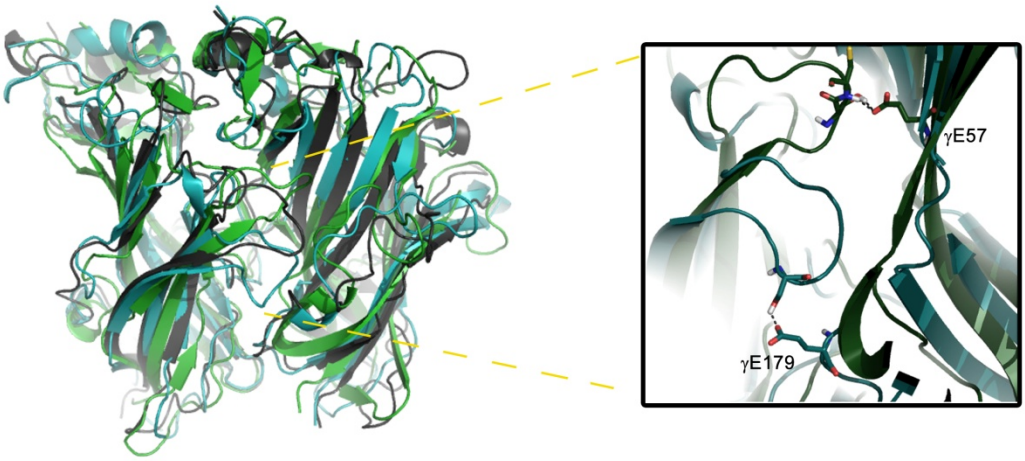

Figure 6.6: Movement of the C-loop in the α/γ interface. The grey structure is the initial structure (post-minimization, pre-MD). The hydrogen bonding between the C-loop and γE57 (WT, green) and γE179 (ester, cyan) are highlighted on the right.

An analysis of the hydrogen-bonding patterns of γW55 did not show any substantial intersubunit interactions between the C-loop and either the backbone or sidechain of this residue. A further look at all the intersubunit hydrogen bonds between the α C-loop and the adjacent subunit revealed the presence of a hydrogen bond between residues in the C-loop and γE57 in the wild-type protein that is completely absent in the ester-modified receptor. Instead, analogous C-loop residues of the ester-containing protein formed significant hydrogen bonding interactions with a different glutamate residue, γE179. As γE57 is separated from γW55 by only one residue, one reasonable hypothesis is that the backbone ester at γW55 subtly alters the side chain position of γE57, preventing the formation of the hydrogen bond between it and the C-loop. Instead, the C-loop finds an alternative hydrogen-bonding partner in γE179, thus accounting for the downward motion of the C-loop.

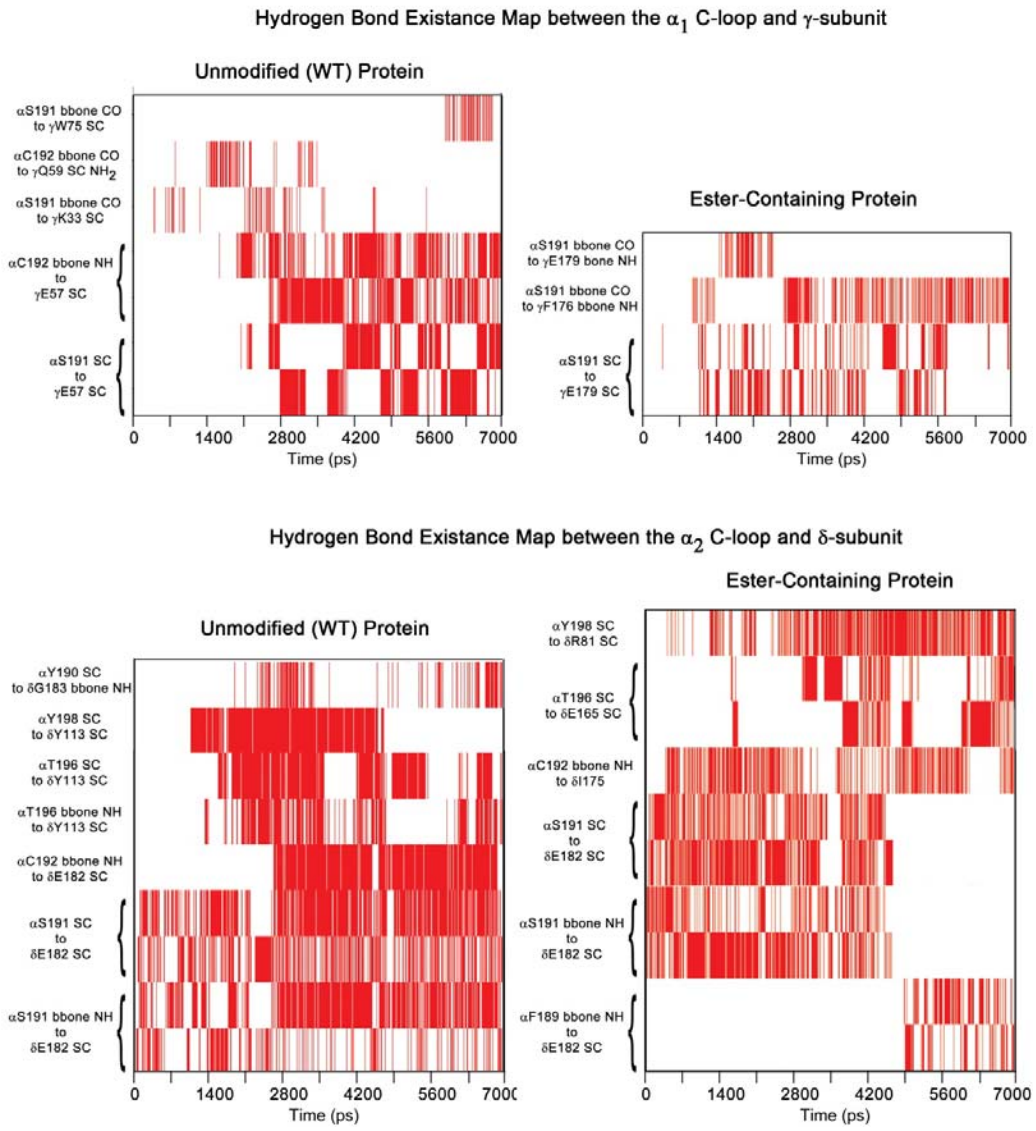

Figure 6.7: The most significantly contributing hydrogen bonds between the α C-loop and the complementary binding subunit.

The analogous residue in the δ-subunit, δE59, does not participate in hydrogen bonding interactions with the C-loop. Instead, these interactions seem to be replaced by hydrogen bonds between αS191 and the side chain of δE182, as well as between αT195 and αY198 with the side chain of δY113. Hydrogen bonds between αS191 and δE182 are also shown to be present for a significant portion of the simulation of the ester-containing protein, although those involving δY113 are largely absent. The greater overlap in the hydrogen bonding patterns

seen in the α/δ binding site of the unmodified and modified proteins likely contributes to the greater similarity in C-loop movement than seen at the α/γ site.

To verify that the movement of the C-loop at the α/γ interface of the ester-containing protein is not an artifact, the first 2700 ps of the simulation were re-run. At the end of this simulation, the C-loop was in a similar position to that in the initial MD simulation (Figure 6.9). Importantly, the key hydrogen bond between αS191 in the C-loop and γE179 forms at around 2600 ps. The formation of this bond occurs later in the second simulation than in the first, where it formed within the first 1200 ps. In addition, there are some differences in the number and nature of hydrogen bonds in both the binding sites between the two simulations. Nonetheless, the movement of the C-loop is retained in the second simulation, making it likely that this motion is related to the ester modification.

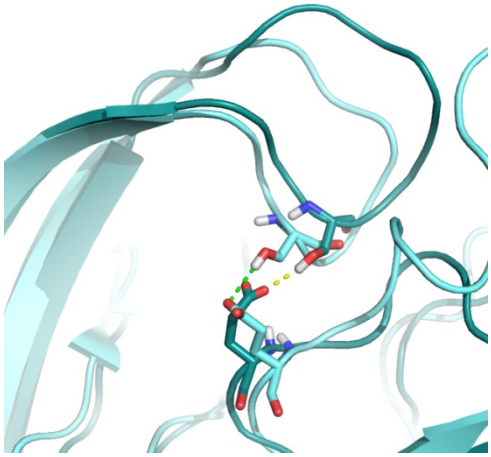

Figure 6.9: Positions of the C-loops in the first (lighter cyan) and second (darker cyan) MD simulations on the ester-containing protein at 2650 ps. Note the hydrogen bond between αS191 in the C-loop and γE179 is present in both structures.

6.2.3.2 Correlated Motion in MD Trajectories

Correlated motions between residues can be analyzed through a covariance analysis of coordinate displacements over the simulation trajectory.[18, 19] Examining correlated motions in a protein provides an understanding of which regions are strongly coupled to one another,

including those that are structurally or sequentially distant. To understand the global impact of the ester mutations on protein dynamics, we performed a covariance analysis on the C^{α} atoms of the wild-type and mutant proteins using the general correlation coefficient. Using this generalized correlation measure based on mutual information (MI) allows for the complete characterization of atomic correlations without suffering from many of the artifacts arising from the use of the standard Pearson correlation coefficient.[20]

From this analysis, an increase in correlated motions is seen in the ester-containing protein. To ensure that this observation was not a result of the structural equilibration during the first 100 ps of the simulation, we evaluated the covariation matrix for the last 5 ns of the simulations only. Again, the ester-containing protein overall displayed a moderately higher degree of coupled motions (Figure 6.9). Examining the difference between the covariation matrices of the wild-type and ester-modified proteins illustrates the overall similarity in the covariation matrices. The regions where the correlated motions deviated the most between the wild-type and ester-containing proteins correspond to regions of high mobility, such as the F-loops on the α_2 and δ subunits. Notably, no substantial differences in the amount of correlated motion around the ester mutation were observed. Combined, this analysis suggests that the ester modification leads to a small change in the overall dynamics of the protein, echoing the observed overall protein RMSD similarities.

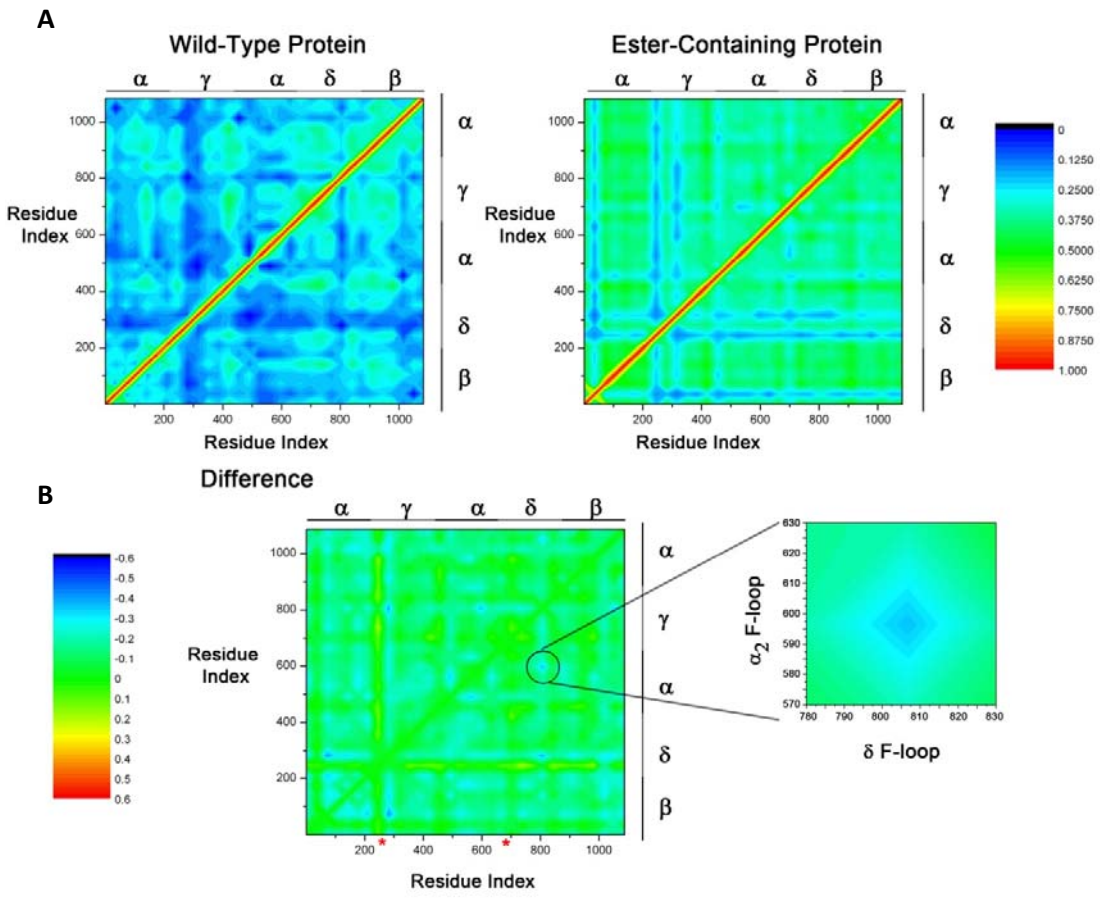

Figure 6.9: A) Correlated fluctuations of the C^{α} atoms in the WT and ester-containing protein. B) The differences in correlated motions between the WT and ester-containing proteins. Negative values (blue) indicate an increase in correlation motion in the ester-containing protein, while positive values (red) indicate a decrease in correlated motion. The green areas have values near zero and indicate regions of similar correlated motion in the two proteins. The red stars indicate the positions of the ester modifications.

6.3 Conclusions and Future Work

In the preliminary experiments described here, we have demonstrated that we can generate a homology model of the extracellular domain of the nAChR bearing an ester modification in two separate subunits and subject it to MD simulations. Unfortunately, the inconclusive nature of the experimental data for ester mutations at these sites makes comparison to experiment difficult in this case (see Chapter 5). However, there is still validity in the computational approach described herein for studying the effect of backbone esters in proteins. Although there are some striking differences between the unmodified and ester-

bearing proteins (hydrogen-bonding patterns, loop movements, etc.), the overall results of the MD simulations show similar RMSD and RMSF patterns, as well as similar movements of the residues in the aromatic box and elsewhere around the mutated residue. Future *in silico* studies of backbone esters might include studies at well-behaved and thoroughly characterized sites in the muscle or neuronal nAChRs.

As more crystal structures of membrane receptors are being solved, our ability to model these proteins expands. The recent β_2 adrenergic GPCR structure[21] opens up the possibility of expanding our computational studies to this exciting class of membrane proteins, which are just beginning to be characterized using unnatural amino acid mutagenesis.

6.4 Materials and Methods

6.4.1 Homology Modeling Protocol

A homology model of the extracellular domain of the mouse muscle nicotinic acetylcholine receptor was constructed using Modeller 9, version 5 (http://salilab.org/modeller/), using the crystal structure of the AChBP from Lymnaea stagnalis as the template. A sequence alignment based on experimental data was used (shown in Figure 6.10). Ten three-dimensional models of the full pentamer of the mouse muscle nAChR were generated using the automodel function (see also appendix 6.1: Constructing a basic homology model using Modeller). Although six of the seven disulfide bonds were correctly calculated based on the AChBP template alone, the disulfide in the β-subunit was missing. Therefore the Cys-loop disulfides were individually specified. Each of the ten homology models were individually evaluated, as discussed in Results and Discussion. Following selection of the best initial homology model, the loop refinement

feature of Modeller (loopmodel) was used to improve the position of several loop regions, again evaluated according to the criteria laid out in the Results and Discussion section.

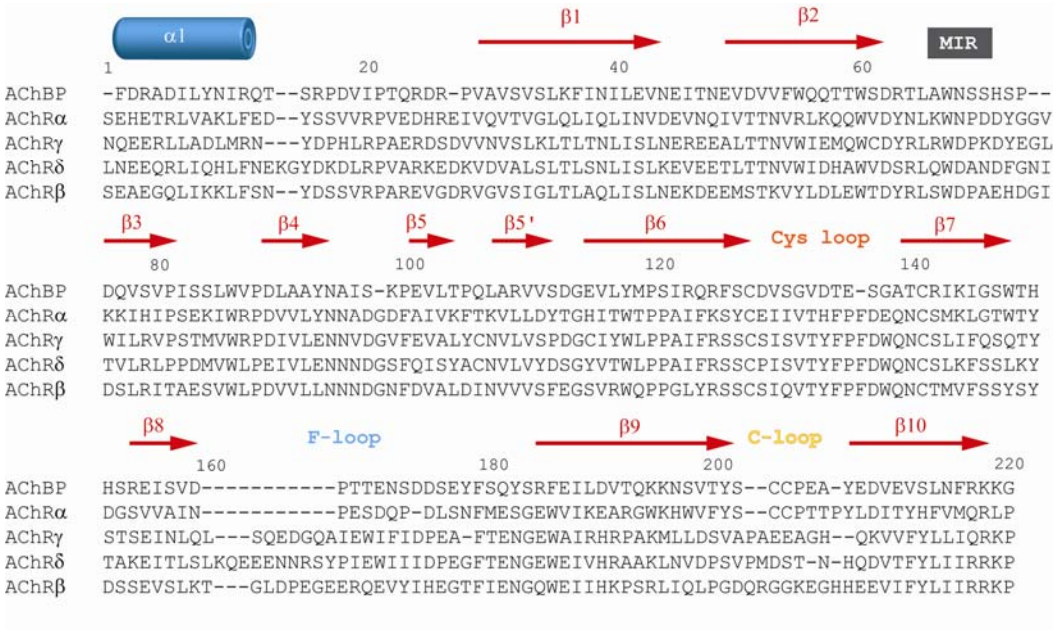

Figure 6.10: The sequence alignment between Lymnaea stagnalis AChBP and the muscle nAChR subunits.

6.4.2 Construction of the ester-containing protein

The homology model for the mouse muscle nAChR extracellular domain was modified using Pymol to create the ester-containing protein. This was accomplished by manually selecting and mutating the desired backbone NH groups to oxygen. Manually, the i-1 residue and the now α-hydroxy tryptophan residue were combined into a single residue with the name "VWA." This is important because the backbone oxygen alters the amide bond between the i-1 and i residues. In order to correctly parameterize the resulting ester bond, this unified residue is used. The i-1 residue in this case was a valine, so the resulting unified dipeptide was termed "VWA." Residues in the pentamer are listed continuously. Residues 264 and 265 from the original input file were unified, as were residues 694 and 695. Since each residue can have only one C^{α}, the designation

CA was changed to CA2 for the second residue. The ester oxygen was designated OA. The resulting pdb file was then imported into GROMACS, as outlined above.

Once the GROMACS input files were initially generated (after pdb2gmx, see below), the parameters related to the backbone ester (given in appendix 6.2: backbone ester parameters) were modified in several different locations.

(1) **The .gro file** The .gro file is a fixed-column coordinate file format. Residue numbering and labeling was verified.

(2) **The local .itp files** An .itp file is a topology that is included within the system topology, and defines a topology for a single specific molecule type. It contains entries for [atoms], [bonds], [angles], [dihedrals], [impropers], and [exclusions]. Because backbone esters are not a standard part of the GROMACS program, proper parameters needed to be specified and/or verified.

> [ATOMS]: In addition to changing the appropriate VAL and TRP residues to VWA, the masses and charges were adjusted, as needed (see appendix 6.2).
>
> [BONDS], [ANGLES], [DIHEDRALS], [IMPROPERS], [EXCLUSIONS]: the bonds, angles, dihedrals, and impropers involving the backbone oxygen in the unified VWA residue needed to be specified (see appendix 6.2).

(3) **ffG43a1.rtp** This is residue topology file and must be modified as root. Each residue entry starts with a directive for the residue abbreviation (i.e., [ALA]), followed by [atoms], [bonds], [angles], [dihedrals], [impropers], and [exclusions], with the specific content dictated by the force field chosen. The new dipeptide VWA was added with parameters specified in appendix 6.2.

(4) **aminoacids.dat** Another global GROMACS file listing the amino acid types. VWA was added to this file.

(5) **ffG43a1.hdb** This is the hydrogen database, containing entries for adding missing hydrogens to residue building blocks present in the force field .rtp file.

(6) **The local .ndx file** This is an index file that contains various categories that are useful for analysis. The standard categories are: System, Protein, Protein-H, C-alpha, Backbone, MainChain, MainChain+Cb, MainChain+H, SideChain, SideChain-H, Prot-Masses, Non-Protein, SOL, NA+, CL-, Other. Because the ester containing dipeptide is a non-standard residue, it will be included in System, Protein, Protein-H, but not in C-alpha, Backbone, MainChain, MainChain+Cb, MainChain+H, SideChain, or SideChain-H. Modifying each of these categories to include the relevant atoms from "VWA" is necessary only to the extent that they will be used for analysis. Since the .ndx file often gets automatically overwritten, this file was renamed upon modification.

6.4.3 Constructing the simulation box in GROMACS

The final, loop-optimized homology model was imported into the GROMACS program using pdb2gmx, e.g.:

```
$pdb2gmx -f input_structure.pdb -o output_structure.gro -p output_topology.top -i
output_topology2.top
```

A rectangular box with dimensions 9.49600 9.36000 6.383900 was generated:

```
$editconf -f output_structure.gro -o output_structure_box.gro -d 0.7
```

The simulation box was then solvated with SPC waters:

```
$genbox -cp output_structure_box.gro -cs spc216.gro -o output_structure_box_h2o.gro -p
output_topology.top
```

A MD parameters file (parameters.mdp) was constructed for the genion run, in which ions were generated to simulate physiological conditions and neutralize the simulation box. Before any minimization or MD run is performed, it is necessary to generate a start file (.tpr). This file contains the starting structure of your simulation (coordinates and velocities), the molecular topology and all the simulation parameters. It is generated by grompp and then executed by mdrun to perform the simulation.

```
$grompp -f parameters.mdp -c output_structure_box_h2o.gro -p output_topology.top -o
run.tpr
```

For the genion run, in order to neutralize the charge in the box, it is critical to note the charge in the output. For instance, if the charge is -62 and you want to mimic a 150 mM NaCl extracellular environment in a 9 nm^3 box, then:

150 mmol/L * $(9\ nm)^3$ * $(1\ cm/\ 10^7\ nm)^3$ * 1 $L/10^3\ cm^3$ * 1 mol/ 10^3 mmol * 6.022×10^{23} ions/mol = 65.9 ions

To neutralize charge, we need 62 more cations than anions, resulting in 66 cationic and 4 anionic species. This number of positively and negatively charged monovalent species is added to the box using genion:

```
$genion -s run.tpr -o output_structure_box_h2o_ion.gro -n index.ndx -g genion.log -np 66 -nn 4
-pname Na+ -nname Cl-
```

Several problems can crop up at this juncture. First, the order of the groups in the .top file must match that of the .gro file. In addition, the way the ions are specified in the .gro and .top files

may need to be adjusted. For instance, it may be necessary to change Cl to CL and Na to NA in the .gro file.

At this stage, the protein in its solvated, neutral box is ready for minimization.

6.4.4 GROMACS energy minimizations

A series of seven minimization steps was performed to prepare the proteins for molecular dynamics simulations:

Minimization 1: High homology residues frozen, protein backbone strongly restrained.

Minimization 2: High homology residues frozen, protein backbone weakly restrained.

Minimization 3: Aromatic box residues frozen, protein backbone weakly restrained.

Minimization 4: No residues frozen, high homology residues strongly restrained.

Minimization 5: No residues frozen, high homology residues weakly restrained.

Minimization 6: All non-hydrogen atoms strongly restrained.

Minimization 7: Completely unrestrained.

Minimization 1:

To achieve the specified position restraints, a position restraint file is generated (restrain_backbone.itp) with the specified force constants in the X, Y, and Z directions.

```
$genpr -f output_structure_box_h2o_ion.gro -n index.ndx -o restrain_backbone.itp -fc 1000
1000 1000
```

This position restraint file is then specified in the .mdp file in the line "define = -dBACKBONE_1000" and the end of each subunit's .itp file using an if statement:

```
; Include Backbone restraint file
```

```
#ifdef BACKBONE_1000
#include "restrain_backbone.itp"
#endif
```

A new .mdp file is specified with the desired run parameters (see appendix 6.3: Minimization and Molecular Dynamics Parameter files) and compiled into an input file for the minimization run:

```
$grompp -f structure_min1.mdp -c output_structure_box_h2o_ion.gro -n index.ndx -p
output_topology.top -o structure_min1.tpr
```

The input file (.tpr) is used to initiate the minimization run, as follows:

```
$mdrun -s structure_min1.tpr -o structure_min1.trr -x structure_min1.xtc -c structure_min1.gro
-e structure_min1.edr -g structure_min1.log &
```

The file extensions designate the following:

.trr: full-precision trajectory containing coordinate, velocity, and force information

.xtc: a compressed version of the trajectory, containing only coordinate, time, and box vector information

.gro: fixed-column coordinate file format first used in the GROMOS simulation package

.edr: a portable energy file, containing all the energy terms that are saved in a simulation

.log: a log file with run information, including errors encountered

Minimization 2:

To achieve the specified position restraints, a position restraint file is generated (restrain_backbone2.itp) with the specified force constants in the X, Y, and Z directions. Note that the input coordinate file is now the output from the first minimization.

```
$genpr -f structure_min1.gro -n index.ndx -o restrain_backbone2.itp -fc 500 500 500
```

This position restraint file is then specified in the .mdp file in the line "define = -dBACKBONE_500" and the end of each subunit's .itp file using an if statement:

```
; Include Backbone restraint file
#ifdef BACKBONE_500
#include "restrain_backbone2.itp"
#endif
```

A new .mdp file is specified with the desired run parameters (see appendix 6.3: Minimization and Molecular Dynamics Parameter files) and compiled into an input file for the minimization run:

```
$grompp -f structure_min2.mdp -c structure_min1.gro -n index.ndx -p output_topology.top -o structure_min2.tpr
```

The input file (.tpr) is used to initiate the minimization run, as follows:

```
$mdrun -s structure_min2.tpr -o structure_min2.trr -x structure_min2.xtc -c structure_min2.gro -e structure_min2.edr -g structure_min2.log &
```

Minimization 3:

No additional position restraint files were needed for this minimization. A new .mdp file is specified with the desired run parameters (see appendix 6.3: Minimization and Molecular Dynamics Parameter files) and compiled into an input file for the minimization run:

```
$grompp -f structure_min3.mdp -c structure_min2.gro -n index.ndx -p output_topology.top -o structure_min3.tpr
```

The input file (.tpr) is used to initiate the minimization run, as follows:

```
$mdrun -s structure_min3.tpr -o structure_min3.trr -x structure_min3.xtc -c structure_min3.gro
-e structure_min3.edr -g structure_min3.log &
```

Minimization 4:

To achieve the specified position restraints, a position restraint file is generated (Homology_1000.itp) with the specified force constants in the X, Y, and Z directions. Note that the input coordinate file is now the output from the third minimization.

```
$genpr -f structure_min2.gro -n index.ndx -o Homology_1000.itp -fc 1000 1000 1000
```

This position restraint file is then specified in the .mdp file in the line "define = -dHomology_1000" and the end of each subunit's .itp file using an if statement:

```
; Include Backbone restraint file
#ifdef Homology_1000
#include "Homology_1000.itp"
#endif
```

A new .mdp file is specified with the desired run parameters (see appendix 6.3: Minimization and Molecular Dynamics Parameter files) and compiled into an input file for the minimization run:

```
$grompp -f structure_min4.mdp -c structure_min3.gro -n index.ndx -p output_topology.top -o
structure_min4.tpr
```

The input file (.tpr) is used to initiate the minimization run, as follows:

```
$mdrun -s structure_min4.tpr -o structure_min4.trr -x structure_min4.xtc -c structure_min4.gro
-e structure_min4.edr -g structure_min4.log &
```

Minimization 5:

To achieve the specified position restraints, a position restraint file is generated (Homology_500.itp) with the specified force constants in the X, Y, and Z directions. Note that the input coordinate file is now the output from the fourth minimization.

```
$genpr -f structure_min2.gro -n index.ndx -o Homology_500.itp -fc 500 500 500
```

This position restraint file is then specified in the .mdp file in the line "define = -dHomology_500" and the end of each subunit's .itp file using an if statement:

```
; Include Backbone restraint file
#ifdef Homology_500
#include "Homology_500.itp"
#endif
```

A new .mdp file is specified with the desired run parameters (see appendix 6.3: Minimization and Molecular Dynamics Parameter files) and compiled into an input file for the minimization run:

```
$grompp -f structure_min5.mdp -c structure_min4.gro -n index.ndx -p output_topology.top -o
structure_min5.tpr
```

The input file (.tpr) is used to initiate the minimization run, as follows:

```
$mdrun -s structure_min5.tpr -o structure_min5.trr -x structure_min5.xtc -c structure_min5.gro
-e structure_min5.edr -g structure_min5.log &
```

Minimization 6:

To achieve the specified position restraints, a position restraint file is generated (nonH_1000.itp) with the specified force constants in the X, Y, and Z directions. Note that the input coordinate file is now the output from the fifth minimization.

```
$genpr -f structure_min2.gro -n index.ndx -o nonH_1000.itp -fc 1000 1000 1000
```

This position restraint file is then specified in the .mdp file in the line "define = -dnonH_1000" and the end of each subunit's .itp file using an if statement:

```
; Include Backbone restraint file
#ifdef nonH_1000
#include " nonH_1000.itp"
#endif
```

A new .mdp file is specified with the desired run parameters (see appendix 6.3: Minimization and Molecular Dynamics Parameter files) and compiled into an input file for the minimization run:

```
$grompp -f structure_min6.mdp -c structure_min5.gro -n index.ndx -p output_topology.top -o
structure_min6.tpr
```

The input file (.tpr) is used to initiate the minimization run, as follows:

```
$mdrun -s structure_min6.tpr -o structure_min6.trr -x structure_min6.xtc -c structure_min6.gro
-e structure_min6.edr -g structure_min6.log &
```

Minimization 7:

The final minimization had no position restraints. A new .mdp file is specified with the desired run parameters (see appendix 3: Minimization and Molecular Dynamics Parameter files) and compiled into an input file for the minimization run:

```
$grompp -f structure_min7.mdp -c structure_min6.gro -n index.ndx -p output_topology.top -o
structure_min7.tpr
```

The input file (.tpr) is used to initiate the minimization run, as follows:

```
$mdrun -s structure_min7.tpr -o structure_min7.trr -x structure_min7.xtc -c structure_min7.gro
-e structure_min7.edr -g structure_min7.log &
```

Upon completion of all the minimization steps, the trajectories were concatenated and the energy and RMSD profiles of these runs were examined, along with the final structure (Figure 6.4).

```
trjcat -f structure_min1.trr structure_min2.trr structure_min3.trr structure_min4.trr
structure_min5.trr structure_min6.trr structure_min7.trr -o concat_min1_7.xtc -n index.ndx

g_rms -s structure_min1.tpr -f concat_min1_7.xtc -o concat_min1_7_rms.xvg

g_energy -f structure_min1.edr -o structure_min1_nrg.xvg (and so on for each minimization)

editconf -f structure_min7.gro -n index.ndx -o structure_min7.pdb
```

6.4.5 GROMACS Molecular Dynamics Simulations

Once it was confirmed that the energy and structure from the minimizations were sensible (i.e. no dramatic deviations from the initial homology model and no anomalous energy fluctuations, see Figure 6.4), a series of molecular dynamics runs were initiated.

The MD runs were begun at 0 K and the temperature was gradually increased to 310 K with a linear annealing function over the first 25 ps (see appendix 6.3: Minimization and Molecular Dynamics Parameter files). The protein was strongly constrained during this warm-up phase and then the restraints were relaxed over the subsequent 125 ps. After this point the simulations proceeded unrestrained.

MD1: 50 ps. Annealing from 0 to 310 K over the first 25 ps, held at 310 K for the remaining 25 ps. Protein strongly restrained.

MD2: 50 ps. Backbone strongly restrained.

MD3: 50 ps. Backbone weakly restrained.

MD4-11: 850 ps each. No restraints.

MD1:

Position restraints were fulfilled and specified in the appropriate places, as was done in the minimization runs.

```
$genpr -f structure_min7.gro -n index.ndx -o restrain_protein.itp -fc 1000 1000 1000
```

MD input file was compiled:

```
$grompp -f structure_md1.mdp -c structure_min7.gro -n index.ndx -p  output_topology.top -o
structure_md1.tpr
```

MD run initiated:

```
$mdrun -s structure_md1.tpr -o structure_md1.trr -x structure_md1.xtc -c
structure_md1.gro -e structure_md1.edr -g structure_md1.log &
```

MD2-11:

Position restraints were fulfilled and specified in the appropriate places, as was done in the minimization runs. No additional positional restraint files were needed, because the backbone constraint files had already been generated during the minimizations. The time designated at the start of the run, tint, is changed in each of these MD runs to reflect the simulation time of the previous MD runs (e.g. MD2 begins at 50 ps instead of 0 ps, where MD1 ended).

MD input file was compiled:

```
$grompp -f structure_md2.mdp -c structure_md1.gro -n index.ndx -p output_topology.top -o
structure_md2.tpr
```

MD run initiated:

```
$mdrun -s structure_md2.tpr -o structure_md2.trr -x structure_md2.xtc -c
structure_md2.gro -e structure_md2.edr -g structure_md2.log &
```

6.4.5 Analysis

RMSD values were calculated using g_rms. RMSF values were calculated on the concatenated trajectories using g_rmsf.

Side chain plane angles were calculated using g_sgangle. Index groups were defined for each side chain. Tryptophan side chains were defined by CG, CZ3, and NE atoms. Tyrosine side chains were defined by the CG, CE1, and CE2 atoms. g_sgangle was used with the option -noone to calculated interplane angles between two residues.

Hydrogen bonding patterns were evaluated using g_hbond. Non-overlapping groups were created in the index file for this analysis. The resulting .xpm file was converted to an .eps format using xpm2ps.

The correlation matrices were calculated on the protein α-carbons using g_correlation, downloaded from http://www.mpibpc.mpg.de/groups/grubmueller/olange/gencorr.html and installed in GROMACS. MATLAB[22] was used to read the *.dat output generated by g_correlation and produce the matrix of correlation coefficients. This matrix was written to Microsoft Excel before being exported and plotted using the Origin software program.[23]

6.5 References

1. Brejc, K. et al. Crystal structure of an ACh-binding protein reveals the ligand-binding domain of nicotinic receptors. *Nature* **411**, 269-76 (2001).
2. Fiser, A., Do, R.K. & Sali, A. Modeling of loops in protein structures. *Protein Sci* **9**, 1753-73 (2000).
3. Sali, A. & Blundell, T.L. Comparative protein modelling by satisfaction of spatial restraints. *J Mol Biol* **234**, 779-815 (1993).
4. Notredame, C., Higgins, D.G. & Heringa, J. T-Coffee: A novel method for fast and accurate multiple sequence alignment. *J Mol Biol* **302**, 205-17 (2000).
5. Sine, S.M., Wang, H.L. & Bren, N. Lysine scanning mutagenesis delineates structural model of the nicotinic receptor ligand binding domain. *J Biol Chem* **277**, 29210-23 (2002).
6. Shen, M.Y. & Sali, A. Statistical potential for assessment and prediction of protein structures. *Protein Sci* **15**, 2507-24 (2006).
7. Czajkowski, C. & Karlin, A. Agonist binding site of Torpedo electric tissue nicotinic acetylcholine receptor. A negatively charged region of the delta subunit within 0.9 nm of the alpha subunit binding site disulfide. *J Biol Chem* **266**, 22603-12 (1991).
8. Czajkowski, C. & Karlin, A. Structure of the nicotinic receptor acetylcholine-binding site. Identification of acidic residues in the delta subunit within 0.9 nm of the 5 alpha subunit-binding. *J Biol Chem* **270**, 3160-4 (1995).
9. Karlin, A. Chemical Modification of the Active Site of the Acetylcholine Receptor. *J Gen Physiol* **54**, 245-264 (1969).
10. Delano, W.L. (Delano Scientific, Palo Alto, CA, 2002).
11. Amiri, S., Sansom, M.S. & Biggin, P.C. Molecular dynamics studies of AChBP with nicotine and carbamylcholine: the role of water in the binding pocket. *Protein Eng Des Sel* **20**, 353-9 (2007).
12. Cheng, X., Ivanov, I., Wang, H., Sine, S.M. & McCammon, J.A. Nanosecond-timescale conformational dynamics of the human alpha7 nicotinic acetylcholine receptor. *Biophys J* **93**, 2622-34 (2007).
13. Cheng, X., Wang, H., Grant, B., Sine, S.M. & McCammon, J.A. Targeted molecular dynamics study of C-loop closure and channel gating in nicotinic receptors. *PLoS Comput Biol* **2**, e134 (2006).
14. Liu, L.T., Willenbring, D., Xu, Y. & Tang, P. General anesthetic binding to neuronal alpha4beta2 nicotinic acetylcholine receptor and its effects on global dynamics. *J Phys Chem B* **113**, 12581-9 (2009).
15. Yi, M., Tjong, H. & Zhou, H.X. Spontaneous conformational change and toxin binding in alpha7 acetylcholine receptor: insight into channel activation and inhibition. *Proc Natl Acad Sci U S A* **105**, 8280-5 (2008).
16. Hansen, S.B. et al. Structures of Aplysia AChBP complexes with nicotinic agonists and antagonists reveal distinctive binding interfaces and conformations. *EMBO J* **24**, 3635-46 (2005).
17. Shi, J., Koeppe, J.R., Komives, E.A. & Taylor, P. Ligand-induced conformational changes in the acetylcholine-binding protein analyzed by hydrogen-deuterium exchange mass spectrometry. *J Biol Chem* **281**, 12170-7 (2006).

18. Hunenberger, P.H., Mark, A.E. & van Gunsteren, W.F. Fluctuation and cross-correlation analysis of protein motions observed in nanosecond molecular dynamics simulations. *J Mol Biol* **252**, 492-503 (1995).
19. Ichiye, T. & Karplus, M. Collective motions in proteins: a covariance analysis of atomic fluctuations in molecular dynamics and normal mode simulations. *Proteins* **11**, 205-17 (1991).
20. Lange, O.F. & Grubmuller, H. Generalized correlation for biomolecular dynamics. *Proteins* **62**, 1053-61 (2006).
21. Rasmussen, S.G. et al. Crystal structure of the human beta2 adrenergic G-protein-coupled receptor. *Nature* **450**, 383-7 (2007).
22. MATLAB version 7.0.4 (MathWorks Inc., Natick, MA, 2005).
23. Deschenes, L.A. Origin 6.0: Scientific Data Analysis and Graphing Software Origin Lab Corporation (formerly Microcal Software, Inc.). Web site: www.originlab.com. Commercial price: $595. Academic price: $446. *Journal of the American Chemical Society* **122**, 9567-9568 (2000).

Appendix 6.1: Constructing a basic homology model using Modeller

Step 1: Construct a good target-template alignment.

The target sequence- sequence of desired homology model

The template sequence- sequence of the existing structure (ie AChBP)

The quality of your sequence alignment will strongly influence the quality of your homology model. I recommend using a sequence alignment that is based partially on experimental results (when possible).

The format of your sequence alignment should be as is shown in the file mm_nAChR.ali

-The first line of each sequence entry specifies the protein code after the >P1; line identified.

-The second line contains information necessary to extract the atomic coordinates of the segment from the original PDB coordinate set. Fields are separated by colon characters.

-**Field 1**: specification of whether or not the 3D structure is available. For our purposes, this will be either structureX (for x-ray structure of template) or sequence (for the target).
-**Field 2**: The PDB code
-**Field 3-6**: the residue and chain identifiers for the first and last residue of the sequence given in the subsequent lines. Note in the example file, this field is **1:A:+1025:E:** for the template, specifying that the first residue is 1 in chain A and the last is 1025 in chain E. In the target sequence, these fields are unnecessary.
-**Field 7**: Protein name (optional)
-**Field 8**: Source of protein (optional)
-**Field 9**: Resolution (optional)
-**Field 10**: R-factor (optional)

-The subsequent lines have the aligned sequence in them**.** Chain breaks are indicated by " / ". **If you are using AChBP for a template, this is the only part of this file you will need to change.**

Step 2: Build your model using model.py

Once the target-template alignment is ready, MODELLER calculates a 3D model of the target completely automatically, using the automodel class. The model.py script will generate 5 similar models of your target based on the template. There are several features of this script that you should be aware of.

- The **special_restraints** (below) part of the script constrains the C_αs in chains A and C to be the same. This was done because there are 2 alpha subunits in the muscle nicotinic receptor. It is not strictly necessary to do this.

```
def special_restraints(self, aln):
                    s1 = selection(self.chains['A']).only_atom_types('CA')
                    s2 = selection(self.chains['C']).only_atom_types('CA')
                    self.restraints.symmetry.append(symmetry(s1, s2, 1.0))
                    rsr = self.restraints
                    at = self.atoms
```

-The special_patches (below) part of the script forces a disulfide bond between the specified residues (in the specified chain) and to specify secondary structural elements. Neither of these things is strictly necessary, however, it is sometimes handy to be able to do. # is used to "comment out" a line, i.e., if you put it before a line, the program will ignore that line.

```
def special_patches(self, aln):
        # A disulfide between residues 128 and 142, ie the Cys-loop:
        #self.patch(residue_type='DISU', residues=(self.residues['128:A'], self.residues['142:A']))
        #self.patch(residue_type='DISU', residues=(self.residues['338:B'], self.residues['352:B']))
        #self.patch(residue_type='DISU', residues=(self.residues['557:C'], self.residues['571:C']))
        #self.patch(residue_type='DISU', residues=(self.residues['770:D'], self.residues['784:D']))
        self.patch(residue_type='DISU', residues=(self.residues['993:E'], self.residues['1007:E']))
#residues 1 thru 10 of chain A and B should be an alpha helix
        #rsr.add(secondary_structure.alpha(self.residue_range('1:A', '10:A')))
        #rsr.add(secondary_structure.alpha(self.residue_range('483:C', '499:C')))
        #rsr.add(secondary_structure.alpha(self.residue_range('239:B', '251:B')))
```

-The last several lines of the script are crucial:

```
a = MyModel(env, alnfile='mm_nAChR-mult.ali',

                knowns=('1I9B'), sequence='mm_nAChR',
                assess_methods=(assess.DOPE, assess.GA341))

a.starting_model = 1
a.ending_model = 5
a.make()
```

The name, as specified in your .ali file, of the template you are using.

The name, as specified in your .ali file, of the target sequence

Assessment methods provide a quick way of evaluating various models relative to one another.

Dictates # of models to generate.

Once you have model.py specified the way you want, you should open the Modeller program from the start menu of your computer. This will give you a DOS command prompt window. Now you need to be in the proper directory. To change directories, type cd followed by the directory you want (use tab to auto complete the folder name). Your default start directory will be in the Modeller9v5 directory in your program files directory:

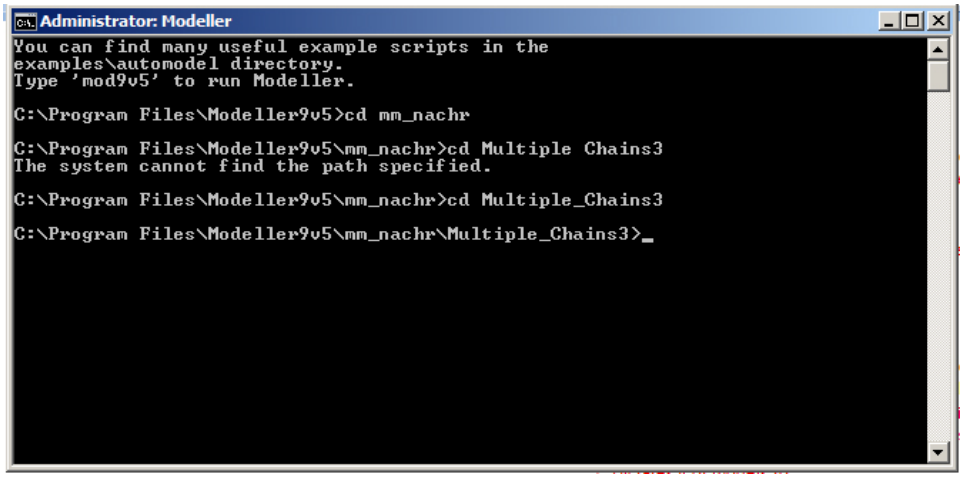

Once you are in the proper directory, type: **mod9v5 model.py**, which will run the script for you. It will take several minutes for the script to finish.

Step 3: Evaluate your model

Step 3A: Since we included assess_methods in our model.py script, the bottom of the output log file (named model.log) will have a summary of the produced models, listing both DOPE and GA341 scores. These provide a quick and dirty way to assess which model is best.

-The DOPE (Discrete Optimized Protein Energy) is the more reliable of the two. The lowest (most negative) value is the best.

-GA341 is another method. Here 0.0 is worst and 1.0 is best.

Step 3B: Since the assessment scores mentioned above are for the entire protein, you might want to know which residues/regions of the model are the "worst." To do this, you need to run an assessment. The script for this is called evaluate_model.py. The output file will be *.profile that you specify at the end of the script (below-mm_nAChR_min7.profile).

```
s.assess_dope(output='ENERGY_PROFILE NO_REPORT', file='mm_nAChR_min7.profile',
              normalize_profile=True, smoothing_window=15)
```

-To run the script, type: mod9v5 evaluate_model.py

-You will want to paste the output contained in the *.profile file into excel, using the text-to-column delimited option. From there you can plot the DOPE score on a residue by residue basis. This is convenient because you are then able to hone in on potential problem spots in your homology model when looking at them using whatever visualization program you prefer.

Step 4: Refine loops (optional)

Depending on how your model looks, you may decide to refine some of the loops in your structure. For example, Loop F is much shorter in AChBP than it is in the d and g subunits of the muscle receptor, which lead to some odd loop conformations in my original homology models. These could be fixed using the loop_refine.py script.

-You will want to specify the amino acids that define the loop, as well as which homology model you want to refine (remember in step 3 we generated 5 separate models). You will also get to specify the number of independent loop refinements you want the program to run.

-To run, type: mod9v5 loop_refine.py

```
# Loop refinement of an existing model

from modeller import *
from modeller.automodel import *

log.verbose()
env = environ()

# directories for input atom files
env.io.atom_files_directory = './:../atom_files'

# Create a new class based on 'loopmodel' so that we can redefine
# select_loop_atoms (necessary)
class myloop(loopmodel):
        # This routine picks the residues to be refined by loop modeling
   def select_loop_atoms(self):
        # 10 residue insertion
      return selection(self.residue_range('394:B', '406:B'))

m = myloop(env,
        inimodel='mm_nAChR6A.pdb',                  # initial model of the target
        sequence='mm_nAChR')                        # code of the target

m.loop.starting_model= 1        # index of the first loop model
m.loop.ending_model  = 1        # index of the last loop model

m.loop.md_level = refine.very_fast      # loop refinement method

m.make()
```

Starting residue: chain

Name of model to be refined

Number of loop refinement models to be produced

Appendix 6.2: Backbone Ester Parameters for GROMACS

[VWA]
[atoms]

N	N	-0.28000	0
H	H	0.28000	0
CA	CH1	0.00000	1
CB	CH1	0.00000	1
CG1	CH3	0.00000	1
CG2	CH3	0.00000	1
C	C	0.270	2
O	O	-0.190	2
OA	OA	-0.18000	0
CA2	CH1	0.10000	1
CB2	CH2	0.00000	1
CG3	C	-0.14000	2
CD1	C	-0.10000	2
HD1	HC	0.10000	2
CD2	C	0.00000	2
NE1	NR	-0.05000	2
HE1	H	0.19000	2
CE2	C	0.00000	2
CE3	C	-0.10000	3
HE3	HC	0.10000	3
CZ2	C	-0.10000	4
HZ2	HC	0.10000	4
CZ3	C	-0.10000	5
HZ3	HC	0.10000	5
CH2	C	-0.10000	6
HH2	HC	0.10000	6
C2	C	0.380	7
O2	O	-0.380	7

[bonds]

N	H gb_2
N	CA gb_20
CA	C gb_26
C	O gb_4
C	OA gb_17
CA	CB gb_26
CB	CG1 gb_26
CB	CG2 gb_26
OA	CA2 gb_17
CA2	C2 gb_26
C2	O2 gb_4
C2	+N gb_9
CA2	CB2 gb_26
CB2	CG3 gb_26
CG3	CD1 gb_9
CG3	CD2 gb_15
CD1	HD1 gb_3
CD1	NE1 gb_9
CD2	CE2 gb_15
CD2	CE3 gb_15
NE1	HE1 gb_2
NE1	CE2 gb_9
CE2	CZ2 gb_15
CE3	HE3 gb_3
CE3	CZ3 gb_15
CZ2	HZ2 gb_3
CZ2	CH2 gb_15
CZ3	HZ3 gb_3
CZ3	CH2 gb_15
CH2	HH2 gb_3

[exclusions]
; ai aj
CB2 HD1
CB2 NE1
CB2 CE2
CB2 CE3
CG3 HE1
CG3 HE3
CG3 CZ2
CG3 CZ3
CD1 CE3
CD1 CZ2
HD1 CD2
HD1 HE1
HD1 CE2
CD2 HE1
CD2 HZ2
CD2 HZ3
CD2 CH2
NE1 CE3
NE1 HZ2
NE1 CH2
HE1 CZ2
CE2 HE3
CE2 CZ3
CE2 HH2
CE3 CZ2
CE3 HH2
HE3 HZ3
HE3 CH2
CZ2 HZ3
HZ2 CZ3
HZ2 HH2
HZ3 HH2

[angles]
; ai aj ak gromos type
-C N H ga_31
H N CA ga_17
-C N CA ga_30
N CA C ga_12
CA C OA ga_18
CA C O ga_29
O C OA ga_32
N CA CB ga_12
C CA CB ga_12
CA CB CG1 ga_14
CA CB CG2 ga_14
CG1 CB CG2 ga_14
C OA CA2 ga_9
OA CA2 C2 ga_12
CA2 C2 +N ga_18
CA2 C2 O2 ga_29
O2 C2 +N ga_32
OA CA2 CB2 ga_12
C2 CA2 CB2 ga_12
CA2 CB2 CG3 ga_14
CB2 CG3 CD1 ga_36
CB2 CG3 CD2 ga_36
CD1 CG3 CD2 ga_6
CG3 CD1 HD1 ga_35
HD1 CD1 NE1 ga_35
CG3 CD1 NE1 ga_6
CG3 CD2 CE2 ga_6
CD1 NE1 CE2 ga_6
CD1 NE1 HE1 ga_35
HE1 NE1 CE2 ga_35
NE1 CE2 CD2 ga_6
CG3 CD2 CE3 ga_38
NE1 CE2 CZ2 ga_38
CD2 CE2 CZ2 ga_26
CE2 CD2 CE3 ga_26
CD2 CE3 HE3 ga_24
HE3 CE3 CZ3 ga_24
CD2 CE3 CZ3 ga_26
CE2 CZ2 HZ2 ga_24
HZ2 CZ2 CH2 ga_24
CE2 CZ2 CH2 ga_26
CE3 CZ3 HZ3 ga_24
HZ3 CZ3 CH2 ga_24
CE3 CZ3 CH2 ga_26
CZ2 CH2 HH2 ga_24
HH2 CH2 CZ3 ga_24
CZ2 CH2 CZ3 ga_26

[impropers]
; ai aj ak al gromos type
N -C CA H gi_1
C CA OA O gi_1
CA N C CB gi_2
CB CG2 CG1 CA gi_2
C2 CA2 +N O2 gi_1
CA2 OA C2 CB2 gi_2
CG3 CD1 CD2 CB2 gi_1
CD2 CG3 CD1 NE1 gi_1
CD1 CG3 CD2 CE2 gi_1
CG3 CD1 NE1 CE2 gi_1
CG3 CD2 CE2 NE1 gi_1
CD1 NE1 CE2 CD2 gi_1
CD1 CG3 NE1 HD1 gi_1
NE1 CD1 CE2 HE1 gi_1
CD2 CE2 CE3 CG3 gi_1
CE2 CD2 CZ2 NE1 gi_1
CE3 CD2 CE2 CZ2 gi_1
CD2 CE2 CZ2 CH2 gi_1
CE2 CD2 CE3 CZ3 gi_1
CE2 CZ2 CH2 CZ3 gi_1
CD2 CE3 CZ3 CH2 gi_1
CE3 CZ3 CH2 CZ2 gi_1
CE3 CD2 CZ3 HE3 gi_1
CZ2 CE2 CH2 HZ2 gi_1
CZ3 CE3 CH2 HZ3 gi_1
CH2 CZ2 CZ3 HH2 gi_1

[dihedrals]
; ai aj ak al gromos type
-CA -C N CA gd_4
-C N CA C gd_19
N CA C OA gd_20
N CA CB CG1 gd_17
CA C OA CA2 gd_3
C OA CA2 C2 gd_12
OA CA2 C2 +N gd_17
OA CA2 CB2 CG3 gd_20
CA2 CB2 CG3 CD2 gd_20

Appendix 6.3: Minimization and Molecular Dynamics Parameter files
WT and ester-containing files are equivalent with the sole exception of the title.

Minimization 1: mm_nachr_min1.mdp, wah_nachr_min1.mdp

```
title                    = wah_nachr_min1
cpp                      = /lib/cpp
define                   = -dBACKBONE_1000
integrator               = steep
emstep                   = 0.01
tinit                    = 0.0
nsteps                   = 5000
nstlog                   = 10
nstlist                  = 10
ns_type                  = grid
rlist                    = 0.8
coulombtype              = PME
fourierspacing           = 0.10
pme_order                = 4
ewald_rtol               = 1e-5
epsilon_r                = 80
rcoulomb                 = 0.8
rvdw                     = 0.8
freeze_grps              = high_homology
freeze_dim               = y y y
```

Minimization 2: mm_nachr_min2.mdp, wah_nachr_min2.mdp

```
title                    = wah_nachr_min2
cpp                      = /lib/cpp
define                   = -dBACKBONE_500
integrator               = steep
emstep                   = 0.01
tinit                    = 0.0
nsteps                   = 5000
nstlog                   = 10
nstlist                  = 10
ns_type                  = grid
rlist                    = 0.8
coulombtype              = PME
fourierspacing           = 0.10
pme_order                = 4
ewald_rtol               = 1e-5
epsilon_r                = 80
rcoulomb                 = 0.8
rvdw                     = 0.8
freeze_grps              = high_homology
freeze_dim               = y y y
```

Minimization 3: mm_nachr_min3.mdp, wah_nachr_min3.mdp

```
title                    = wah_nachr_min3
cpp                      = /lib/cpp
define                   = -dBACKBONE_500
integrator               = steep
emstep                   = 0.01
tinit                    = 0.0
nsteps                   = 5000
nstlog                   = 10
nstlist                  = 10
```

```
ns_type                  = grid
rlist                    = 0.8
coulombtype              = PME
fourierspacing           = 0.10
pme_order                = 4
ewald_rtol               = 1e-5
epsilon_r                = 80
rcoulomb                 = 0.8
rvdw                     = 0.8
freeze_grps              = boxes
freeze_dim               = y y y
```

Minimization 4: mm_nachr_min4.mdp, wah_nachr_min4.mdp

```
title                    = wah_nachr_min4
cpp                      = /lib/cpp
define                   = -dHomology_1000
integrator               = steep
emstep                   = 0.01
tinit                    = 0.0
nsteps                   = 10000
nstlog                   = 10
nstlist                  = 10
ns_type                  = grid
rlist                    = 0.8
coulombtype              = PME
fourierspacing           = 0.10
pme_order                = 4
ewald_rtol               = 1e-5
epsilon_r                = 80
rcoulomb                 = 0.8
rvdw                     = 0.8
```

Minimization 5: mm_nachr_min5.mdp, wah_nachr_min5.mdp

```
title                    = wah_nachr_min5
cpp                      = /lib/cpp
define                   = -dHomology_500
integrator               = steep
emstep                   = 0.01
tinit                    = 0.0
nsteps                   = 6000
nstlog                   = 10
nstlist                  = 10
ns_type                  = grid
rlist                    = 0.8
coulombtype              = PME
fourierspacing           = 0.10
pme_order                = 4
ewald_rtol               = 1e-5
epsilon_r                = 80
rcoulomb                 = 0.8
rvdw                     = 0.8
```

Minimization 6: mm_nachr_min6.mdp, wah_nachr_min6.mdp

```
title                    = wah_nachr_min6
cpp                      = /lib/cpp
define                   = -dnonH_1000
integrator               = steep
```

```
emstep                  = 0.01
tinit                   = 0.0
nsteps                  = 6000
nstlog                  = 10
nstlist                 = 10
ns_type                 = grid
rlist                   = 0.8
coulombtype             = PME
fourierspacing          = 0.10
pme_order               = 4
ewald_rtol              = 1e-5
epsilon_r               = 80
rcoulomb                = 0.8
rvdw                    = 0.8
```

Minimization 7: mm_nachr_min7.mdp, wah_nachr_min7.mdp

```
title                   = wah_nachr_min7
cpp                     = /lib/cpp
define                  =
integrator              = steep
emstep                  = 0.01
tinit                   = 0.0
nsteps                  = 10000
nstlog                  = 10
nstlist                 = 10
ns_type                 = grid
rlist                   = 0.8
coulombtype             = PME
fourierspacing          = 0.10
pme_order               = 4
ewald_rtol              = 1e-5
epsilon_r               = 80
rcoulomb                = 0.8
rvdw                    = 0.8
```

MD Run 1: mm_nachr_md1.mdp, wah_nachr_md1.mdp

```
title                   = wah_nachr_md1
cpp                     = /lib/cpp
define                  = -dProtein_1000
integrator              = md
dt                         = 0.002
tinit                   = 0.0
nsteps                  = 25000
nstxout                 = 5000
nstvout                 = 5000
nstlog                  = 250
nstenergy               = 500
nstxtcout               = 250
xtc_grps                = Protein  SOL  Na+  Cl-
energygrps              = Protein  SOL  Na+  Cl-
nstlist                 = 10
ns_type                 = grid
rlist                   = 1.0
coulombtype             = PME
fourierspacing          = 0.10
pme_order               = 4
ewald_rtol              = 1e-5
optimize_fft            = yes
```

```
rcoulomb                = 1.0
rvdw                    = 1.0
pbc                     = xyz
tcoupl                  = berendsen
tc-grps                 = Protein  SOL  Na+  Cl-
tau_t                   = 0.1 0.1 0.1 0.1
ref_t                   = 310 310 310 310
annealing               = single single single single
annealing_npoints       = 2 2 2 2
annealing_time          = 0 25    0 25   0 25   0 25
annealing_temp          = 0 310   0 310  0 310  0 310
Pcoupl                  = berendsen
pcoupltype              = anisotropic
tau_p                = 1.0 1.0 1.0 1.0 1.0 1.0
compressibility         = 4.5e-5 4.5e-5 4.5e-5 0 0 0
ref_p                   = 1.0 1.0 1.0 1.0 1.0 1.0
E_z                     = 1 -0.05 1
gen_vel                 = no
gen_temp                = 310
gen_seed                = 173529
constraints             = all-bonds
constraint_algorithm    = lincs
unconstrained_start     = no
```

MD Run 2: mm_nachr_md2.mdp, wah_nachr_md2.mdp

```
title                   = wah_nachr_md2
cpp                     = /lib/cpp
define                  = -dBackbone_1000
integrator              = md
dt                         = 0.002
tinit                   = 50.0
nsteps                  = 25000
nstxout                 = 5000
nstvout                 = 5000
nstlog                  = 250
nstenergy               = 500
nstxtcout               = 250
xtc_grps                = Protein  SOL  Na+  Cl-
energygrps              = Protein  SOL  Na+  Cl-
nstlist                 = 10
ns_type                 = grid
rlist                   = 1.0
coulombtype             = PME
fourierspacing          = 0.10
pme_order               = 4
ewald_rtol              = 1e-5
optimize_fft            = yes
rcoulomb                = 1.0
rvdw                    = 1.0
pbc                     = xyz
tcoupl                  = berendsen
tc-grps                 = Protein  SOL  Na+  Cl-
tau_t                   = 0.1 0.1 0.1 0.1
ref_t                   = 310 310 310 310
Pcoupl                  = berendsen
pcoupltype              = anisotropic
tau_p                = 1.0 1.0 1.0 1.0 1.0 1.0
compressibility         = 4.5e-5 4.5e-5 4.5e-5 0 0 0
ref_p                   = 1.0 1.0 1.0 1.0 1.0 1.0
E_z                     = 1 -0.05 1
```

```
gen_vel                 = no
gen_temp                = 310
gen_seed                = 173529
constraints             = all-bonds
constraint_algorithm    = lincs
unconstrained_start     = no
```

MD Run 3: mm_nachr_md3.mdp, wah_nachr_md3.md

```
title                   = wah_nachr_md3
cpp                     = /lib/cpp
define                  = -dBackbone_500
integrator              = md
dt                          = 0.002
tinit                   = 100.0
nsteps                  = 25000
nstxout                 = 5000
nstvout                 = 5000
nstlog                  = 250
nstenergy               = 500
nstxtcout               = 250
xtc_grps                = Protein  SOL  Na+  Cl-
energygrps              = Protein  SOL  Na+  Cl-
nstlist                 = 10
ns_type                 = grid
rlist                   = 1.0
coulombtype             = PME
fourierspacing          = 0.10
pme_order               = 4
ewald_rtol              = 1e-5
optimize_fft            = yes
rcoulomb                = 1.0
rvdw                    = 1.0
pbc                     = xyz
tcoupl                  = berendsen
tc-grps                 = Protein  SOL  Na+  Cl-
tau_t                   = 0.1 0.1 0.1 0.1
ref_t                   = 310 310 310 310
Pcoupl                  = berendsen
pcoupltype              = anisotropic
tau_p                 = 1.0 1.0 1.0 1.0 1.0 1.0
compressibility         = 4.5e-5 4.5e-5 4.5e-5 0 0 0
ref_p                   = 1.0 1.0 1.0 1.0 1.0 1.0
E_z                     = 1 -0.05 1
gen_vel                 = no
gen_temp                = 310
gen_seed                = 173529
constraints             = all-bonds
constraint_algorithm    = lincs
unconstrained_start     = no
```

MD Run 4: mm_nachr_md4.mdp, wah_nachr_md4.mdp

```
title                   = wah_nachr_md4
cpp                     = /lib/cpp
define                  =
```

```
integrator              = md
dt                     = 0.002
tinit                   = 150.0
nsteps                  = 425000
nstxout                 = 5000
nstvout                 = 5000
nstlog                  = 250
nstenergy               = 500
nstxtcout               = 250
xtc_grps                = Protein  SOL  Na+  Cl-
energygrps              = Protein  SOL  Na+  Cl-
nstlist                 = 10
ns_type                 = grid
rlist                   = 1.0
coulombtype             = PME
fourierspacing          = 0.10
pme_order               = 4
ewald_rtol              = 1e-5
optimize_fft            = yes
rcoulomb                = 1.0
rvdw                    = 1.0
pbc                     = xyz
tcoupl                  = berendsen
tc-grps                 = Protein  SOL  Na+  Cl-
tau_t                   = 0.1 0.1 0.1 0.1
ref_t                   = 310 310 310 310
Pcoupl                  = berendsen
pcoupltype              = anisotropic
tau_p                  = 1.0 1.0 1.0 1.0 1.0 1.0
compressibility         = 4.5e-5 4.5e-5 4.5e-5 0 0 0
ref_p                   = 1.0 1.0 1.0 1.0 1.0 1.0
E_z                     = 1 -0.05 1
gen_vel                 = no
gen_temp                = 310
gen_seed                = 173529
constraints             = all-bonds
constraint_algorithm    = lincs
unconstrained_start     = no
```

MD Run 5: mm_nachr_md5.mdp, wah_nachr_md5.mdp

```
title                   = wah_nachr_md5
cpp                     = /lib/cpp
define                  =
integrator              = md
dt                     = 0.002
tinit                   = 1850.0
nsteps                  = 425000
nstxout                 = 5000
nstvout                 = 5000
nstlog                  = 250
nstenergy               = 500
nstxtcout               = 250
xtc_grps                = Protein  SOL  Na+  Cl-
energygrps              = Protein  SOL  Na+  Cl-
nstlist                 = 10
ns_type                 = grid
rlist                   = 1.0
coulombtype             = PME
```

```
fourierspacing          = 0.10
pme_order               = 4
ewald_rtol              = 1e-5
optimize_fft            = yes
rcoulomb                = 1.0
rvdw                    = 1.0
pbc                     = xyz
tcoupl                  = berendsen
tc-grps                 = Protein  SOL  Na+  Cl-
tau_t                   = 0.1 0.1 0.1 0.1
ref_t                   = 310 310 310 310
Pcoupl                  = berendsen
pcoupltype              = anisotropic
tau_p                   = 1.0 1.0 1.0 1.0 1.0 1.0
compressibility         = 4.5e-5 4.5e-5 4.5e-5 0 0 0
ref_p                   = 1.0 1.0 1.0 1.0 1.0 1.0
E_z                     = 1 -0.05 1
gen_vel                 = no
gen_temp                = 310
gen_seed                = 173529
constraints             = all-bonds
constraint_algorithm    = lincs
unconstrained_start     = no
```

MD Run 6: mm_nachr_md6.mdp, wah_nachr_md6.mdp

```
title                   = wah_nachr_md6
cpp                     = /lib/cpp
define                  =
integrator              = md
dt                      = 0.002
tinit                   = 1850.0
nsteps                  = 425000
nstxout                 = 5000
nstvout                 = 5000
nstlog                  = 250
nstenergy               = 500
nstxtcout               = 250
xtc_grps                = Protein  SOL  Na+  Cl-
energygrps              = Protein  SOL  Na+  Cl-
nstlist                 = 10
ns_type                 = grid
rlist                   = 1.0
coulombtype             = PME
fourierspacing          = 0.10
pme_order               = 4
ewald_rtol              = 1e-5
optimize_fft            = yes
rcoulomb                = 1.0
rvdw                    = 1.0
pbc                     = xyz
tcoupl                  = berendsen
tc-grps                 = Protein  SOL  Na+  Cl-
tau_t                   = 0.1 0.1 0.1 0.1
ref_t                   = 310 310 310 310
Pcoupl                  = berendsen
pcoupltype              = anisotropic
tau_p                   = 1.0 1.0 1.0 1.0 1.0 1.0
compressibility         = 4.5e-5 4.5e-5 4.5e-5 0 0 0
ref_p                   = 1.0 1.0 1.0 1.0 1.0 1.0
E_z                     = 1 -0.05 1
gen_vel                 = no
```

```
gen_temp                 = 310
gen_seed                 = 173529
constraints              = all-bonds
constraint_algorithm     = lincs
unconstrained_start      = no
```

MD Run 7: mm_nachr_md7.mdp, wah_nachr_md7.mdp

```
title                    = wah_nachr_md7
cpp                      = /lib/cpp
define                   =
integrator               = md
dt                       = 0.002
tinit                    = 2700.0
nsteps                   = 425000
nstxout                  = 5000
nstvout                  = 5000
nstlog                   = 250
nstenergy                = 500
nstxtcout                = 250
xtc_grps                 = Protein  SOL  Na+  Cl-
energygrps               = Protein  SOL  Na+  Cl-
nstlist                  = 10
ns_type                  = grid
rlist                    = 1.0
coulombtype              = PME
fourierspacing           = 0.10
pme_order                = 4
ewald_rtol               = 1e-5
optimize_fft             = yes
rcoulomb                 = 1.0
rvdw                     = 1.0
pbc                      = xyz
tcoupl                   = berendsen
tc-grps                  = Protein  SOL  Na+  Cl-
tau_t                    = 0.1 0.1 0.1 0.1
ref_t                    = 310 310 310 310
Pcoupl                   = berendsen
pcoupltype               = anisotropic
tau_p                    = 1.0 1.0 1.0 1.0 1.0 1.0
compressibility          = 4.5e-5 4.5e-5 4.5e-5 0 0 0
ref_p                    = 1.0 1.0 1.0 1.0 1.0 1.0
E_z                      = 1 -0.05 1
gen_vel                  = no
gen_temp                 = 310
gen_seed                 = 173529
constraints              = all-bonds
constraint_algorithm     = lincs
unconstrained_start      = no
```

MD Run 8: mm_nachr_md8.mdp, wah_nachr_md8.mdp

```
title                    = wah_nachr_md8
cpp                      = /lib/cpp
define                   =
integrator               = md
```

```
dt                      = 0.002
tinit                    = 3550.0
nsteps                   = 425000
nstxout                  = 5000
nstvout                  = 5000
nstlog                   = 250
nstenergy                = 500
nstxtcout                = 250
xtc_grps                 = Protein  SOL  Na+  Cl-
energygrps               = Protein  SOL  Na+  Cl-
nstlist                  = 10
ns_type                  = grid
rlist                    = 1.0
coulombtype              = PME
fourierspacing           = 0.10
pme_order                = 4
ewald_rtol               = 1e-5
optimize_fft             = yes
rcoulomb                 = 1.0
rvdw                     = 1.0
pbc                      = xyz
tcoupl                   = berendsen
tc-grps                  = Protein  SOL  Na+  Cl-
tau_t                    = 0.1 0.1 0.1 0.1
ref_t                    = 310 310 310 310
Pcoupl                   = berendsen
pcoupltype               = anisotropic
tau_p                   = 1.0 1.0 1.0 1.0 1.0 1.0
compressibility          = 4.5e-5 4.5e-5 4.5e-5 0 0 0
ref_p                    = 1.0 1.0 1.0 1.0 1.0 1.0
E_z                      = 1 -0.05 1
gen_vel                  = no
gen_temp                 = 310
gen_seed                 = 173529
constraints              = all-bonds
constraint_algorithm     = lincs
unconstrained_start      = no
```

MD Run 9: mm_nachr_md9.mdp, wah_nachr_md9.mdp

```
title                    = wah_nachr_md9
cpp                      = /lib/cpp
define                   =
integrator               = md
dt                      = 0.002
tinit                    = 4400.0
nsteps                   = 425000
nstxout                  = 5000
nstvout                  = 5000
nstlog                   = 250
nstenergy                = 500
nstxtcout                = 250
xtc_grps                 = Protein  SOL  Na+  Cl-
energygrps               = Protein  SOL  Na+  Cl-
nstlist                  = 10
ns_type                  = grid
rlist                    = 1.0
coulombtype              = PME
fourierspacing           = 0.10
```

```
pme_order               = 4
ewald_rtol              = 1e-5
optimize_fft            = yes
rcoulomb                = 1.0
rvdw                    = 1.0
pbc                     = xyz
tcoupl                  = berendsen
tc-grps                 = Protein  SOL  Na+  Cl-
tau_t                   = 0.1 0.1 0.1 0.1
ref_t                   = 310 310 310 310
Pcoupl                  = berendsen
pcoupltype              = anisotropic
tau_p                   = 1.0 1.0 1.0 1.0 1.0 1.0
compressibility         = 4.5e-5 4.5e-5 4.5e-5 0 0 0
ref_p                   = 1.0 1.0 1.0 1.0 1.0 1.0
E_z                     = 1 -0.05 1
gen_vel                 = no
gen_temp                = 310
gen_seed                = 173529
constraints             = all-bonds
constraint_algorithm    = lincs
unconstrained_start     = no
```

MD Run 10: mm_nachr_md10.mdp, wah_nachr_md10.mdp

```
title                   = wah_nachr_md10
cpp                     = /lib/cpp
define                  =
integrator              = md
dt                      = 0.002
tinit                   = 5250.0
nsteps                  = 425000
nstxout                 = 5000
nstvout                 = 5000
nstlog                  = 250
nstenergy               = 500
nstxtcout               = 250
xtc_grps                = Protein  SOL  Na+  Cl-
energygrps              = Protein  SOL  Na+  Cl-
nstlist                 = 10
ns_type                 = grid
rlist                   = 1.0
coulombtype             = PME
fourierspacing          = 0.10
pme_order               = 4
ewald_rtol              = 1e-5
optimize_fft            = yes
rcoulomb                = 1.0
rvdw                    = 1.0
pbc                     = xyz
tcoupl                  = berendsen
tc-grps                 = Protein  SOL  Na+  Cl-
tau_t                   = 0.1 0.1 0.1 0.1
ref_t                   = 310 310 310 310
Pcoupl                  = berendsen
pcoupltype              = anisotropic
tau_p                   = 1.0 1.0 1.0 1.0 1.0 1.0
compressibility         = 4.5e-5 4.5e-5 4.5e-5 0 0 0
ref_p                   = 1.0 1.0 1.0 1.0 1.0 1.0
```

```
E_z                     = 1 -0.05 1
gen_vel                 = no
gen_temp                = 310
gen_seed                = 173529
constraints             = all-bonds
constraint_algorithm    = lincs
unconstrained_start     = no
```

MD Run 11: mm_nachr_md11.mdp, wah_nachr_md11.mdp

```
title                   = wah_nachr_md11
cpp                     = /lib/cpp
define                  =
integrator              = md
dt                      = 0.002
tinit                   = 6100.0
nsteps                  = 425000
nstxout                 = 5000
nstvout                 = 5000
nstlog                  = 250
nstenergy               = 500
nstxtcout               = 250
xtc_grps                = Protein  SOL  Na+  Cl-
energygrps              = Protein  SOL  Na+  Cl-
nstlist                 = 10
ns_type                 = grid
rlist                   = 1.0
coulombtype             = PME
fourierspacing          = 0.10
pme_order               = 4
ewald_rtol              = 1e-5
optimize_fft            = yes
rcoulomb                = 1.0
rvdw                    = 1.0
pbc                     = xyz
tcoupl                  = berendsen
tc-grps                 = Protein  SOL  Na+  Cl-
tau_t                   = 0.1 0.1 0.1 0.1
ref_t                   = 310 310 310 310
Pcoupl                  = berendsen
pcoupltype              = anisotropic
tau_p                   = 1.0 1.0 1.0 1.0 1.0 1.0
compressibility         = 4.5e-5 4.5e-5 4.5e-5 0 0 0
ref_p                   = 1.0 1.0 1.0 1.0 1.0 1.0
E_z                     = 1 -0.05 1
gen_vel                 = no
gen_temp                = 310
gen_seed                = 173529
constraints             = all-bonds
constraint_algorithm    = lincs
unconstrained_start     = no
```

Chapter 7: Investigations into the Role of the Unusual Disulfide in the nAChR Agonist Binding Site

7.1 Introduction

Disulfide bonds are generally viewed as stabilizing elements in protein function. However, available high-resolution structural data over the last two decades have revealed that many important proteins contain so-called "forbidden disulfides," or highly constrained S-S linkages that may be a net destabilizing presence in the protein. Various potential roles have been ascribed to these special case disulfide bonds, including as redox, mechanochemical, or structural switches.[1, 2] One of the most interesting "forbidden disulfides" is the vicinal disulfide, in which two adjacent cysteines form a disulfide bond. Examples of this type of disulfide have been found near the active site of a small number of enzymes,[3, 4] as well as in the agonist binding site of the nicotinic acetylcholine receptor (nAChR).[3-6]

In the case of the nAChR, conformational changes in the ring formed by this vicinal disulfide have been proposed to play a role in modulating receptor function.[5-7] Specifically, changes in the *cis-trans* preferences of the peptide backbone between these residues could be altered by the binding of acetylcholine, contributing to the opening of the central ion conducting pore. In support of this hypothesis, it has been known for some time that proper function of the nicotinic receptor is highly sensitive to the oxidation state of these cysteines.[8] In addition, Cys-to-Ser mutations at either residue lead to a non-functional receptor.[9] Alternatively, this unusual disulfide bond could be important in localizing a diffuse negative potential near the agonist binding site or conferring additional rigidity on the C-loop.

Computational and NMR studies of small model peptides have yielded conflicting results about the putative native conformation of this unusual eight-membered, disulfide-containing

ring.[5, 6] Part of this is likely due to the unique nature of these eight-membered rings. Although otherwise unconstrained peptide bonds have a strong *trans* preference, small amide-containing rings may adopt a *cis* conformation to minimize ring strain. In a systematic study of the conformational preferences of amide-containing rings,[10] it was found that rings with fewer than eight atoms prefer the *cis* geometry, while those with greater than eight atoms adopt the *trans* conformation. In rings containing exactly eight atoms, such as the one formed by the vicinal disulfide, both *cis* and *trans* isomers can be accommodated, making it difficult to predict which geometry will be preferred.

Avizonis et al.[5] performed natural abundance ^{13}C and proton NMR spectroscopy in aqueous solution on a pentapeptide (TCCPD) corresponding to amino acids 191-195 of the nAChR. They additionally performed molecular mechanics calculations to predict the lowest energy conformers and to estimate the barriers to interconversion. Good agreement was found between theory and experiment, with both *cis* and *trans* conformations detected and having $\Delta G^{\neq}$ values at 20 ^{o}C of approximately 15 and 21 kcal/mol, respectively. Molecular mechanics calculations found the lowest energy conformation to be a *cis*-boat-chair conformation. Similarly, high level (B3LYP/6-31++ G(d,g)) ab initio calculations on the eight-membered ring 4,5-ditiaheptano-7-lactam and a small model dipeptide HCO-*ox*-[Cys-Cys]-NH_2 identified the lowest energy conformers for both molecules as containing *cis* amide bonds.[4]

NMR and Monte Carlo simulations by Creighton et al.[6] on the small peptide fragment Ac-*ox*-[Cys-Cys]-NH_2 also revealed interconverting *cis* and *trans* conformations. However, in this study the *trans* amide was found to be preferred over the *cis* amide by a ratio of 60:40, a ratio subsequently confirmed by Hondal and co-workers.[11] Similar to the study by Avizonis et al., this ratio implies a relatively low barrier to interconversion between the two conformers.

Both the Acetycholine Binding Protein (AChBP) crystal structures[12-15] and the α_1 nAChR crystal structure[16] reveal a *trans* amide bond, regardless of the presence of agonist or antagonist (Figure 7.1). However, these structures are static snapshots, and, in the case of the AChBPs, they are images of a binding protein - a protein lacking an ion conducting pore and thus presumably lacking some of the elements that enable signal transduction. As such, one must always interpret these structures with care.

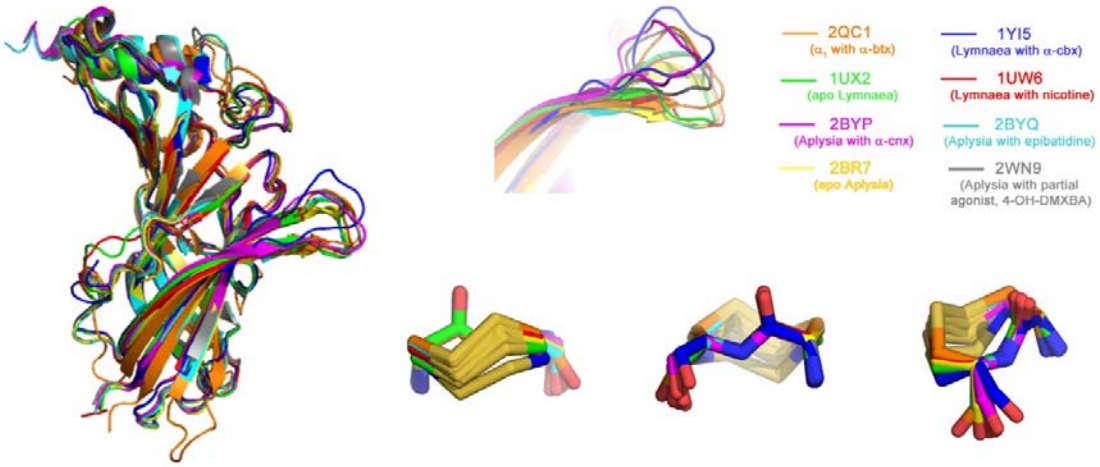

Figure 7.1: Crystal structures of α_1 (orange) and AChBP in the absence (green and yellow) and presence of various antagonists (magenta and blue) and agonists (red, cyan, and grey).

In addition, the ability to correctly identify the amide-bond conformation relies on the structure refinement program used in structure determination. Many of these programs allow for the *cis* conformation only in the instance of a proline residue or where explicitly defined by the crystallographer. Furthermore, at medium resolution the electron density of a *cis* peptide bond appears remarkably similar to that of a *trans* peptide bond and the wrong conformation can easily be accommodated with only minor distortions in the surrounding protein environment.[17, 18] The C-loop vicinal disulfide in the original medium resolution structure of AChBP could not be definitively identified as in the *trans* conformation,[19] although this bond

preference is shown in the crystal structure. This structure was used to aid in structure determination for subsequent, higher-resolution structures[12-14, 16], drawing into question the *trans* bond assignment given in these AChBP structures.

Functional studies probing the role of *cis-trans* isomerization of this vicinal disulfide are largely absent in the current literature. One hint as to the conformational proclivities of this region comes from a solution NMR study of AChBP, where ^{15}N-cysteine was incorporated at the native cysteines involved in both the C-loop and Cys-loop disulfide bonds.[20] In the absence of agonist, five distinct cross-peaks associated with the C-loop vicinal disulfide are observed, where only two are anticipated. Additional cross-peaks indicate multiple distinct conformations and could potentially be ascribed to *cis-trans* isomerization of the peptide backbone at this position. In the presence of the agonist acetylcholine, the number of cross-peaks associated with this disulfide is reduced to the expected two cross-peaks, indicating a single predominant conformation in the agonist-bound state.

Structure-function studies at the C-loop vicinal disulfide have largely failed due to the intolerance for substitutions at these positions. While conventional mutagenesis of these residues has been unable to provide insight as to the specific functional role of this unusual disulfide, unnatural amino acid mutagenesis may afford us the opportunity to probe the role of conformational flexibility in this region. Specifically, N-methyl amino acids (Figure 2A) have a lower energy barrier between *cis* and *trans* isomers.[21] In addition, N-methylation of the amide bond has been shown to increase the population of the *cis* conformer in peptides.[22, 23] Most recently, the presence of the N-methyl group in a model vicinal disulfide-containing dipeptide led to a dominant *cis*-conformation (by NMR), whereas both *cis* and *trans* conformations were observed in the amide-containing dipeptide.[11] Thus, incorporation of N-methyl cysteine affords

one possible opportunity to better understand the role of backbone isomerization at this position.

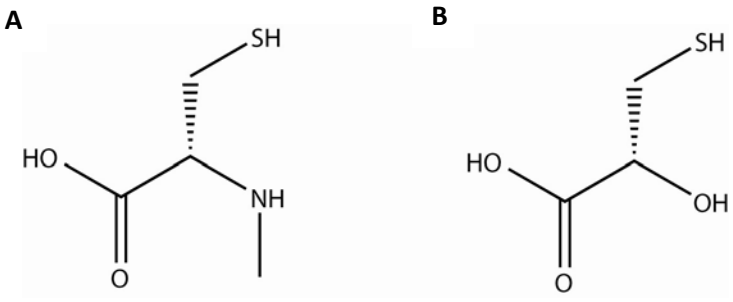

Figure 7.2: Cysteine analogues used in this study. A) N-methyl cysteine B) α-hydroxy cysteine

Incorporation of an α-hydroxy cysteine analogue (Figure 2B) could provide another avenue for addressing this question. Generally speaking, the resulting ester backbone has a lower barrier for *cis*-*trans* isomerization, but a stronger overall *trans* preference.[24]

Before incorporating these analogues into full-length receptors, *ab initio* calculations using the Gaussian software package[25] were undertaken, comparing the native eight-member, disulfide-containing ring with model peptides containing the two unnatural analogues. By finding the lowest energy conformations and the relative energy differences between the *cis* and *trans* backbone conformations in each of these three cases (amide, ester, and N-methyl), we seek to gain a better understanding of the influence of the unnatural substitutions on the backbone conformations of the vicinal disulfide.

7.2 Results and Discussion

The *cis* and *trans* isomers of a model peptide of the form CH_3CO-ox-[Cys-Cys]-NH_2 were constructed using GausView[25] molecule building tools with the S-S disulfide torsional angles of +/-90. The dihedral angles for these starting structures were derived from the lowest energy conformers from high-level ab initio calculations on a similar model peptide, HCO-ox-[Cys-Cys]-

NH_2.[4] These structures were then subject to B3LYP/6-311++G(d,p) level of theory. The optimized structures then served as the starting point for the ester and N-methyl model systems, where GausView was used to replace the backbone NH between the two cysteines with an oxygen or N-methyl moiety, respectively. In total, the energies for twelve geometry-optimized structures were calculated, with four conformers for each model system (Table 7.1, Figure 7.3).

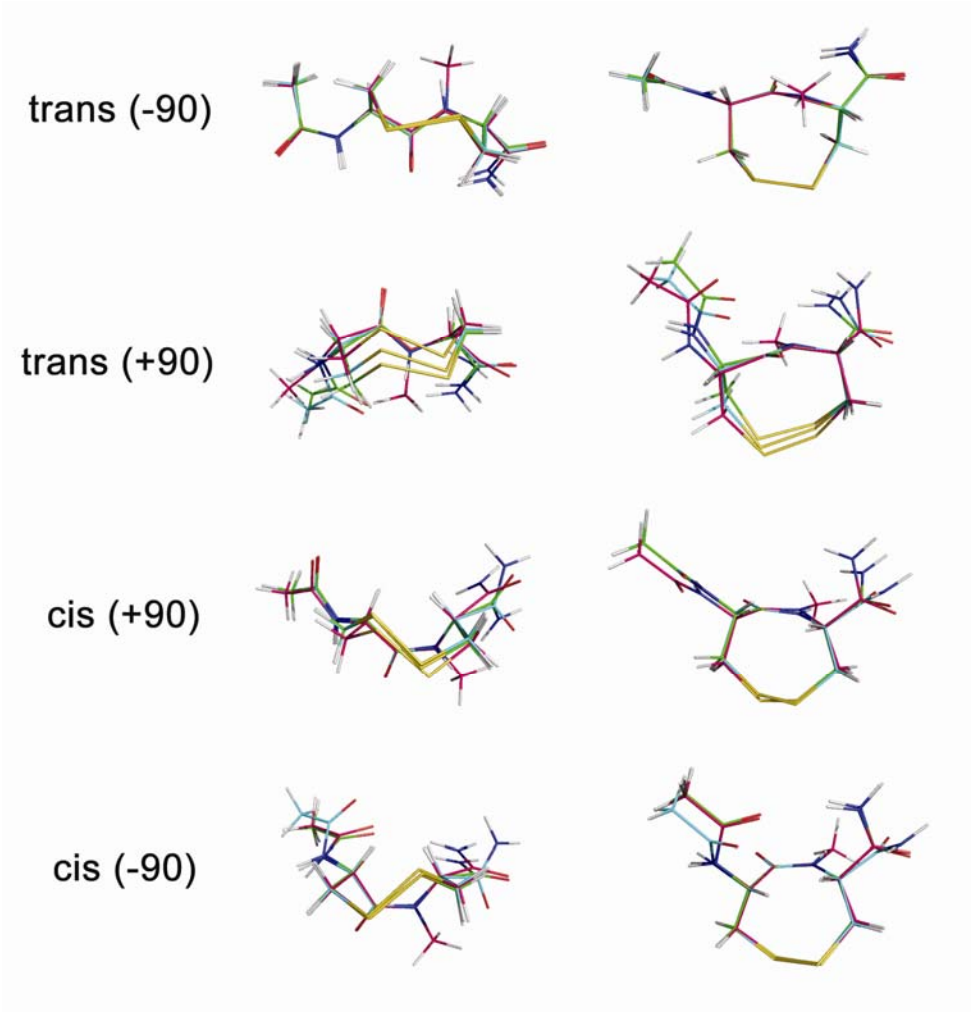

Figure 7.3: Geometry optimized structures. The amide is shown in cyan, the ester in green, and the N-methyl in pink.

	Energy (Hartrees)	ϕ_1	ϕ_2	ψ_1	ψ_2	ω_1	χ_{11}	χ_{21}	χ_{13}
Cis WT (+90)	-1499.30857804	-153.77	-139.05	151.87	143.30	6.80	-159.45	-54.61	95.53
Cis WT (-90)	-1499.30727674	-104.83	-152.82	130.89	148.79	-1.83	177.16	-94.14	-80.94
Trans WT (+90)	-1499.30315553	68.60	-166.68	-77.03	23.25	-146.12	175.91	43.10	90.12
Trans WT (-90)	-1499.29771128	-147.27	81.89	173.00	-43.19	144.01	77.08	-55.71	-86.81
Cis Ester (+90)	-1519.16938950	-155.17	-135.07	150.70	-3.48	7.48	-161.49	-58.20	95.37
Cis Ester (-90)	-1519.16561903	-63.07	-142.84	129.31	61.65	-2.90	175.34	-86.42	-92.62
Trans Ester (+90)	-1519.17167390	67.48	-161.54	-86.89	8.42	-154.74	179.98	44.28	85.90
Trans Ester (-90)	-1519.16449190	-146.02	80.28	176.17	-36.01	147.11	74.05	-56.52	-83.20
Cis N-methyl (+90)	-1538.62309456	-155.54	-133.60	146.86	34.85	13.82	-162.22	-55.58	95.68
Cis N-methyl (-90)	-1538.62226175	-70.28	-134.67	131.89	69.80	-6.52	176.43	-84.12	-92.57
Trans N-methyl (+90)	-1538.59575667	-32.31	-158.51	-67.98	63.27	-148.05	173.35	30.46	91.96
Trans N-methyl (-90)	-1538.60825774	-147.99	85.38	172.74	-49.22	144.11	73.56	-55.06	-86.15

Table 7.1: Relevant parameters for the geometry-optimized structures in this study. See Figure 7.4 for definitions of dihedral angles.

Given that the amide structures served as a starting point for the ester and N-methyl structure geometry optimizations, it is not surprising that geometric preferences of the resulting amide, ester, and N-methyl structures are, on the whole, similar (Figure 7.4). The largest differences between these molecules is seen in the external dihedral angles, ϕ_1 and ψ_2. In general, a larger range of values is observed for the *cis*-conformers, versus the *trans* conformers. The internal angles, by contrast, remain tightly clustered among the three molecules in both the *cis* and *trans* conformations.

Energetically, however, there are some striking differences among the three molecules. In agreement with previous studies, a moderate energy difference of 3.4 kcal/mol is seen between the two lowest energy conformers of the amide, with the preference for the *cis*-form (Figure 7.5). As would be predicted from the literature, the N-methylation of the internal amide leads to a stronger *cis* preference, resulting in a 9.3 kcal/mol energy difference between the *cis* and *trans* conformations. The ester modification has exactly the opposite effect. In fact, the lowest energy ester conformer contained a *trans* bond (ω = -154.74˚), which was 1.4 kcal/mol lower in energy than the lowest energy *cis* conformer.

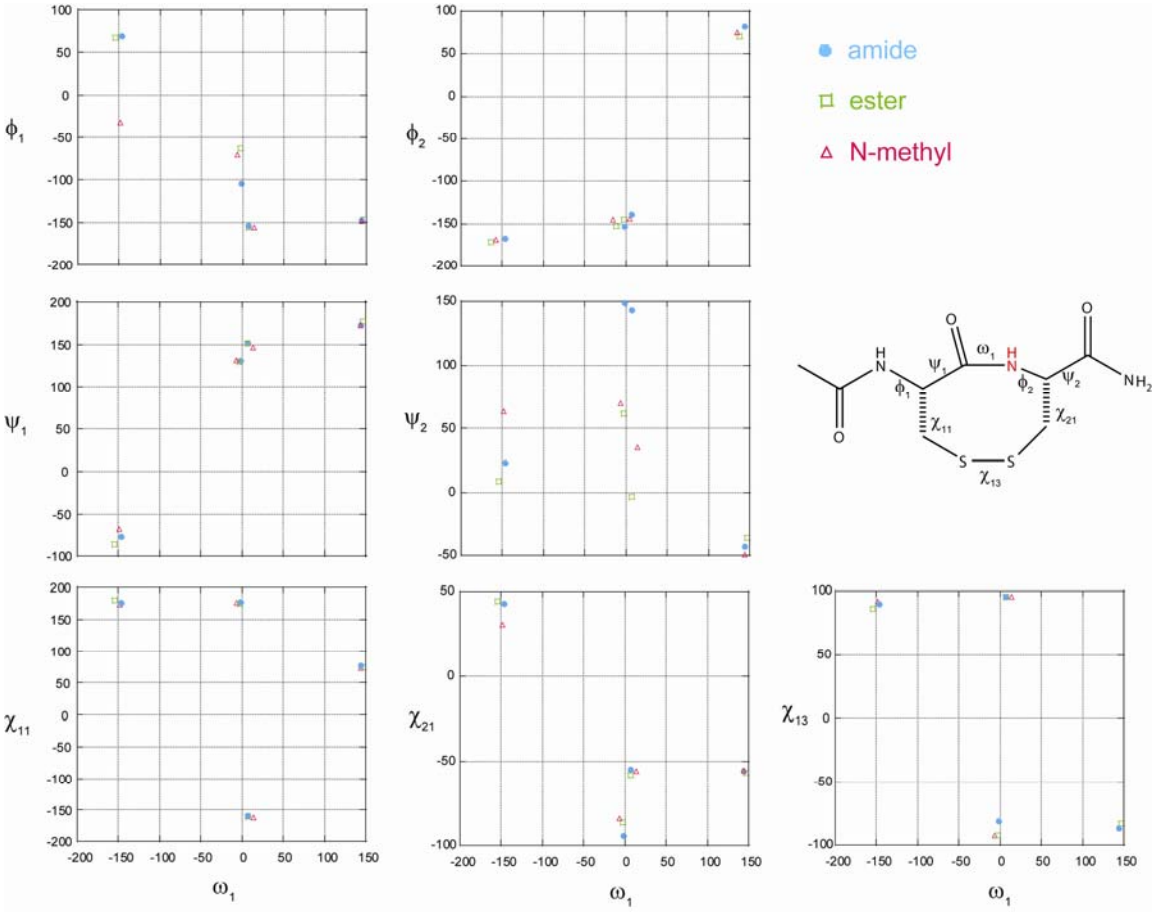

Figure 7.4: Selected conformational parameters of the structures evaluated in this study. Torsion angles are defined in the structure on the right.

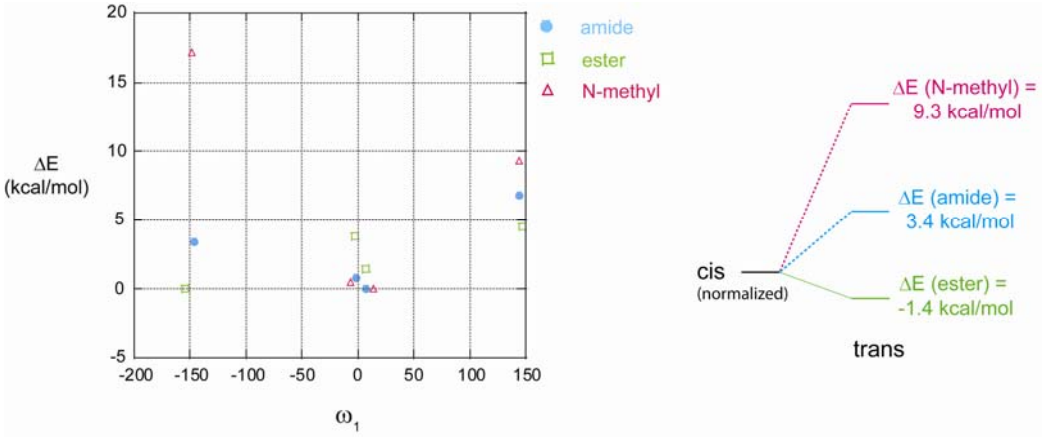

Figure 7.5: A) Correlation of the relative energies of the conformers in this study with the dihedral angle, ω. B) Relative ΔE between the lowest energy *cis* and *trans* isomers.

These results lead to some clear experimental predictions for models of nAChR function that implicate the vicinal disulfide. In the first model, the *cis*/*trans* preferences of the vicinal disulfide are altered by agonist binding. This leads to a conformational change in the C-loop that contributes to receptor activation. In this case, both the N-methyl or ester modifications should impact receptor function and these effects should be opposite. In other words, if the native conformation has a slight *cis* preference in the absence of agonist, then the N-methylation of the amide nitrogen will stabilize the apo conformation, making the receptor more difficult to open.

A second model ascribes a primarily structural role to this unusual disulfide; the conformational constraints of the eight-membered ring provide the correct geometry to the C-loop, allowing it to make the necessary intermolecular interactions with the agonist and intramolecular interactions with other residues in the receptor. If this is the case, one reasonable expectation would be that only the modification that contains the same conformational inclination as the native peptide bond will be able to produce functional receptors (e.g., α-hydroxy cysteine, if the wild-type receptor is predominantly *trans* or N-methyl cysteine, if the wild-type receptor is predominantly *cis* at the vicinal disulfide).

In our simple model system, the *cis* over *trans* preference was strengthened by 6 kcal/mol in the case of the N-methyl- containing compound. In the case of the ester, the backbone conformational preference was reversed, an energetic effect worth nearly 5 kcal/mol. A ten-fold shift in macroscopic EC_{50} is approximately equivalent to a $\Delta\Delta G$ of ± 1.4 kcal/mol. While these simple model dipeptides cannot possibly capture the complexity of a 280 kilodalton protein such as the nAChR, even moderately attenuated effects on the *cis*-*trans* preferences of

the vicinal disulfide should be easily detectable in a full-length receptor, provided that the bond conformation at this position is important for receptor function.

7.3 Conclusions and Future Directions

Ab initio studies with model peptides indicate that the N-methyl and ester modifications in the eight-membered ring created by the vicinal disulfide do alter the *cis-trans* preferences of the protein backbone. The amide backbone has a slight *cis* preference, which is strengthened by N-methylation of the amide nitrogen. In contrast, the ester backbone leads to a preference for the *trans* conformation. As such, the incorporation of these cysteine analogues into the full-length nAChR should provide insight as to the importance of *cis-trans* preferences at the C-loop vicinal disulfide. However, the calculated *cis-trans* preferences tell us little about the relative barrier to *cis-trans* isomerization for the constrained eight-membered ring. To address this issue, future ab-initio characterization of the transition states for *cis-trans* isomerization in the model peptides is additionally planned.

Synthesis of N-methyl cysteine and α-hydroxy cysteine by Angela Blum is currently underway. Incorporation of these unnatural analogues at positions 192 and 193 in the muscle nAChR, followed by electrophysiological characterization is planned. In the event of no detectable ionic currents, surface expression will need to be confirmed using radiolabeled α-bungarotoxin and binding studies or fluorescently labeled α-bungarotoxin and TIRF microscopy.

7.4 Materials and Methods

Geometric parameters used in this study are defined in Figure 7.4. Structure building and subsequent ab initio calculations were carried out using the Gaussian 03 software package.[25] at the B3LYP/6-31++G(d,p) level of theory in the gas phase. Geometric parameters

for the initial structures of the amide-containing model dipeptides were derived from the work of Hudaky et al.[4] *Cis* and *trans* isomers with both the +90 and -90 conformations of the disulfide dihedral (χ_{13}) were considered. These geometry-optimized structures then served as starting points for the ester and N-methyl calculations. Conformational characterization of the optimized structures was done in GausView and Pymol.[26]

7.5 References

1. Sandal, M., Grandi, F. & Samorì, B. Single molecule force spectroscopy discovers mechanochemical switches in biology: The case of the disulfide bond. *Polymer* **47**, 2571-2579 (2006).
2. Wouters, M.A., George, R.A. & Haworth, N.L. "Forbidden" disulfides: their role as redox switches. *Curr Protein Pept Sci* **8**, 484-95 (2007).
3. Carugo, O. et al. Vicinal disulfide turns. *Protein Eng* **16**, 637-9 (2003).
4. Hudaky, I. et al. Vicinal disulfide bridge conformers by experimental methods and by ab initio and DFT molecular computations. *Proteins* **55**, 152-68 (2004).
5. Avizonis, D.Z., Farr-Jones, S., Kosen, P.A. & Basus, V.J. Conformations and Dynamics of the Essential Cysteinyl-Cysteine Ring Derived from the Acetylcholine Receptor. *Journal of the American Chemical Society* **118**, 13031-13039 (1996).
6. Creighton, C.J., Reynolds, C.H., Lee, D.H., Leo, G.C. & Reitz, A.B. Conformational analysis of the eight-membered ring of the oxidized cysteinyl-cysteine unit implicated in nicotinic acetylcholine receptor ligand recognition. *J Am Chem Soc* **123**, 12664-9 (2001).
7. Kao, P.N. & Karlin, A. Acetylcholine receptor binding site contains a disulfide cross-link between adjacent half-cystinyl residues. *J Biol Chem* **261**, 8085-8 (1986).
8. Walker, J.W., Lukas, R.J. & McNamee, M.G. Effects of thio-group modifications on the ion permeability control and ligand binding properties of Torpedo californica acetylcholine receptor. *Biochemistry* **20**, 2191-9 (1981).
9. Mishina, M. et al. Location of functional regions of acetylcholine receptor alpha-subunit by site-directed mutagenesis. *Nature* **313**, 364-9 (1985).
10. Cumberbatch, S., North, M. & Zagotto, G. The synthesis and conformational analysis of a pair of diastereomeric, conformationally constrained peptides with opposite amide bond geometries. *Tetrahedron* **49**, 9049-9066 (1993).
11. Ruggles, E.L., Deker, P.B. & Hondal, R.J. Synthesis, redox properties, and conformational analysis of vicinal disulfide ring mimics. *Tetrahedron* **65**, 1257-1267 (2009).
12. Celie, P.H. et al. Crystal structure of acetylcholine-binding protein from Bulinus truncatus reveals the conserved structural scaffold and sites of variation in nicotinic acetylcholine receptors. *J Biol Chem* **280**, 26457-66 (2005).
13. Celie, P.H.N. et al. Nicotine and Carbamylcholine Binding to Nicotinic Acetylcholine Receptors as Studied in AChBP Crystal Structures. *Neuron* **41**, 907-914 (2004).
14. Hansen, S.B. et al. Structures of Aplysia AChBP complexes with nicotinic agonists and antagonists reveal distinctive binding interfaces and conformations. *EMBO J* **24**, 3635-3646 (2005).
15. Rucktooa, P., Smit, A.B. & Sixma, T.K. Insight in nAChR subtype selectivity from AChBP crystal structures. *Biochemical Pharmacology* **78**, 777-787 (2009).
16. Dellisanti, C.D., Yao, Y., Stroud, J.C., Wang, Z.-Z. & Chen, L. Crystal structure of the extracellular domain of nAChR [alpha]1 bound to [alpha]-bungarotoxin at 1.94 A resolution. *Nat Neurosci* **10**, 953-962 (2007).
17. Jabs, A., Weiss, M.S. & Hilgenfeld, R. Non-proline cis peptide bonds in proteins. *J Mol Biol* **286**, 291-304 (1999).
18. Weiss, M.S. & Hilgenfeld, R. A method to detect nonproline cis peptide bonds in proteins. *Biopolymers* **50**, 536-44 (1999).

19. Sixma, T.K. & Smit, A.B. Acetylcholine binding protein (AChBP): a secreted glial protein that provides a high-resolution model for the extracellular domain of pentameric ligand-gated ion channels. *Annu Rev Biophys Biomol Struct* **32**, 311-34 (2003).
20. Gao, F. et al. Solution NMR of acetylcholine binding protein reveals agonist-mediated conformational change of the C-loop. *Mol Pharmacol* **70**, 1230-5 (2006).
21. Fischer, G. Chemical aspects of peptide bond isomerisation. *Chem Soc Rev* **29**, 119-127 (2000).
22. Aubry, A., Vitoux, B., Boussard, G. & Marraud, M. N-Methyl peptides. IV. Water and beta-turn in peptides. Crystal structure of N-pivaloyl-L-prolyl-N,N'-dimethyl-D-alaninamide in the anhydrous and monohydrated states. *Int J Pept Protein Res* **18**, 195-202 (1981).
23. Vitoux, B., Aubry, A., Cung, M.T., Boussard, G. & Marraud, M. N-methyl peptides. III. Solution conformational study and crystal structure of N-pivaloyl-L-prolyl-N-methyl-N'-isopropyl-L-alaninamide. *Int J Pept Protein Res* **17**, 469-79 (1981).
24. Christophe, D. in Cis-Trans Isomerization in Biochemistry (ed. Christophe, D.) 143-166 (2006).
25. Frisch, M.J. et al. (Gaussian, Wallingford, CT, 2003).
26. Delano, W.L. (Delano Scientific, Palo Alto, CA, 2002).